IZMIR KATIP CELEBI UNIVERSITY

GRADUATE SCHOOL OF NATURAL AND APPLIED SCIENCES

SYNTHESIS AND APPLICATION OF THE IRIDIUM SEMICONDUCTOR
COMPLEXES FOR ORGANIC LIGHT EMITTING DIODES

Ph.D. THESIS

Caner KARAKAYA

Department of Materials Science and Engineering

DECEMBER 2017

IZMIR KATIP CELEBI UNIVERSITY

GRADUATE SCHOOL OF NATURAL AND APPLIED SCIENCES

SYNTHESIS AND APPLICATION OF THE IRIDIUM SEMICONDUCTOR COMPLEXES FOR ORGANIC LIGHT EMITTING DIODES

Ph.D. THESIS

Caner KARAKAYA
(D120111001)

Department of Materials Science and Engineering

Thesis Advisor: Prof. Dr. Şerafettin DEMİÇ

DECEMBER 2017

İZMİR KATİP ÇELEBİ ÜNİVERSİTESİ

FEN BİLİMLERİ ENSTİTÜSÜ

ORGANİK IŞIK YAYAN DİYOTLAR İÇİN İRİDYUM YARIİLETKEN KOMPLEKSLERİNİN SENTEZİ VE UYGULAMASI

DOKTORA TEZİ

Caner KARAKAYA
(D120111001)

Malzeme Bilimi ve Mühendisliği Anabilim Dalı

Tez Danışmanı: Prof. Dr. Şerafettin DEMİÇ

ARALIK 2017

Caner KARAKAYA, a **Ph.D.** student of **IKCU Graduate School of Science and Engineering**, student ID D120111001, successfully defended the thesis entitled ''**SYNTHESIS AND APPLICATION OF THE IRIDIUM SEMICONDUCTOR COMPLEXES FOR ORGANIC LIGHT EMITTING DIODES**'', which he prepared after fulfilling the requirements specified in the associated legislations, before the jury whose signatures are below.

Thesis Advisor:	**Prof. Dr. Şerafettin DEMİÇ** Izmir Katip Celebi University	....
Jury Members:	**Prof. Dr. Mahmut KUŞ** Konya Selcuk University	....
	Assoc. Prof. Dr. Sermet KOYUNCU Canakkale Onsekiz Mart University	....
	Asist. Prof. Dr. Nesrin HORZUM POLAT Izmir Katip Celebi University	....
	Asist. Prof. Dr. Fethullah GÜNEŞ Izmir Katip Celebi University	....

Date of Submission : 27 November 2017
Date of Defense : 29 December 2017

*To my **spouse** and **daughter**,*

x

ACKNOWLEDGMENTS

TABLE OF CONTENTS

ABBREVIATIONS

Alq₃	:	Tris-(8-hydroxyquinoline)aluminum
a.u.	:	Arbitrary unit
C^N ligand	:	Cyclometallating ligand (e.g. 2-phenylpyridine)
CBP	:	4,4′-N,N′-dicarbazol-biphenyl
CD₃CN	:	Acetonitrile-d3
CH₂Cl₂	:	Dichloromethane
CIE	:	the Commission International de l'Eclairage
CRT	:	Cathode ray tube
CuPc	:	Copper phthalocyanine
CV	:	Cyclic voltammetry
DFT	:	Density functional theory
DME	:	1,2-dimethoxy ethane
DMSO	:	Dimethyl sulfoxide
EBL	:	Electron blocking layer
EDG	:	Electron donating group
EIL	:	Electron injection layer
EL	:	Electroluminescence
E$_{ox}$	:	Oxidation potential
EQE	:	External quantum efficiency
E$_{red}$	:	Reduction potential
Et₂O	:	Diethyl ether
ETL	:	Electron transfer layer
EWG	:	Electron withdrawing group
eV	:	Electron volt
HBL	:	Hole blocking layer
HIL	:	Hole injection layer
H-NMR	:	Proton nuclear magnetic resonance spectroscopy
HOMO	:	Highest occupied molecular orbital
HTL	:	Hole transport layer
IL	:	Ionic liquid
ISC	:	Intersystem crossing
ITO	:	Indium tin oxide
iTMC	:	Ionic transition metal complex
LC	:	Ligand centered transition
LCD	:	Liquid crystal display
LEC	:	Light-emitting electrochemical cell
LED	:	Light-emitting diode
LMCT	:	Ligand to metal charge transfer
LUMO	:	Lowest unoccupied molecular orbital

MC	: Metal centered transition
MeCN	: Acetonitrile
MeOH	: Methanol
MLCT	: Metal-ligand charge transfer
N^N ligand	: Polypyridine ligand
NMR	: Nuclear magnetic resonance
NPB	: N,N'-diphenyl-N,N'-bis(1-naphthyl)–(1,1'-biphenyl)-4,4'-diamine
OLED	: Organic light emitting diode
PEDOT/PSS	: Poly(3,4-ethylenedioxythiophene)/polystyrene sulfonate
PL	: Photoluminescence
PLED	: Polymer light emitting diode
PPV	: Polyphenylene vinylene
PtOEP	: Platinum octaethylporphyrin
SiC	: Silicon carbide
TFH	: Tetrahydrofuran
TLC	: Thin-layer chromatography
UV-vis	: Ultraviolet-visible
ZnS	: Zinc selenide

SYMBOLS

δ	: Chemical shift [ppm]
λ_{abs}	: Absorption wavelength
λ_{em}	: Emission wavelength
λ_{ex}	: Excitation wavelength
χ_e	: Work function of cathode
χ_h	: Work function of anode

LIST OF TABLES

LIST OF FIGURES

SYNTHESIS AND APPLICATION OF THE IRIDIUM SEMICONDUCTOR COMPLEXES FOR ORGANIC LIGHT EMITTING DIODES

ABSTRACT

Organic light emitting diodes (OLEDs) is a multi-disciplinary research area. Due to the possibility of being produced in different designs and low costs, studies on the research and development of energy efficient structures have increased. These expectations have increased so much that research on new types of molecules and device designs is increasing with the expectation that OLEDs will be more efficient than all available light sources and that almost 100% of the energy used can be converted to light. Transition metal complexes, especially Iridium(III) complexes, which make them phosphorescent due to their high quantum yield and broad emission colors, have been the most widely used emission material for OLED applications. Because the materials with this property provide both singlet and triplet transitions, all excited states contribute to light emission, so the theoretical internal quantum yield of these complexes can reach 100%.

In this work, 4 spiro-based ligands were synthesized by Suzuki cross-linking methodology and 8 novel Ir(III) complexes were synthesized with these ligands. The synthesized molecules were characterized by ^{1}HNMR, ^{13}CNMR, UV-Vis, photoluminescence (PL) and cyclic voltammetry (CV) techniques.

Ir(III) complexes have been prepared functionalized as two series. The photophysical properties of the functionalization have been examined to determine the effect on the emission. It was determined that complexes with solution phase emission studies had green and orange emissions ranging from 510 to 578 nm with the effect of functionalized electron donating group (EDG) and electron withdrawing group (EWG) groups. These results showed that substituent groups are effective on the emission of complexes. The results from cyclic voltammograms show that EDG and EWG groups and complexes have different energy band intervals (E_g value).

Some of the synthesized iridium complexes were made with a light emitting device (single active layer OLED, light emitting electrochemical cell, LEC device). It has been observed that these devices can operate at low voltages. LEC devices were prepared in the ITO/PEDOT:PSS/Ir(III)complex/Ag configuration. It was determined

that the prepared LEC devices started to radiate at on average of 5.5 V and the highest luminance value (in C2 complex) was measured as 1107 cd/m^2.

ORGANİK IŞIK YAYAN DIYOTLAR İÇİN IRIDIUM YARI İLETKEN KOMPLEKSLERİNIN SENTEZİ VE UYGULAMASI
ÖZET

Işık yayan organik diyotlar (OLED'ler) disiplinler arası çalışma alanına sahip araştırma konusudur. Farklı tasarımlarla üretilebilme olanağı ve düşük maliyetleri sebebi ile enerji tasarruflu yüksek verimli aygıtların araştırılması ve geliştirilmesi üzerine çalışmalar çoğalmıştır. Bu beklentiler o kadar çoğalmıştır ki OLED tipi aydınlatma aygıtları mevcut uygulamalardan ayrılmakta, teorik olarak kullanılan enerjiyi neredeyse %100 oranda ışığa çevirebilecek oldukları için, bu sebeple de yeni tür moleküller ve cihaz tasarımları üzerine araştırmalar artmaktadır. Yüksek kuantum verimi ve geniş emisyon renkleri nedeniyle fosforesans yapan geçiş metal kompleksleri, özellikle iridyum(III) kompleksleri, OLED uygulamaları için en yaygın kullanılan emisyon malzemesi olmuştur. Bu özelliğe sahip malzemeler hem singlet hem de triplet geçişlerini sağladığından dolayı, tüm uyarılmış durumlar ışık emisyonuna katkıda bulunur, bu nedenle bu komplekslerin teorik iç kuantum verimi % 100'e ulaşabilir.

Bu çalışmada, Suzuki çapraz bağlanma sentez yöntemi ile spiro karbonu içeren 4 yeni ligand sentezi ve bu ligantların kullanıldığı 8 adet yeni tür iyonik Ir(III) kompleksi sentezlenmiştir. Sentezlenen bileşiklerin kimyasal yapıları ^{1}H ve ^{13}C NMR ile doğrulanmış, fotofiziksel özellikleri ise UV-Vis, fotolüminesans (PL) ve döngüsel voltammetri (CV) tekniği ile aydınlatılmıştır.

Ir(III) kompleksleri iki seri olacak şekilde fonksiyonelleştirilmiş olarak hazırlanmıştır. Fonksiyonelleştirmenin emisyon üzerindeki etkisini belirlemek için fotofiziksel özellikleri incelenmiştir. Çözelti fazı emisyon çalışmaları yapılan komplekslerin, fonksiyonelleştirilmiş elektron veren (EDG) ve elektron çeken (EWG) grupların etkisiyle 510 ve 578 nm arasında değişen yeşil ve turuncu emisyona sahip olduğu tespit edildi. Bu sonuçlar, ikame edici grupların komplekslerin emisyonu üzerinde etkili olduğunu gösterdi. Döngüsel voltamogramlardan elde edilen sonuçlar, EDG ve EWG grupları ile komplekslerin sahip oldukları enerji bant aralıklarının (E_g değeri) değiştiğini göstermiştir.

Sentezlenen iridyum komplekslerinin bazıları ile ışık yayan aygıt çalıştığı (tek aktif katmanlı OLED denilen ışık yayan elektrokimyasal hücre, LEC aygıtı) yapılmıştır. Bu

aygıtların düşük voltajda çalışabildiği gözlenmiştir. LEC aygıtları ITO/PEDOT:PSS/Ir(III)kompleksi/Ag konfigürasyonunda hazırlanmıştır. Hazırlanan LEC aygıtlarının ortalama olarak 5.5 V civarında ışıma yapmaya başladığı tespit edilmiş ve en yüksek parlaklık değeri (C2 kompleksinde) 1107 cd/m^2 olarak ölçülmüştür.

1. INTRODUCTION

Light emitting diodes (LEDs), using both for lighting and displaying, provide highly efficient illumination compared to the incandescent sources such as light bulbs [1] and fluorescent tubes containing toxic mercury gas [2] and also LED-based screens, which have lower manufacturing costs and power consumption, and significantly less weight and bulk, have begun to take the place of cathode ray tubes (CRTs) since the late 2000s [3]. On the other hand the soft functional material based light emitting diodes such as organic light emitting diodes (OLEDs) and light emitting electrochemical cells (LECs) have the potential to complement LEDs in the future. These soft functional materials can be deposited on large-area, low energy consumption, flexible and light weight substrates which cannot be possible for semiconductor based LEDs.

1.1   History of Organic Electroluminescence

Electroluminescence (EL) was firstly observed in 1907, by Captain Henry Joseph Round who reported that a yellow light was emitted from silicon carbide (SiC) when a current was applied [4]. In 1936, Destriau et al was reported luminescence from zinc selenide (ZnS) [5]. The first observation of organic electroluminescence was utilized from 5 mm thick anthracence crystal under 100V driving voltage. In 1963, this organic semiconductor device architected by Pope et al [6]. In the next work, multilayer organic light-emitting diode (OLED) was operated in the laboratories of the Eastman Kodak company in 1987 [7] with working voltage less than 10 V and external quantum efficiency (EQE) as high as 1%. This multilayered OLED structure has organic emitting layer sandwiched between hole transport, electron transport layers. [7] In 1990 the first polymer light emitting diode (PLED) using polyphenylene vinylene (PPV) emissive layer only between anode (indium tin oxide, ITO) and cathode (Al) [8]. Since these developments, the OLED technology was interested by the scientists all over the world. After about ten years, the first commercial OLED display, which utilized in a car radio, was presented by the Pioneer Corporation in 1997 [9] In 1998, the first phosphorescence OLED (ph-OLED) was fabricated by using a

phosphorescence transition metal complexes (iTMC) as an emissive material in OLED structure by Baldo et. al. In 2000 for the break fresh ground work on conductive polymers, the chemistry Nobel Prize was awarded to Hideki Shirakawa, Alan Heeger and Alan MacDiarmid [10]. These developments were followed by applications in mobile phones, digital cameras and TVs. The first OLED lamp was introduced by OSRAM in 2008, this started a new market in lighting industry [11] Another OLED applications such as luminescent wallpapers [12] rollable notebooks [13] or MP3-bracelets [14] can be mentioned for the creativity to design new gadgets. In 2012, data-eye-glasses based on bidirectional OLED micro-displays were developed at Frauenhofer IPMS and this was honored by the Society for Information Display (SID) [15]

OLEDs can be separated into three types according to structure and emissive layers; small molecule OLEDs (SMOLEDs) [16], PLEDs [17] and light emitting electrochemical cells (LECs) which has a simple structure containing highly emissive transition metal complexes between anode and cathode [18].

Pure organic light emitting diodes have a lot of advantages, however, most of their emitting materials are only based on fluorescence emitting. Because of the spin forbidden rule [19-21] in fluorescence, the internal quantum efficiency of these materials are limited only up to 25%. Whereas, organometallic materials, which contain heavy metal atoms, can emit light through both phosphorescence and fluorescence. For this reason, the strong spin-orbit coupling, which causes to efficient triplet states, occurs in that materials and they can theoretically achieve a maximum internal quantum efficiency of 100% [22]

In the development of highly efficient OLEDs, the most widely studied organometallic complexes are iridium(III) complexes [23] due to their prevalent advantages. The phosphorescence lifetime of the iridium(III) complexes is less than 1 s, which decreases the energy loss and causes more enhancement of efficiency. On the other hand, by modifying the ligands of the iridium(III) complexes, the emission wavelength can be finely tuned.[24-27]

1.2 OLED Light Generating Mechanism and Structure

Electroluminescence is obtained by combining light emitting layers (LEDs) between anode and cathode electrodes. The simple components of the OLED constructions are anode, light emitting layer and cathode. Along with this, however, there are OLED structures made up of many layers. Multilayer OLEDs, due to different mobility of holes and electrons, result in consumed electricity without proper recombination, which adversely affects the efficiency of the device. (Figure 1.1) [28]. In order to compensate the charge injection and control recombination hole injection/transport layer (HTL) and electron injection/transport layer (ETL) are added to the device configuration. To limit the loads on the active layer, the hole blocking layer (HBL) and the electron blocking layer (EBL) are placed.

After applying a voltage to the device, holes are injected from the anode to the active layer, electrons from the cathode are injected, and this hole and electron migrate along the transport layers. Light emissions are produced when the excitons reach the ground state from the excited state. The wavelength of the light related to the energy difference between the excited states and the ground states, which is dominated by the emissive layer material.
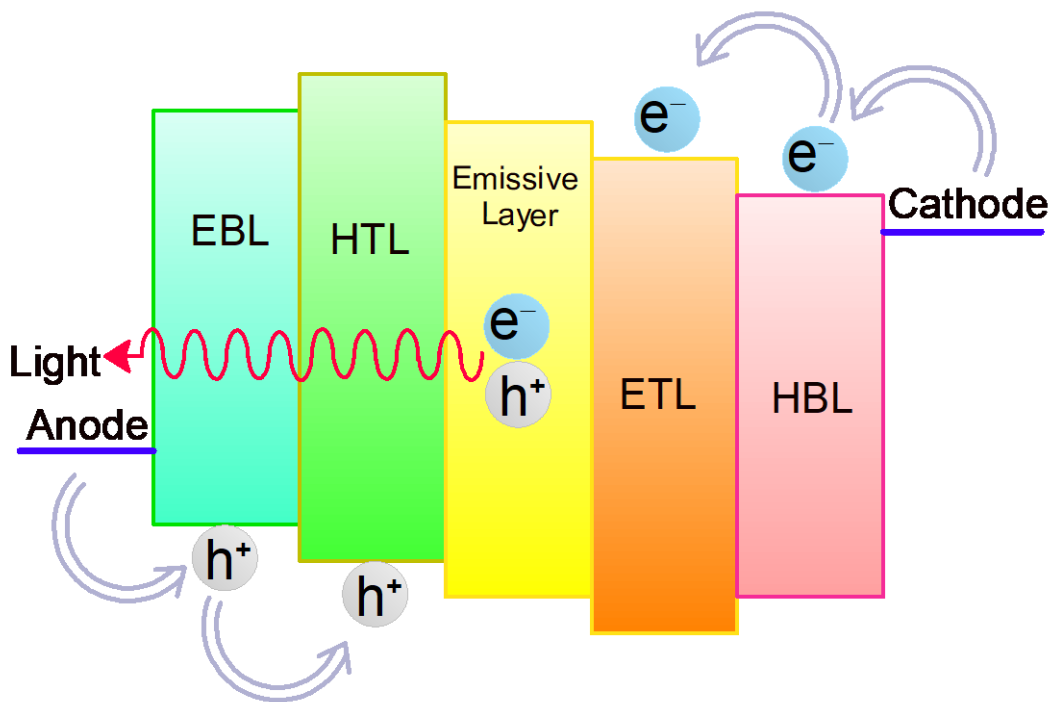
Figure 1.1 : Generating mechanism of OLEDs.

1.2.1 Anode

Indium-tin oxide (ITO) coated glass substrate as anode material for OLEDs is a widely used choice. In addition to high transparency (90%) under visible light, the high operating function is the main point of broadband range ($E_g = 3.5 - 4.3$ eV) and it sticks well to the active material. The ITO should be ultrasonically cleaned with the washing solution before use and rinsed with deionized water consecutively after each treatment. After cleaning, the injection of holes is facilitated using plasma and UV-ozone to increase the working function. These sequential processes are crucial to increase the stability of the OLED [29, 30].

1.2.2 Hole Injection Materials

ITO has work function which is lower than the highest occupied molecular orbital (HOMO) level of most organic materials (active materials) and hole transport materials. A hole injection layer is placed between ITO and HTL, in order to increase the device performance, and to improve the surface morphology of ITO.

Copper phthalocyanine (CuPc) [31, 32] and poly(3,4-ethylenedioxythiophene) poly(styrenesulfonate) (PEDOT/PSS) [33, 34] are widely used hole injection materials. In particular, PEDOT/PSS allows the ITO surface to be smooth. The possibility of opening voltage of the device and the possibility of electric shorts are reduced. CuPc and PEDOT/PSS structures are shown in Figure 1.2.
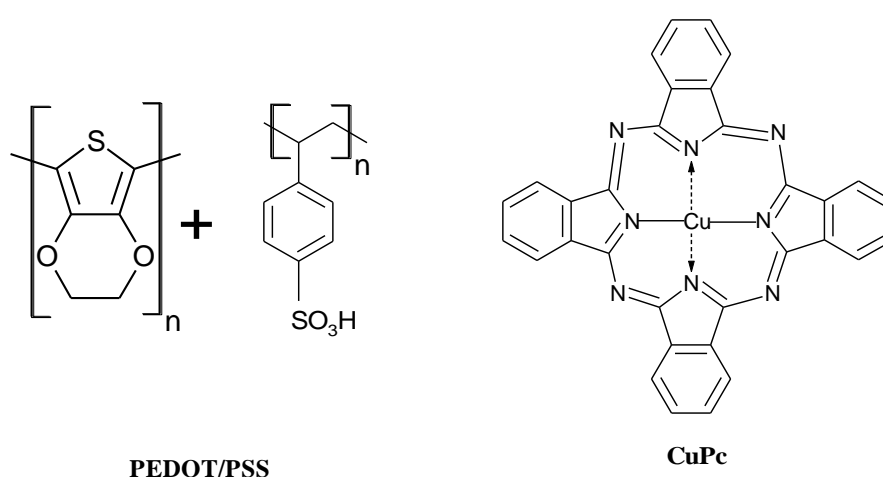
PEDOT/PSS　　　　　**CuPc**

Figure 1.2 : Structures of PEDOT/PSS and CuPc.

1.2.3 Hole Transporting Materials

In OLEDs, hole and electron transport layers are used to enhance device efficiency and balance the transport of charges. A hole transport layer supports hole injection and also satisfy a better matching with the work function of the anode. In addition, hole transporting materials prevent the accumulating of holes on the interface of the anode and the hole transport layer. Because of the low electron affinity of hole transport materials, they constitute the majority of organic materials. In the electroluminescence applications, HTL materials are selected especially according to their thermal stability, low ionization potential, and good coating process [35].

There are many hole transporting materials. The most common ones used are triarylamine and carbazole derivatives, such as N,N′-bis(3-methylphenyl)-N,N′-diphenylbenzidine (TPD) [36], 4,4′-N,N′-dicarbazol-biphenyl (CBP) [37], and N,N'-diphenyl-N,N'-bis(1-naphthyl)–(1,1'-biphenyl)-4,4'-diamine (NPB) [38], (Figure 1.3).

NPB   CBP

TPD
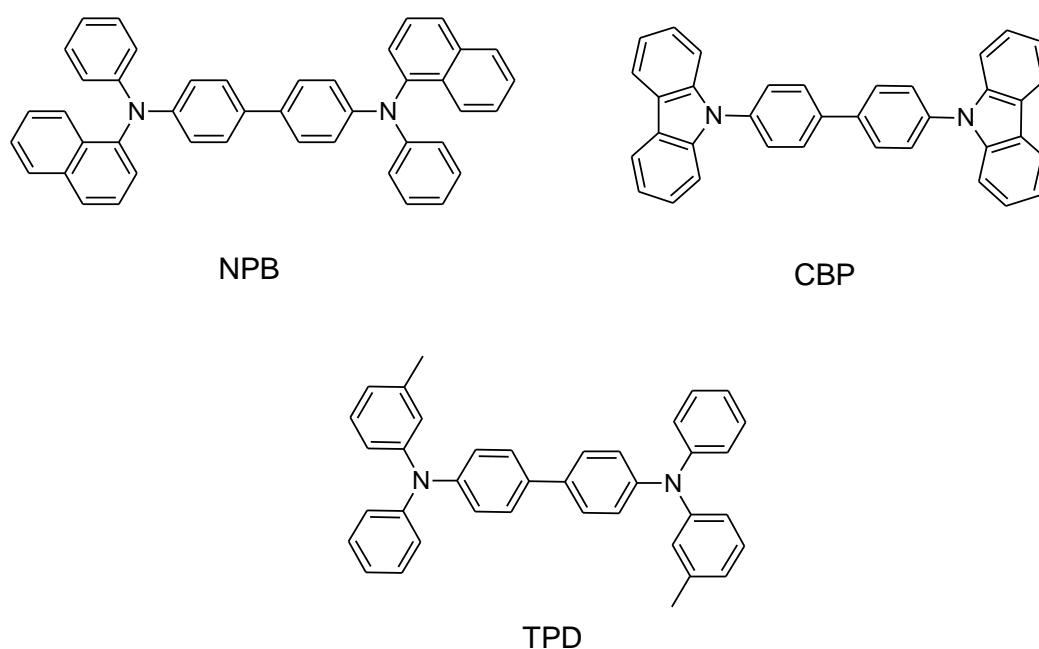
Figure 1.3 : Most commonly used hole transporting materials in OLEDs.

1.2.4 Emissive Materials

Electrons and holes flowing in the device under voltage are recombined into the emissive layer. As a result of the recombination of an electron and a hole, a photon is

emitted. The energy or wavelength of the photon directly depends on the energy band structure of the emissive material. As an example of organic emissive materials, the commonly used tris-(8-hydroxyquinoline)aluminum (Alq$_3$) can be indicated. The reason for the use of this material is its capability of emitting with a very good operation stability [39].

1.2.5 Electron Transporting Materials

An electron-transport layer (ETL) is coated between cathode and emissive layer to reduce the electron injection barrier of the cathode and to satisfy effective recombination of electrons and holes onto emissive layer [40]. An effective electron transfer material should have a low lowest unoccupied molecular orbital (LUMO) level and a high ionization potential.

In constructing organic EL devices, frequently used electron transporting materials are some metal chelates such as Alq$_3$, and Zn chelates, 3-(4-biphenyl)-4-phenyl-5-tert-butylphenyl-1,2,4-triazole (TAZ) [41, 42], 2,2',2''-(1,3,5-phenylene)tris(1-phenyl-1H-benzimidazole) (TPBI) [37, 43, 44], 2-(4-tert-Butylphenyl)-5-(4-biphenylyl)-1,3,4-oxadiazole (PBD) [45] (Figure 1.4), and their oxadiazole derivatives [46, 47].
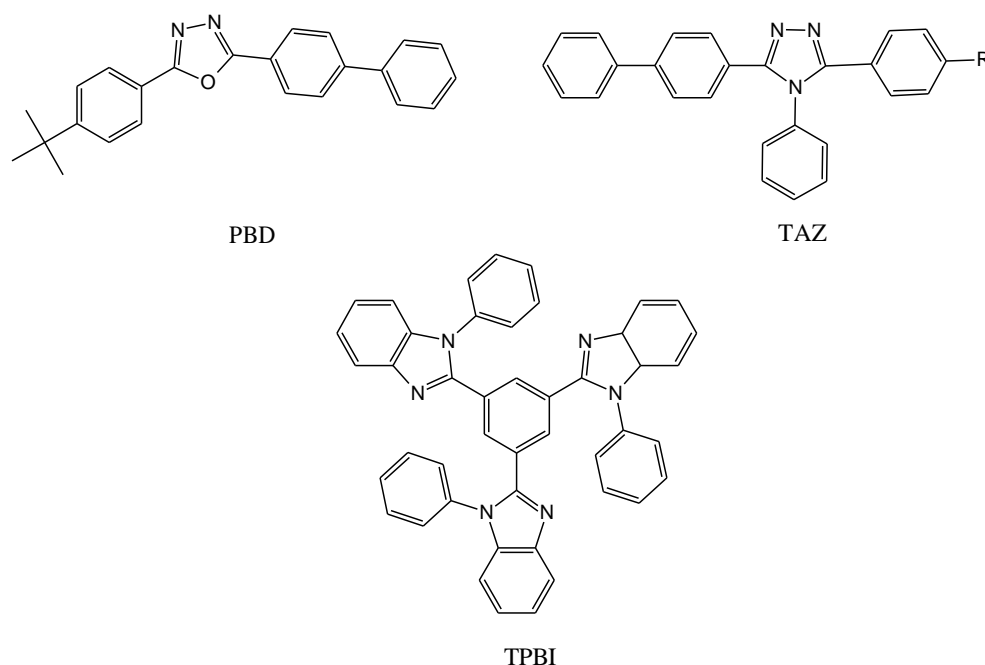
Figure 1.4 : Electron-transporting materials for OLEDs.

1.2.6 Cathodes

As cathodes for OLEDs, low work function and electropositive metals are preferred. For this reason, it is necessary to reduce the energy barrier for the electron injection of the cathode material to the organic material and to maintain the load current density [48, 49].

Ca, K and Li have been used as cathode materials but have been shown to exhibit a high chemical reaction with weak corrosion resistance and organic layer. As a solution, metal alloys such as Al-Li and Mg-Ag, which are more stable and have lower work function, are used. Nowadays, the use of LiF/Al has widespread acceptance because of the increased performance of the OLED devices.

When we look at the energy diagrams of single-layered and multi-layered OLEDs in Figure 1.5 , it can be shown that the hole injection layer and the electron injection layer effectively balance the barrier for charge injection. The harmonious energy levels between the layers will significantly increase the efficiency of the OLEDs.
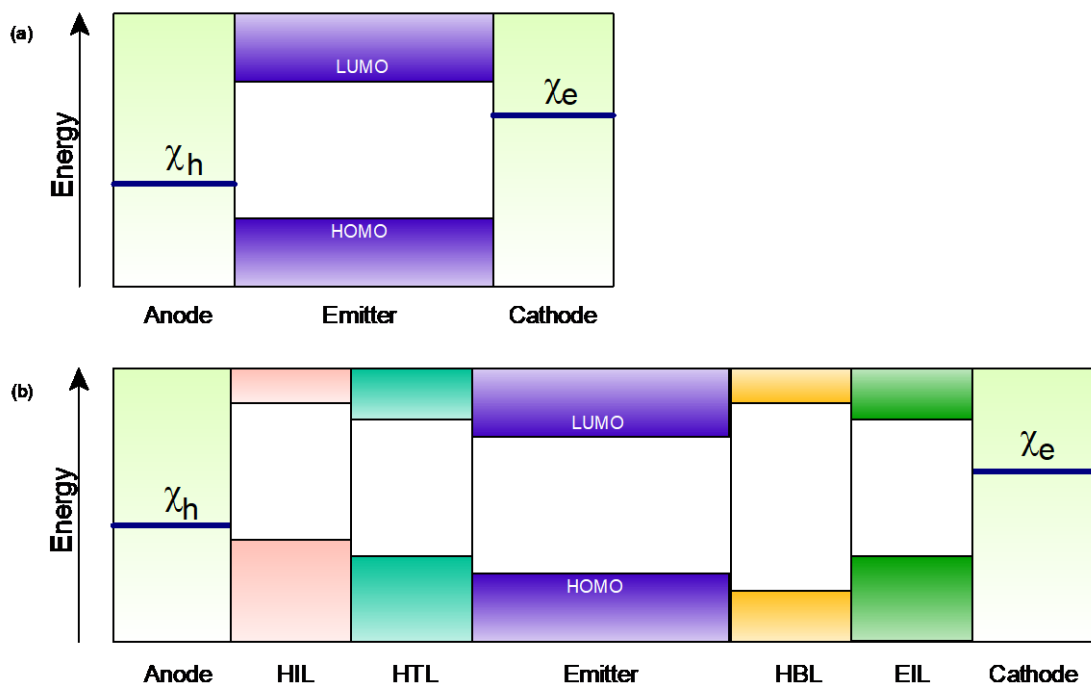
Figure 1.5 : Illustration of energy levels of (a) a single-layered and (b) a multi-layered OLED.

Depending on the configuration and mechanism of OLEDs, device performance is affected by two main aspects: emissive material and device structure. The focus of this thesis is primarily on the research of luminescent materials.

1.3 Photoluminescence and Electroluminescence

Luminescence is the production of light from organic and inorganic compounds. This light comes out of a number of different mechanisms. The light emission of the organic compounds to be used in the OLED applications according to the excited states will be described in detail below. In order for a substance to emit light, it must return to the ground state by energizing it in a way that is not caused by high-energy excitation and this energy is not photon or radiation. This exciting state occurs with electronic excitation (electroluminescence, EL) or light excitation (photoluminescence, PL). PL and EL both express light emission. But they get excited by different types of energy.

PL is the radiative decay that occurs when the photon is absorbed. EL is the light produced when a material is exposed to an electric field, without generating thermal energy.

1.3.1 Photoluminescence

PL occurs by the stimulation of an electron by a photon up to the level of the highest occupied molecular orbital (HOMO) to the lowest un-occupied molecular orbital (LUMO). There is an environment for the excited electrons to come back to the HOMO. This process can be radiation, that is, a photon stuck, or it can be inverse to radiation and help the electron return to the HOMO. The PL scheme can be seen in Figure 1.6.
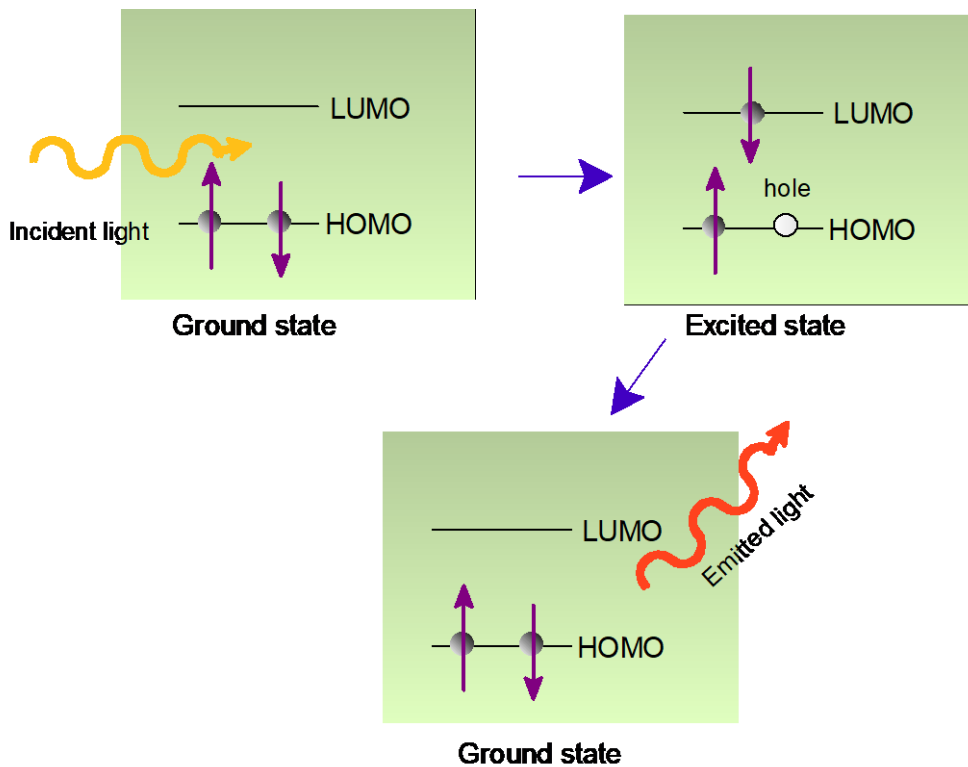
Figure 1.6 : Schematic of photoluminescence.

1.3.2 Electroluminescence

EL can be defined as the light generated by the application of electric field to the material. In order for this to happen, the electrons that reach the highest energy level as a result of excitation through various mechanisms must relax to the lower energy state. Inorganic semiconductors were used in light-emitting diodes before the organic materials were considered to be materials.

Its first examples were given to editors of the Electricity World on a note more than 100 years ago [4]. A yellowish light was observed when an electric field was applied across the crystal of a carborundum (silicon carbide). Unfortunately this discovery did not go behind. And then in the middle of the 1920s the trials started to work on them [50].

When an electric field is applied to inorganic light emitting diodes, charges are injected into the electrons; and thus the charge flows through the anode into the cathode. The semiconductor material forms a photon by the combination of counter charges. This light is defined as the recombination mechanism of formation [51].

1.3.2.1 Organic Electroluminescence

Organic EL is the phenomenon of light emission after the application of an electric field to organic compounds. With the applied electric field, the electrons in the cathodes pass to LUMO, and electrons pass from to anode. Thus, when radical anions (negatively charged) are formed on the LUMO, radical cations (positively charged) are formed on the HOMO (Figure 1.7).
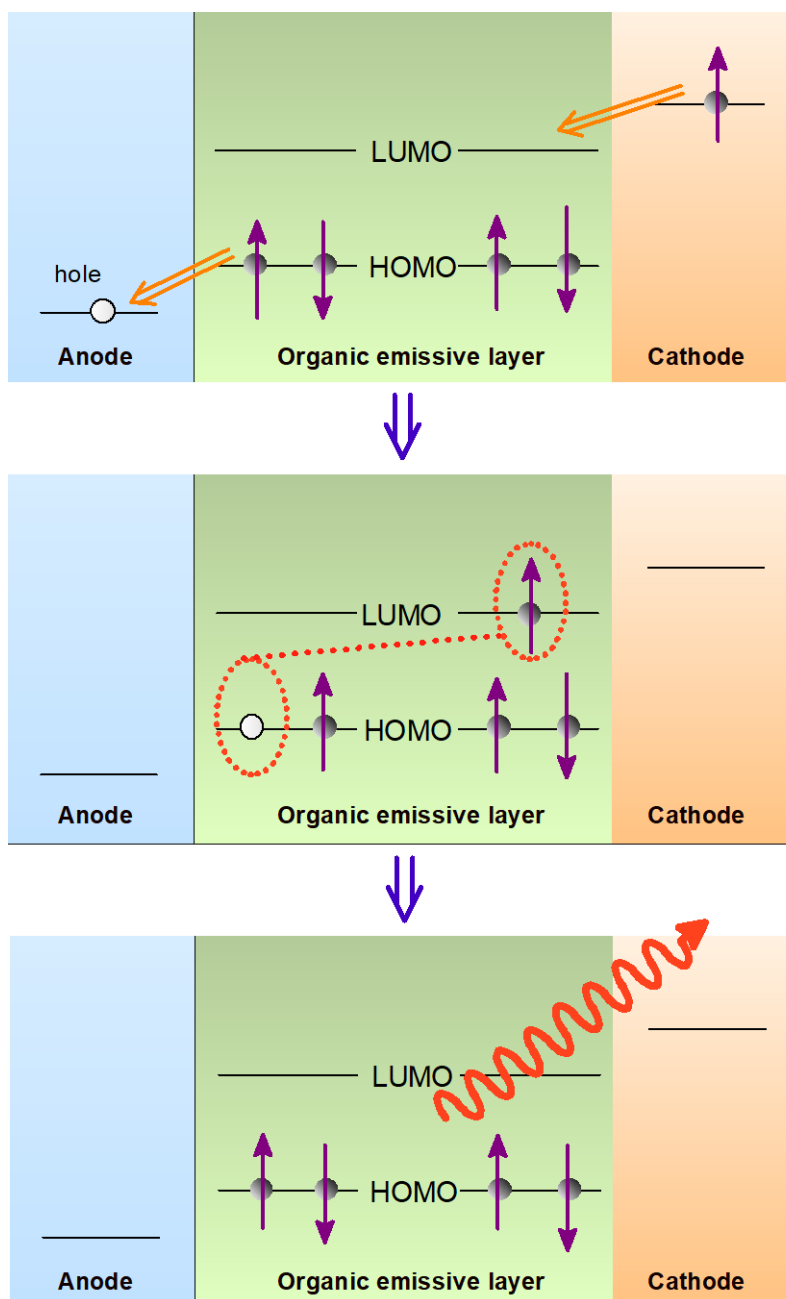
Figure 1.7 : Schematic of organic electroluminescence.

These charges change their positions through a hopping mechanism towards the organic material. If the charges are incorporated in the emission material, the molecular state can become excited sate. The state in which these exciton pairs occur is the excited state. They can decay to the ground state by emitting photons. The schematic demonstration of exciton formation is also given in Figure 1.8.
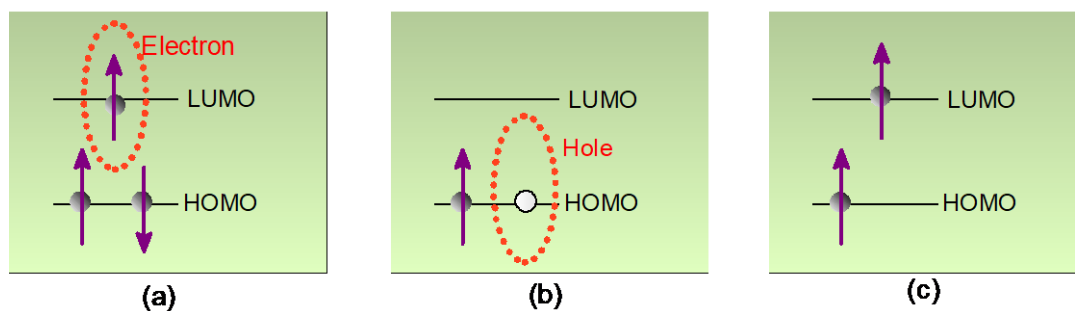
Figure 1.8 : Formation of exciton; (a) electron, (b) hole (c) excited state.

The total of spin moments, of the exciton pairs can be 0 or 1. If the spin moment of the exciton pairs is 0, then there is one possible state, as the spin magnetic moment can be only zero, and this state is called singlet state. If the spin moment of the exciton pairs is 1, the spin magnetic moment may be in three different states of 1, 0, -1, so this is called triplet state. In this system, which has a total of 4 states, each can create an equal situation, possibly creating a singlet or triplet exitons with a probability of 25% and 75%, respectively. This 1:3 ratio has been experimentally proven [52], but it has been reported that this ratio in the polymer material is slightly higher than the singlet state [53].

Electron transition from singlet excitation state to ground state (HOMO) is relatively fast and easy, and consequence of this, the photon emission is called as fluorescence. On the other hand electron transition from triplet excitation state to ground state are relatively slow, and consequence of this, the photon emission is called as phosphorescence. In fluorescence, the electron decay is allowed according to the Pauli Exclusion Principle. However, in phosphorescence electron decay from the triplet exciton to the ground state is forbidden. Due to this forbidden nature of phosphorescence, fluorescence occurs faster. At the same time, this causes the lifetime of the phosphorescence event to be longer. Thus, the probability of the phosphorescence is very low and for most materials this does not occur very often. Because of the reduced repulsion of the electrons, the energy of a singlet exciton is

higher than the energy of a triplet exciton. In order to allow the phosphorescence emission, excited electron will decay from a mixing of singlet and triplet states to the lower triplet state. As a result the triplet state with partial singlet character make possible electron to decay to the ground state. This process called as intersystem crossing (ISC). In phosphorescence, photon emission is red shifted compared to fluorescence. Because energy gap between excited and ground state in phosphorescence is lower so wavelength of emitted photon is longer.

Phosphorescent materials are suitable for OLED applications, because they emit light from triplet excitons and have high lifetime that cause high efficiencies and color purity. Phosphorescent materials are usually dispersed within the charge transport layer in OLEDs. This phosphorescent material placed in the charge transport layer is called as the guest and hence the charge transport layer is also called as the host. Efficient exciton transmission can take place between the host and the guest material when the absorption spectrum of the guest overlaps the emission spectrum of the host. In OLEDs, in order to obtain emission only in the emissive layer, efficient singlet and triplet exciton transfer should occur between host and guest. The singlet exciton transfer between host and guest can be explained by Forster transfer. If this transfer occurs by electron exchange between the host and the guest, the triplet can be transferred into the excitons as the total spin is preserved. When Dexter transmissions occur at short distances, Forster transfer takes place at large distances (Figure 1.9).
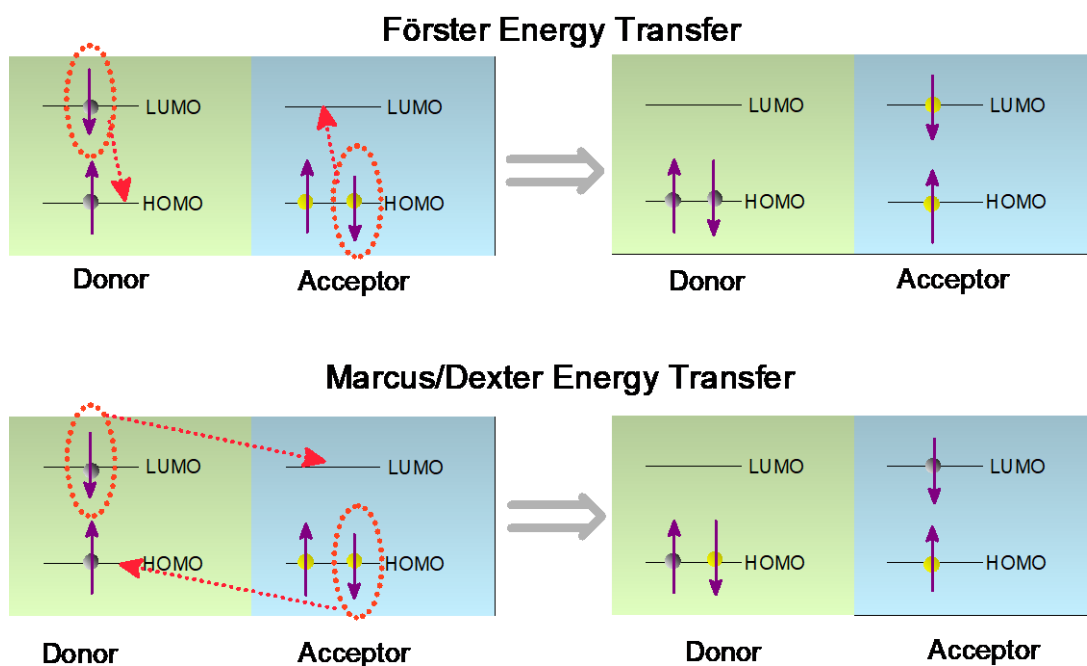
Figure 1.9: Schematic of Forster energy transfer and Marcus/Dexter energy transfer.

1.4   Light Emitting Materials for OLEDs

In OLEDs, the luminescence occurs as a consequence of exciton decay. The singlet and triplet excitons exist in the luminescence. Approximately, three triplet excitons are created corresponding to each singlet exciton. At room temperature, singlet excitons can decay radiatively while triplet excitons cannot. The luminescence processes are shown in Figure 1.10 by Jablonski diagram. The ground, first excited and second excited singlet electronic states are denoted by S_0, S_1 and S_2, respectively. The triplet excited state is also denoted by T_1. The molecule in the ground state can be excited to the first (S_1) or second (S_2) excited state by absorption of energy. The molecule excited to the energy state S_2 relaxes mostly to S_1 state by internal conversion. The molecule in first excited state S_1 can decay directly to the ground energy state S_0 and thus form fluorescence emission. Also the molecule at S_1 state may decay to the T_1 state by intersystem crossing (ISC) and produce phosphorescence emission while decaying from T_1 to S_0 ground state.
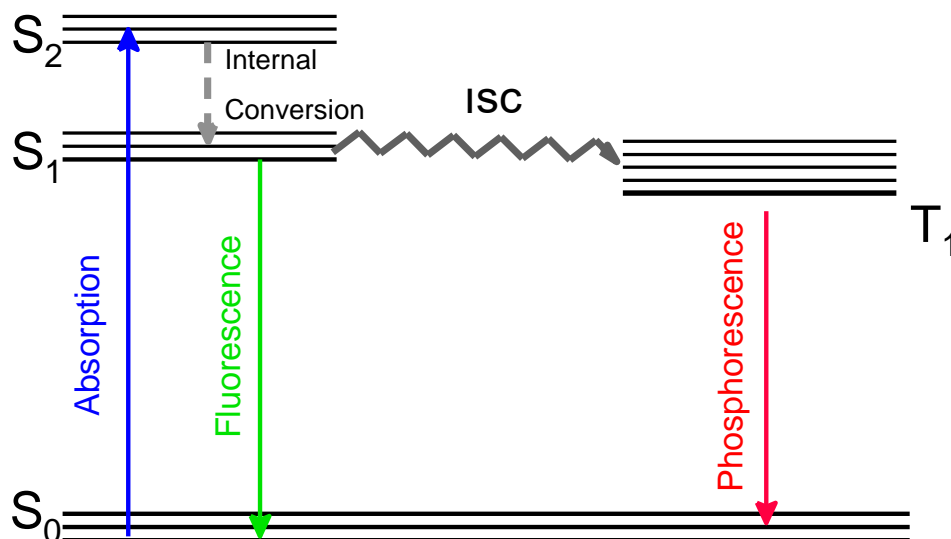
Figure 1.10: Jablonski diagram.

Lifetime of fluorescence, in which singlet exciton decay occur, is on the order of sub-nano-seconds, while lifetime of phosphorescence, in which triplet exciton decay occur, is on the order of 10 - 100 μs [54, 55]. Because of their long lifetimes, triplet excitons show tendency to overcome non-radiative decay, quench emission, deactivated process. In the first organic light emitting material studies, generally fluorescence materials were used due to the forbidden radiative decay nature of triplet excitons of phosphorescence materials. However, phosphorescent materials that radiate at room temperature have been obtained by adding heavy transition metals (Pt, Ru, Ir, Re and Os) to the molecular structure. These heavy metals lead to a mixture of singlet and triplet excitons which cause strong spin-orbit coupling in the molecule.

Light emitting organic molecules are divided into two main categories according to exciton mechanisms: fluorescent and phosphorescent materials.

1.4.1 Fluorescence Materials

Depending on the molecular weight, fluorescence materials are divided into two groups; small molecules and polymers. Small molecules such as Alq_3, coumarin, rubrene and their conjugated molecules and also some metal chelates such as barium chelates, beryllium, copper and zinc are commonly used in OLEDs as light emitting materials (Figure 1.11) [56].
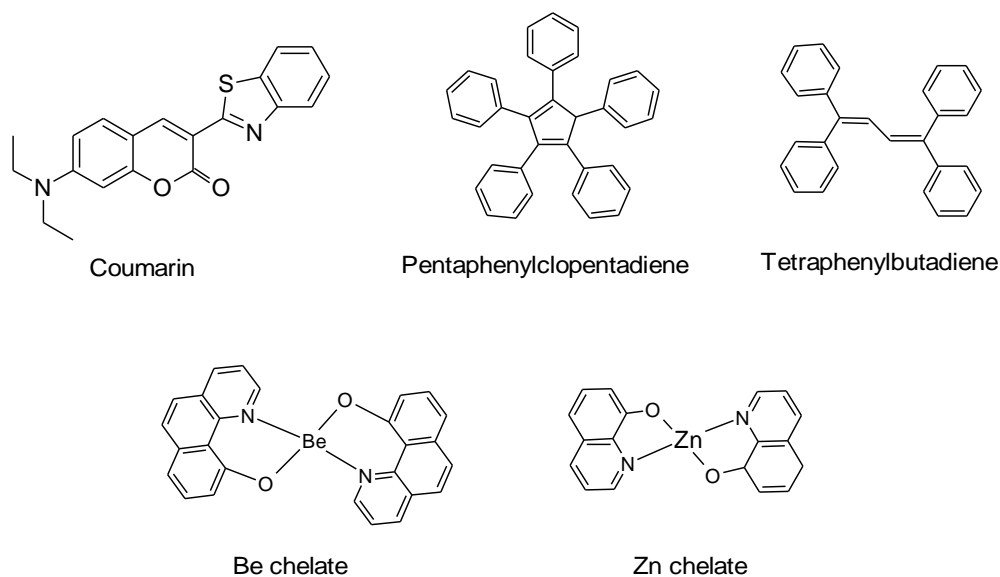
Figure 1.11: Fluorescent small molecules used in OLEDs.

These small molecular fluorescence materials can be easily synthesized and purified. Highly efficient and bright red, green and blue OLEDs can be obtained by using these small molecules. Recently EQE has reached 10%, in green emitting OLEDs with small molecules [57]. However, the low solubility of small molecules makes them unable to be used in solution processes. So that they can be coated only with vacuum vapor deposition processes of higher cost. Another disadvantage is that the small molecules can become easily crystallized, thus it reduce the device lifetime. Therefore, efforts are being made to increase their solubility and to prevent their easy crystallization by introducing some substituents and by designing three dimensional structural molecules.

The development of fluorescent polymers is similar to that of small molecules. Conjugated polymers exhibit semiconducting properties due to their p-orbitals delocalized along polymer chains. PPV that prepared from the precursor route was the first green light emitting polymer [8]. However, due to their insoluble, intractable and infusible properties, the production process is not easy. Thanks to the dialkoxy side chains of MEV-PPV (poly[2-methoxy-5-(2-ethylhexyloxy)-p-phenylenevinylene]) , a derivative of PPV, the solubility is higher but the light emission is red shifted [58, 59]. In fact, adding the substituents to the polymers do not only increase the solubility but also affect electronic properties such as band gap electron affinity and ionization potential. By synthesizing PPV and its derivatives, red green and blue emissions could be obtained. Polythiophene (PT) and its derivatives have also been synthesized as a

newer polymer capable of emitting red green and blue light [60, 61]. As red light emitting polymers, regioregular poly-(3-hexylthiophene) (P3HT) and MEH-PPV have been widely used in optoelectronic applications because of their high charge carrier mobility and uniform thin film formation [62, 63]. Although blue emissions were obtained from PPV and PT derivatives, their OLED performances were not sufficient for commercial display applications. Short conjugate segments and therefore large HOMO-LUMO energy vacancies are required to obtain blue light emitting fluorescence polymers. Poly(para-phenylene) (PPP) [64, 65] and polyfluorene (PF) [59, 66] and their derivatives can be given as examples of these polymers emitting bright and high-efficiency blue light (Figure 1.12).
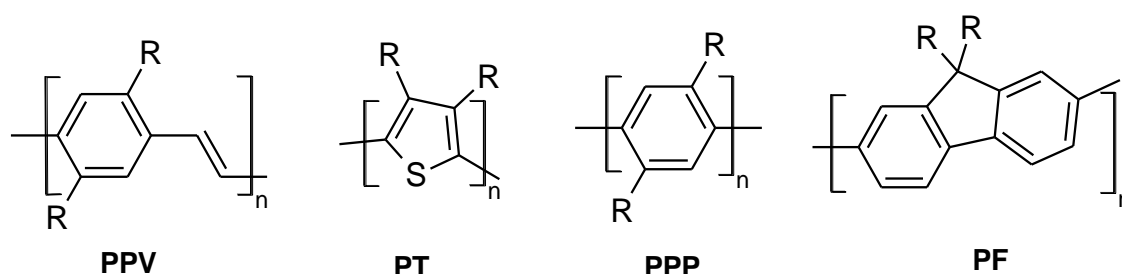
Figure 1.12: Structures of conjugated polymers.

However, OLED efficiency is still lower for materials that emit blue light when compared to molecules that emit light in other colors. As a result, blue light emitting materials in OLED production are the most challenging materials to synthesize and to design a device in terms of efficiency, brightness and color purity. In addition to the conjugated homopolymers mentioned above, conjugated copolymers such as fluorene-thiophene and fluorene-carbazole have been also developed by optimizing their properties and adjusting the band gaps [67, 68]. These copolymers have begun to be preferred due to their superior properties such as solubility, color tenability, charge mobility and high regioselectivity in coupling reactions. These properties considerably vary according to the nature and regularity of the side chains of the copolymers.

The properties of the polymers vary considerably with the exchange of substituents and regioregularities. This provides flexibility according to the area of use of the polymers. Polymers appear to be more advantageous because they can be processed more easily than small molecules. In addition, the polymer structure also provides

information about the efficiency of the material in general. However, since small molecules can be produced more pure than polymers they may be preferred because of their device performance and lifetime.

Another two factors that affect device performance are also mentioned; the excimer and the quenching center in the materials. The excimers, which can be formed when the backbones of neighboring chains are closely packed, broaden the emission spectrum and cause red shift. The quenching sites, which are the defects in polymers, can act as charge carrier traps [69]. In summary, in order to increase the efficiency of OLEDs produced using polymers, main effective ways are improving the purity, suppressing the close packing and reducing defects in polymers.

1.4.2 Phosphorescence Materials

Triplet radiation is different from single excitons due to spin inhibition and low efficiency at room temperature. The existence of transition heavy metal atoms in the cyclometalated complexes offers a strong spin-orbit interaction that leads to inter-system transitions, which cause radiation decay of these triple excitons [70]. Complexes of rare earth metal complexes (Eu, Tb) and transition heavy metals (Pt, Ru, Ir, Re and Os) containing the appropriate ligand have carried out high efficient phosphorescence. Comprehensive photophysicsal investigations of these cyclometalated complexes has shown that the luminescence takes place by the stimulation of ligand charge transfer (^{3}MLCT) from the lowest triplet state of the metal. Since phosphorescent materials can harvest both singlet and triplet states, all excited states contribute to light emission, so the theoretical internal quantum yield of these materials can reach 100%. Compared to single excitons lifetime, triplet excitons have a longer lifetime. In recent years, the interest in OLEDs made with phosphorescent materials has increased due to the high external quantum efficiency. In these studies, external quantum yields of phosphorescence materials can be observed up to 20%. The productivity of the devices has been steadily improving.

1.4.2.1 Transitional Metal Complexes

The material obtained for the first time as a phosphorescent material has been a europium based complex with red emission and EQE of 1.4% [71]. Five years later, the porphyrin complex, platinum octaethylporphyrin (PtOEP) material, which emits deeper red light, has been developed. The EQE of the devices with PtOEP-based

complexes was increased to 4 % by using Alq$_3$ as host material and to 5.6 % by using CBP as host material [72, 73]. Subsequently, phosphorescent materials were obtained using different transition metals such as Ir, Ru, Pt, Eu and Os [74-77]. Examples of these cyclometalled complexes used in OLEDs are given in Figure 1.13.
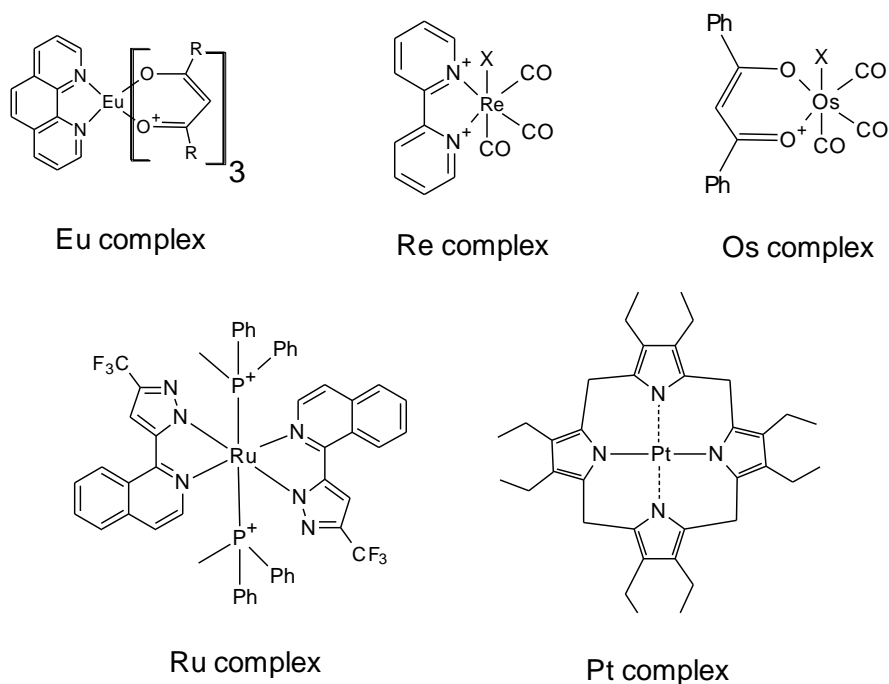
Figure 1.13: Phosphorescence cyclometalated complexes for OLEDs.

In these materials, metals are effective as light-transferring regions. By changing the ligands in these phosphorescence materials, the color of the emitted light, the solubility of the material and the exciton lifetime can be adjusted. Most of the phosphorescence complexes can only emit orange or red light emission while the Ir complexes can be produced in such a way that they can emit any color by modifying their ligand structures. Because the relationship of ligand structure and emission color is more sensitive in Ir complexes.

1.5 Iridium Complexes and Their Advantages

Among the organometallic complexes based on heavy transition elements (Pt, Eu, Os, Re, Ru, Ir) with phosphorescent properties, Ir-based ones are more widely used due to some superior properties. Compared to other organometallic complexes, Ir-based complexes have higher efficiency, more flexible color adjustability, more robust nature and reversible electrochemistry. So far, Ir complexes have been produced as

phosphorescent materials with the best efficiency. Iridium complexes used in OLEDs have +3 oxidation state. In OLEDs fabricated by using iridium complexes, luminescence is emitted from a triple MLCT state or ligand bound (π-π *) excited state [78]. The ligands bound to the metal center are generally derivatives coordinated to form an Ir-N and Ir-C bond. Iridium complexes are sensitive to ligand structures, and cyclometalating and ancillary ligands can be arbitrarily selected. Thus, the desired photophysical and electrochemical properties can be obtained by changing the ligand of complex. By modifying the ligand structures of the Ir complexes, the wavelength of the emission light can be adjusted to obtain the entire spectrum in the visible region. The high efficiency of the Ir complexes is due to their short exciton lifetime (1-14 μs) [79].

Ir complexes are classified as small molecules, dendrimers and polymers depending on the ligand structure they contain. In terms of ease of synthesis and color adjustability, a considerable amount of work has been done in the development of small molecules in Ir complexes. Facial tris(2-phenylpyridine) iridium complex [Ir(ppy)3], bis[2-[2'-benzo(4,5-a)thienyl]pyridinato-N,C3'] iridium(acetylacetonate) [(btp)2Ir(acac)] and bis[(4,6-difluorophenyl)-pyridinato-N,C2'] (picolinate)iridium (FIrpic) are the most well-known of the small molecules. The structures shown in Figure 1.14 emit green, red and blue light with high efficiency.

Ir(ppy)$_3$ (btp)$_2$Ir(acac)   FIrplc
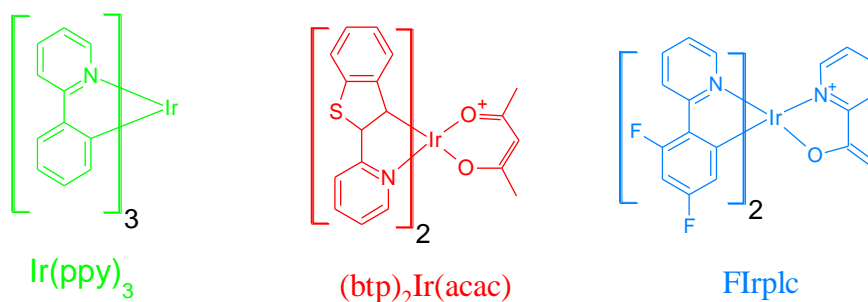
Figure 1.14 : Structure of green, red, and blue emitting Ir complexes.

After it was reported in 1999, the homoleptic Ir complex fac-Ir(ppy) 3 has been highly researched in green light material and device efficiency has been continuously improved. [80, 81]. Due to its simple structure and easy synthesis, numerous Ir(ppy) 3 derivative materials have been synthesized. In one of these examples, complexes emitting blue light were obtained by adding electron withdrawing groups such as fluoride onto the ligand [44].

In 2001, the first blue emissive Ir complex FIrpic was reported by Thompson and Forrest [73]. The device configuration was such that; ITO/CuPc(10nm)/NPB(30 nm)/CBP:6 wt% FIrpic(30nm)/BAlq(30nm)/LiF(1nm)/Al(100nm). With this configuration, the EQE of the blue emitting FIrpic complex reached to 5.7%. In 2003, by using host material (N,N'-dicarbazolyl-3,5-benzene, mCP) in the FIrpic emiting layer, EQE was obtained as 7.5% [82]. Again in 2003, deep blue emission with (0.16, 0.26) CIE coordinates and 11.6% EQE was reached by using material bis(4',6'-difluorophenylpyridinato)tetrakis(1-pyrazolyl)borate (FIr$_6$) as guest and silane based wide energy gap materials as host [83].

1.6   Discovery of LECs

The light emitting electrochemical cell (LEC) which consists of only an emissive layer positioned between two electrodes in a "sandwich structure" was firstly reported in 1995 [84]. In this first LEC, they used a semiconducting polymer, an ion-conducting polymer and an inorganic salt, sandwiched between two electrodes. In addition to these polymer-based LECs, small cationic complex based LECs were also produced. In these LECs, iTMC were used as emissive materials [85, 86]. The first LEC based on iTMC was produced by using ionic iridium (III) complexes in 2004 [87]. iTMC based LECs ensure simpler device structure than polymer based LECs. Because iTMC LECs do not require additional inorganic salts such as in polymer-based LECs. iTMC based LECs ensure simpler device structure than polymer based LECs. Further, the iTMC meets all requirements for operation of the device such as charge injection, charge transfer and emissive recombination. iTMC based LECs are simpler than other OLED structures because they contain only a single active layer (Figure 1.15).
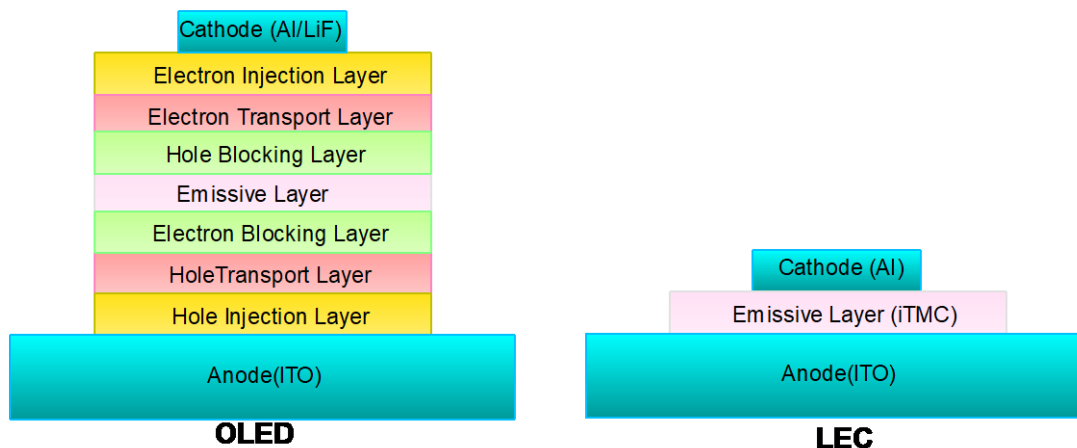
Figure 1.15 : Comparison of an OLED structure and a LEC structure.

In the LECs, ITO is used as the anode material and positive charges or holes are injected into the HOMO of iTMC. As cathode material, aluminum or other conductive metals (e.g. gold, silver) are used and electrons or negative charges are injected into LUMO of iTMC. With the applied current, hole and electrons injected through the anode and cathode, respectively. Electrons and holes meet at the emission floor, creating an exciton that will cause a radiation recombination and the formation of light.

There are many uses of LECs in lighting applications. In addition to the easy production mentioned above, low-energy operation and high-efficiency equipment are possible to produce.

In addition, iTMCs allow spin coating and solution processing methods and do not require solid encapsulation due to their low sensitivity to air.

When a current is applied to a LEC, the charges coming from the anode and the electrons coming from the cathode are injected into the iTMC layer and transported towards the electrodes by hopping. iTMC can recombine to produce emissions in a specific area corresponding to energy gaps. The counter ions (e.g. [PF$_6$]) which have mobility in the film are very important for the LEC operations. Under the applied current, this ionic salt e.g. [Ir(ppy)$_2$(bpy)][PF$_6$] redistributes and helps in the injection of electronic carriers. This arrangement, which facilitates electronic charge injection, makes the working function of the electrons independent. Thus, unlike OLEDs, electrodes that are unaffected by air are used. e.g. gold, silver or aluminum.

Working principle of iTMC-based LECs are still under discussion although extensive research efforts in this field. For understanding of the electric field distribution in an

21

operating LEC device, there are two different models [84, 86, 88]. Due to phosphorescent nature of iTMC materials, they potentially emit light with high efficiencies and their synthesis and purification processes are relatively easy [89]

1.7   Tuning the Emission Maximum

Density functional theory (DFT) calculations of the first iridium(III) LEC [90], which was the yellow emitting device, has given the information about the localization of the HOMO and LUMO of the iridium(III) complex [91]. According to these DFT studies, it has been shown that HOMO generally occurs on cyclometalating C^N ligands and Ir, while LUMO is on ancillary N^N ligands (see Figure 1.16 and Figure 1.17). In order to change the emission maximum of an iridium(III) complex, these are the main parameters.

It is possible to adjust both LUMO and HOMO energy levels to change the band gap between the HOMO and LUMO energy levels and thus it is obtained the desired color emission. If it is desired to increase the energy band gap (i.e. to decrease the wave length) which must be observed as blue-shift in the absorption spectrum, the HOMO energy level is reduced (stabilized) or the LUMO energy level is increased (destabilized) or both of them can occur. If it is desired to reduce the energy band gap (i.e. to increase the wave length) which must be observed as a red-shift), the opposite is done. To reduce (to stabilize) the HOMO energy level, electron-withdrawing substituents such as F or CF_3 are widely used. To increase (to destabilize) the LUMO energy level, electron-donating substituents such as $N(CH_3)_2$ are attached to the ancillary ligand [87, 92, 93].

In order to shift the wavelength of the light to red emission, i.e. to reduce the energy band gap, electron-withdrawing groups are added to the ancillary ligand providing the reduction (stabilization) of the LUMO energy level or the ligand conjugation length is increased   [94, 95]. To obtain white emission, red and blue emitting iridium(III) complexes can be mixed and thin   [96].
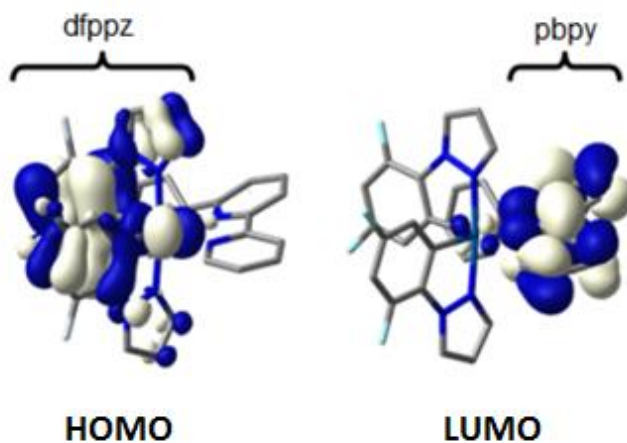
Figure 1.16 : DFT calculations for an Ir complex of HOMO and LUMO of dfppz and pbpy ligands, respectively [97].
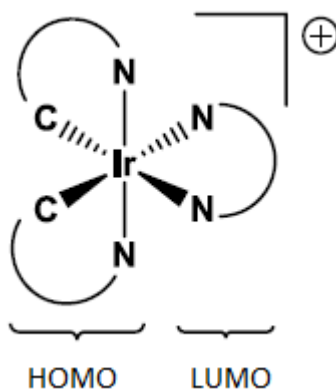
Figure 1.17 : Localization of HOMO and LUMO on an ionic Ir complex [97].

1.8 Coating Techniques

1.8.1 Spin Coating

The most common process used in organic light emitting devices that do not require a hole transport layer or an electron transport layer is spin-coating. The spin-coating method is illustrated schematically in Figure 1.18. With this method, the material, which is solved in a suitable solvent with an appropriate concentration, is dropped on a substrate to be coated. Then a suitable spinning speed is chosen to homogeneously distribute to the surface of the substrate and it is coated on the surface. The film thickness is adjusted by changing both the spinning speed and the concentration of the

material [98]. The spin-coater can be used in a glovebox to obtain more controlled conditions. Besides being easy to spin-coat, another advantage is that small quantity of materials can be coated that is ideal for researches. However, it is not suitable for mass production because almost 90% of the material is wasted during coating. Furthermore, in a multi-layered coating while covering the top layer, the solvent adversely affects the lower layer and consequently negatively affects the performance of the device. Therefore, in the construction of a multilayered device, it may be noted that two hydrophobic materials do not come over or that two hydrophilic materials do not come over. That is, for each layer it is tried to prevent the dissolving of the layer which is coated previously.

(a) Deposition   (b) Spinning   (c) Drying
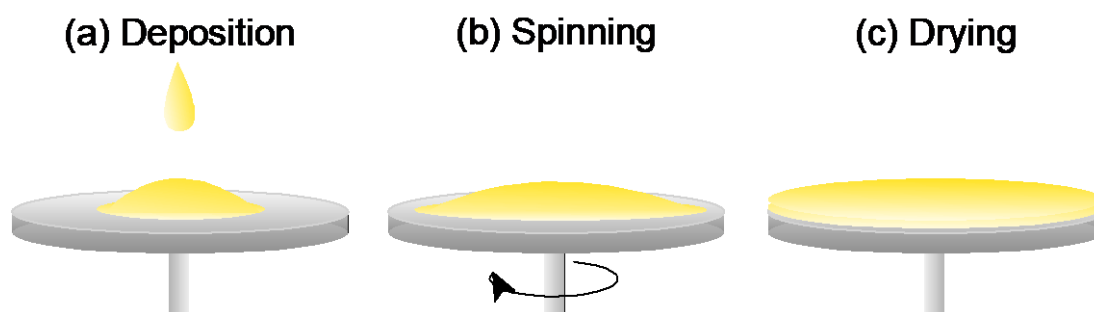
Figure 1.18: Schematic illustration of spin-coating (a) first position of ink on substrate (b) ink is distributed on substrate when spinning (c) at the end ink is coated on substrate homogeneously.

1.8.2 Thermal Evaporation

For fabricating organic light-emitting devices the most effective method is high vacuum thermal evaporation, because this method provide devices with high efficiency and lifetime. With this method, both metal and organic materials can be coated in the form of thin film. The thermal evaporation method does not damage the previous layer because it does not contain solvent and with this method, the thickness is distributed more homogeneously on the surface.

A schematic illustration of the thermal evaporation method is given in Figure 1.19. The heated source material is evaporated and condensate onto the cold sample surface. Thus, the coating process is carried out. While the metal materials are being processed, evaporation takes place at high temperatures, the tungsten crucibles are exposed to

thermal stress and break after about ten uses. When coating with thermal evaporation method, attention should be paid to the temperature and coating speed, otherwise organic film may be damaged [99]. Therefore, this method is disadvantage in terms of time, power and cost.
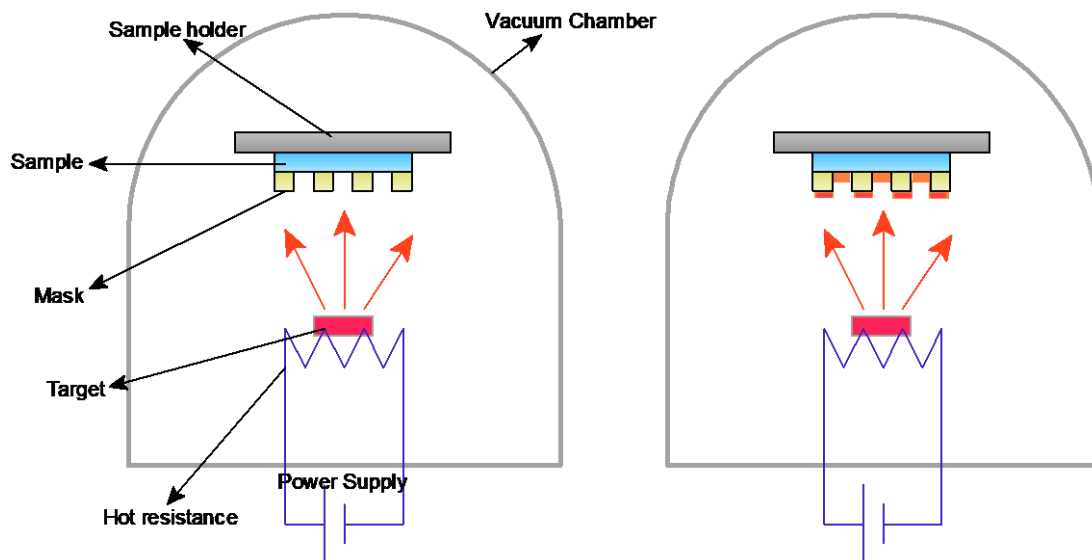
Figure 1.19 : Schematic illustration of thermal evaporation.

1.9 Objectives and Significance

The emission color can be adjusted by adding electron donating molecules onto the Spiro linked ligands of the Ir complexes. Because the color of the emitted light and the band gap energy depends on the chemical structure of the ligands. Thus, in this work, novel iridium complexes which emit light at different wavelengths are synthesized with Spiro-based ligands by electron-donating moieties to the molecular structure.

With novel small molecular iridium complexes containing Spiro-based ligands are designed and synthesized in this thesis, the yield and lifetime of the OLEDs can be increased with novel complexes. The Ir complexes synthesized here provide a useful reference for researchers working on OLEDs.

2. DEVELOPMENT OF IRIDIUM COMPLEXES FOR OLEDS

2.1 Molecular Design

In OLED devices fabricated using small molecules, thin film crystallization can cause excimer and exciplex formation, which adversely affects device efficiency. Small molecules are used to eliminate this problem. Concentration quenching is an option that reduces the efficiency of the device during high currents. The reports show that concentration can suppress damping due to the close stacking of volumetric molecules [100]. In order to solve the above-mentioned problems, it is a good idea to prefer Spiro connected structures. Spiro-type structures are closely aligned due to the three-dimensional molecular geometry and provide good film-forming ability, thus increasing luminescence efficiency in solid state [101, 102]. In addition to all these, thanks to their excellent resolution, their thermal storage capability increases compared to other small molecules. (Figure 2.1). In addition, the donor on the ligands will be replaced with the correct molecules to change the wavelength. Thus, small-molecule Ir complexes based on spirobifluorene ligands are designed to modify structure, increase productivity and adjust light emission.

Figure 2.1 : 3D structure of spirobifluorene.

Spirobifluorene-based ligand structures are shown in Figure 2.2 and the bis-cyclometallated iridium complexes formed from these ligands are shown in Figure 2.3.
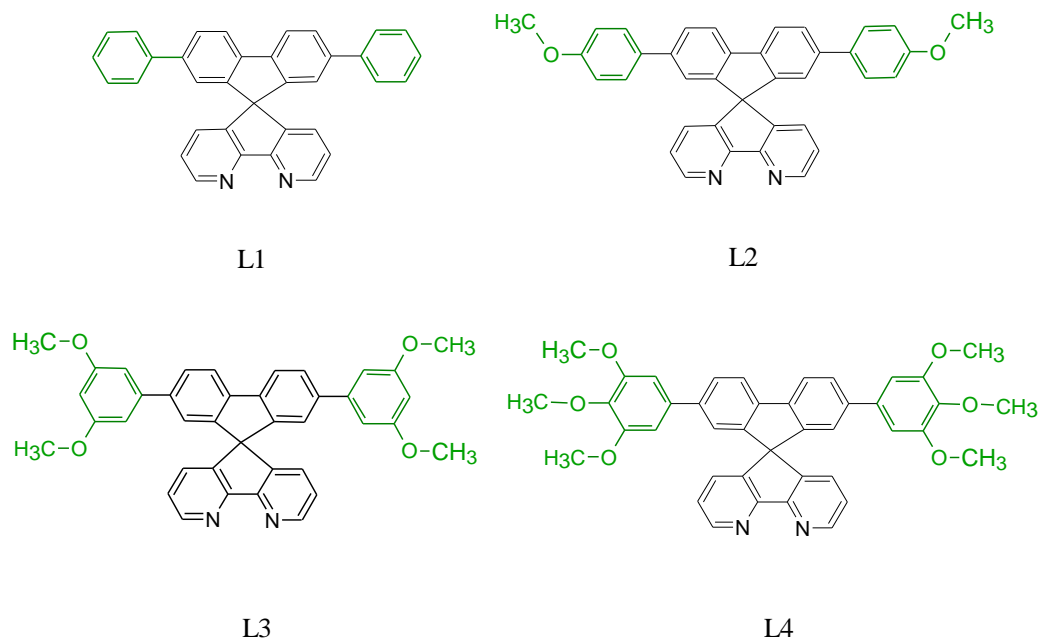

Figure 2.2 : Structures of spirobifluorene based ligands.
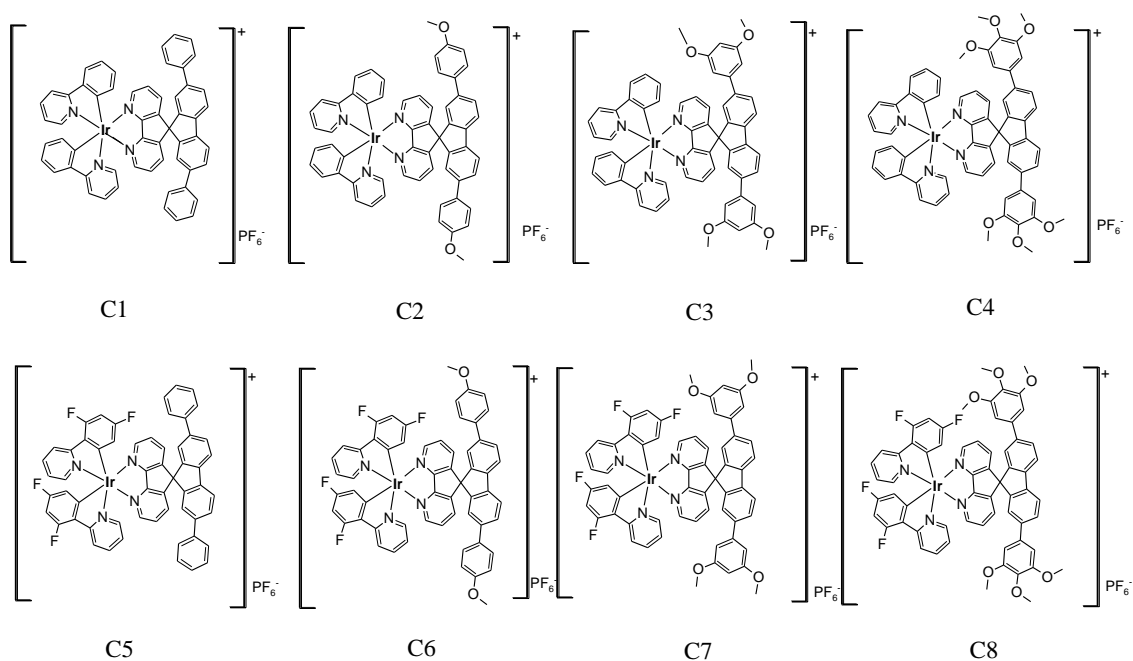

Figure 2.3 : Structures of bis-cyclometalated Ir complexes.

All the starting materials were purchased from, Lumtec, Aldrich, Acros and TCI. Catalyst ([1,1′-bis(diphenylphosphino)ferrocene]dichloropalladium(II), Pd(dppf)Cl$_2$) acetone, tetrahydrofuran (THF), ethylene glycol (1,2-ethanediol), ammonium hexafluorophosphate (NH$_4$PF$_6$), dichloromethane and toluene were purchased from Sigma-Aldrich. Potassium carbonate was obtained from Riedel de Haen. [4-(Methoxycarbonyl)phenyl]boronic acid, benzene boronic acid, 4-methoxybenzeneboronic acid, 3,5-dimethoxybenzeneboronic acid, 3,4,5-trimethoxybenzeneboronic acid, 1,2-dimethoxy ethane (DME), and N,N-dimethylformamide (DMF) were purchased from Alfa-Aesar. 4,5-diaza-2',7'-dibromo-9,9'-spirofluorene, di-μ-chlorotetrakis[(2-pyridinyl-phenyl-KN)-KC]di-iridium and di-μ-chlorotetrakis[3,5-difluoro-2-(2-pyridinyl-KN)phenyl-KC]di-iridium were purchased from Lumtec. All the above chemicals were used without further purification. Anhydrous THF was distilled from sodium-benzophenone immediately prior to use.

^{1}H and ^{13}C NMR spectra were measured in acetonitrile-d$_3$ (CD$_3$CN) solution on a Bruker DPX NMR spectrometer (400 MHz) with tetramethylsilane (TMS) as the internal standard.

2.2   The Suzuki-Miyaura Cross-Coupling Reaction

The Suzuki-Miyaura coupling (Figure 2.4) is an organic reaction with the organohalidine and organoboran to obtain the product in the presence of a palladium catalyst and a weak base [103, 104]. In 2010, the Nobel Prize for Chemistry was awarded in partnership with Richard F. Heck, Ei-ichi Negishi and Akira Suzuki with 'Palladium-Catalyzed Cross-Coupling in Organic Synthesis'. The use of aryl bromides and iodides as aryl halides is preferred [105, 106]. Different coupling ratios of the aryl halides, which influence the strength of the Ar-X bond, make the oxidative addition step more difficult, Ar-I >Ar-Br >Ar-Cl [107, 108]. In the reaction mechanizm, a Pd(II) complex is formed by the oxidative addition of organohalidine to Pd(O). Then, in the presence of a hydroxide or alkoxide base, the R group becomes more nucleophilic by the formation of a borate resistance to the organo-boran while the halide in the palladium complex is replaced. Transmetallation with the borate then proceeds from where the R group in the palladium complex has taken up the halide anion in the complex. After the reductive elimination, the final product is obtained and

the catalyst is regenerated and the catalytic cycle can start again. The most commonly used base in these reactions is Na_2CO_3, but is generally ineffective when working with sterically demanding substrates. In our studies, K_2CO_3 as base was preferred and yielded.
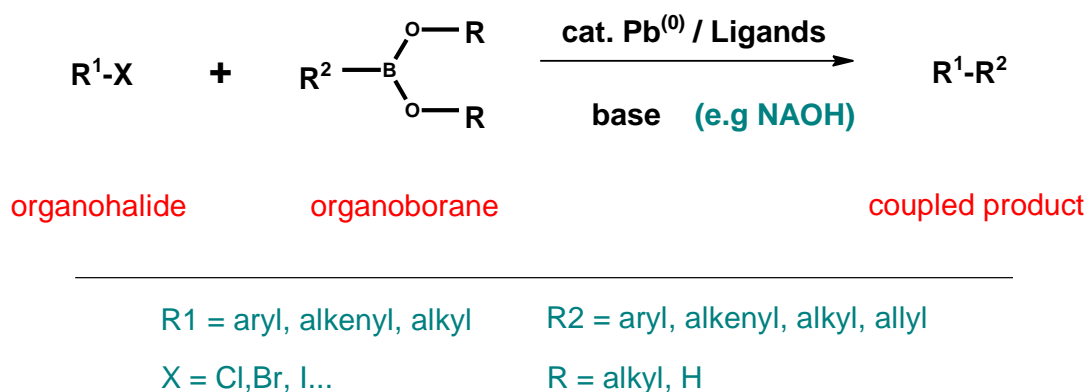
Figure 2.4 : Shematic representation of Suzuki cross-coupling reaction [103].

2.3 Synthesis of Materials

In this thesis, 4 ligands (L1, L2, L3, and L4) and 8 iridium complexes (C1, C2, C3, C4, C5, C6, C7, and C8) total 12 compounds were synthesized. The synthetic routes for all materials are given in Figure 2.5. Some of them were used in OLED fabrication. The names of these compounds are given below and the molecular structures are also shown.

- **L1** : (2',7'-Diphenylspiro(cyclopental(1,2-b')dipyridine-5,9-fluorene)

- **L2** : 2'7'-Bis(methoxyphenyl)spiro(cyclopental(2,3-b:5,4-b')dipyridine-5,9'-fluorene)

- **L3** : 2'7'-Bis(3,5-dimethoxyphenyl)spiro(cyclopental(1,2-b:5,4-b')dipyridine-5,9'-fluorene)

- **L4** : 2'7'-Bis(3,4,5-trimethoxyphenyl)spiro(cyclopental(1,2-b:5,4-b') dipyridine-5,9'-fluorene)

- **C1** :[2',7'-Diphenylspiro(cyclopental(1,2-b')dipyridine-5,9-fluorene)-bis-(2-phenylpyridine-C2′,N)-iridium(III)]

- **C2** :[2'7'-Bis(methoxyphenyl)spiro(cyclopental(2,3-b:5,4-b')dipyridine-5,9'-fluorene)-bis-(2-phenylpyridine-C2′,N)-iridium(III)]

- **C3** :[2'7'-Bis(3,5-dimethoxyphenyl)spiro(cyclopental(1,2-b:5,4-b')dipyridine-5,9'-fluorene)-bis-(2-phenylpyridine-C2′,N)-iridium(III)]

- **C4** : [2'7'-Bis(3,4,5-trimethoxyphenyl)spiro(cyclopental(1,2-b:5,4-b')dipyridine-5,9'-fluorene)-bis-(2-phenylpyridine-C2′,N)-iridium(III)]

- **C5** :[2',7'-Biphenylspiro(cyclopental(1,2-b')dipyridine-5,9-fluorene) -bis-(2-(2′,4′-difluorophenyl)-pyridine-C6′,N)-iridium (III)]

- **C6** : [2'7'-Bis(methoxyphenyl)spiro(cyclopental(2,3-b:5,4-b')dipyridine-5,9'-fluorene)-bis-(2-(2′,4′-difluorophenyl)-pyridine-C6′,N)-iridium (III)]

- **C7** : [2',7'-Diphenylspiro(cyclopental(1,2-b')dipyridine-5,9-fluorene)-bis-(2-(2′,4′-difluorophenyl)-pyridine-C6′,N)-iridium (III)]

- **C8** : [2'7'-Bis(methoxyphenyl)spiro(cyclopental(2,3-b:5,4-b')dipyridine-5,9'-fluorene)-bis-(2-(2′,4′-difluorophenyl)-pyridine-C6′,N)-iridium (III)]
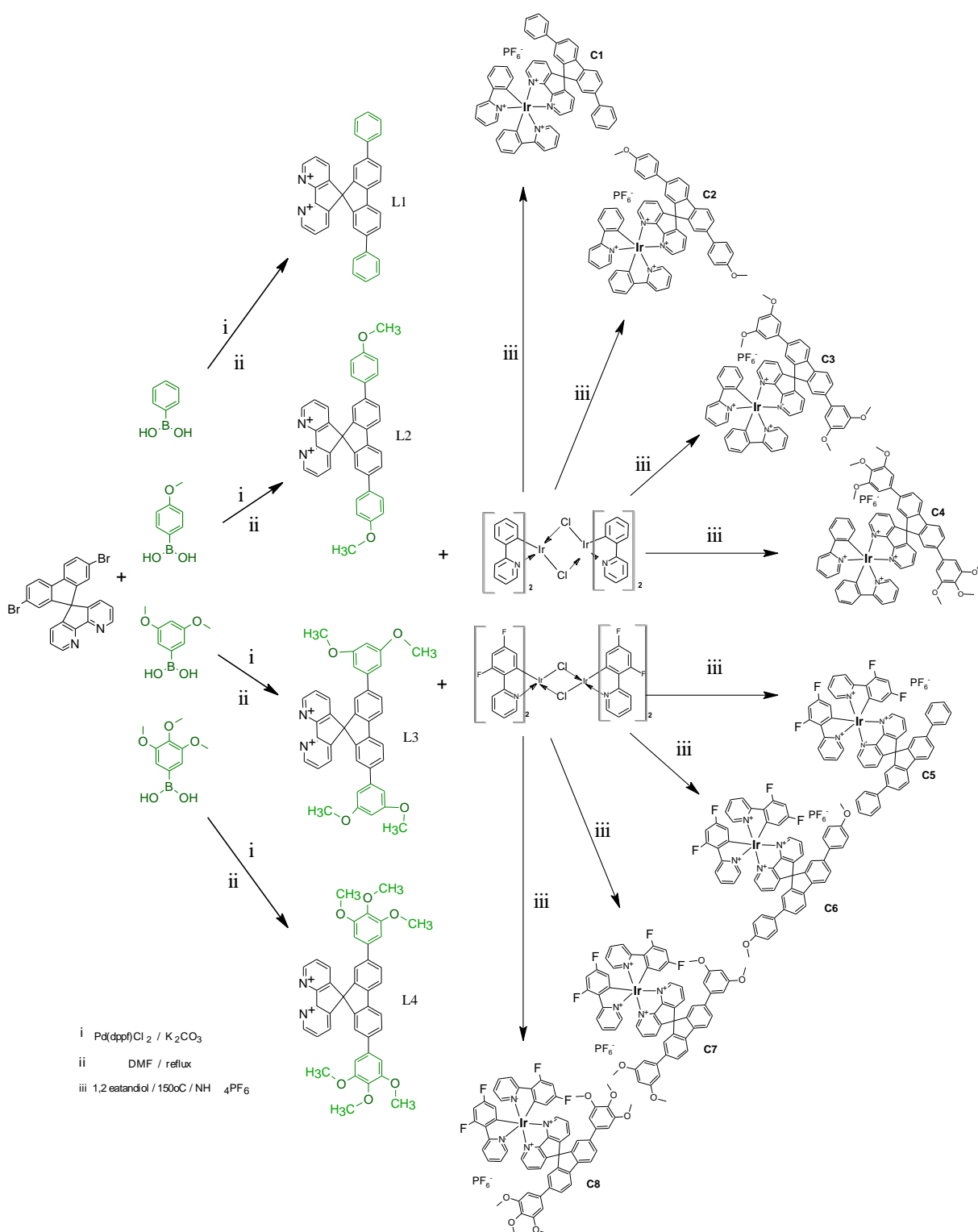
Figure 2.5 : Synthetic routes for all materials.

2.3.1 Experimental Details

2.3.2 Synthesis of Ligands

2.3.2.1 Synthesis of L1 (2',7'-diphenylspiro(cyclopental(1,2-b')dipyridine-5,9-fluorene))

The mixture of 4,5-diaza-2'7'-dibromo-9,9'-spirobifluorene (300 mg, 0,63 mmol) was disolved in DME and phenyl boronic acid (202mg, 1,51mmol), Pd(dppf)Cl$_2$ (52 mg, 0.063 mmol) was dissolved in DME and stirred 10 min. After that, catalyst was added in catalytic amount via stirring and base (1M K$_2$CO$_3$) was added. When the temperature reached boiling point solid base was added in two portion with spatula. Then, the complete solutions waste gassed for 30 min and refluxed for 16 h under argon atmosphere. Reaction mixture refluxed overnight and checked via thin-layer chromatography (TLC). The reaction was cooled to room temperature and then extracted with dichloromethane. The organic phase was washed with water and brine solution, dried over sodium sulfate. Finally organic solvent was evaporated and the crude product was purified by silica gel column chromatography (ethyl acetate: n-hexane 2:1). The synthetic route for L1 is summarized in Figure 2.6.

^{1}H NMR (DMSO, 400MHz): δ, 8.73 (s, 4H), 7.91-7.91 (d, 4H), 7.59-7.57 (d, 4H), 7.19-714 (m, 8H), 6.85 (d, 12H), 6.66-6.62 (d, 4H)

^{13}C NMR (DMSO, 400MHz): δ, 163.1, 162.6, 159.5, 151.9, 147.6, 140.7, 136.7, 132.3, 131.24, 129.9, 123.2, 122.5, 121.1, 115.8, 67.5, 61.3
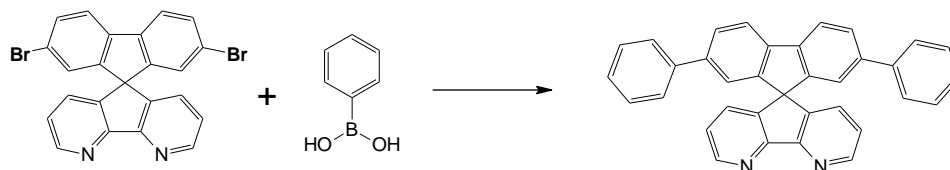

Figure 2.6: Synthetic route for L1.

2.3.2.2 Synthesis of L2 (2'7'-bis(methoxyphenyl)spiro(cyclopental(2,3-b:5,4-b')dipyridine-5,9'-fluorene))

Compound L2 was synthesized by the following procedure described above for L1 molecule, by mixing 4,5-diaza-2'7'-dibromo-9,9'-spirobifluorene (300 mg, 0.063 mmol) (3,5-dimethoxyphenyl) boronic acid (230 mg, 0,151 mmol), Pd(dppf)Cl$_2$ (52 mg, 0.063 mmol) was dissolved in DME. Finally, organic solvent was evaporated and the residue was purified by silica gel column chromatography (ethyl acetate: n-hexane 2:1). The synthetic route for L2 is summarized in Figure 2.7.

^{1}H NMR (DMSO, 400 MHz): δ, 8.87 (d, 2H), 7.95 (d 2H), 7.65 (d 2H), 7.38 (m 4H), 7.23 (d 2H), 7.22 (d 2H), 7.00 (m 4H), 6.9 (s 2H), 3.17 (s 6H)

^{13}C NMR (DMSO, 400 MHz): δ, 164.1, 161.6, 159.3, 150.9, 147.6, 143.9, 140.7, 136.7, 132.3, 131.24, 128.9, 124.2, 122.5, 121.1, 115.8, 68.5, 62.1
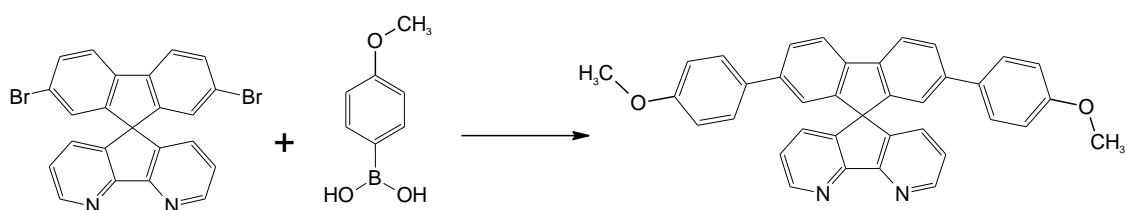

Figure 2.7: Synthetic route for L2.

2.3.2.3 Synthesis of L3 (2'7'-bis(3,5-dimethoxyphenyl)spiro(cyclopental(1,2-b:5,4-b')dipyridine-5,9'-fluorene))

Compound L3 was synthesized by the following procedure described above for L1 molecule, by mixing 4,5-diaza-2'7'-dibromo-9,9'-spirobifluorene (300 mg, 0,063 mmol) (3,5-dimethoxyphenyl) boronic acid (230mg, 1,151mmol), Pd(dppf)Cl$_2$ (52 mg, 0.063 mmol) was dissolved in DME. Finally, organic solvent was evaporated and the residue was purified by silica gel column chromatography (ethyl acetate: n-hexane 2:1). The synthetic route for L3 is summarized in Figure 2.8.

^{1}H NMR (DMSO, 400 MHz): δ, 8.79 (d, 2H), 7.93 (d 2H), 7.68 (d 2H), 7.22-7.16 (m 4H), 6.93 (d 2H), 6.54 (d 4H), 7.00 (m 4H), 6.39 (s 2H), 3.78 (s 12H)

^{13}C NMR (DMSO, 400 MHz): δ, 161.1, 159.0, 150.5, 147.2, 143.6, 142.6, 141.3, 140.9, 132.1, 127.7, 123.8, 122.4, 120.7, 105.3, 99.4, 61.75, 55.5
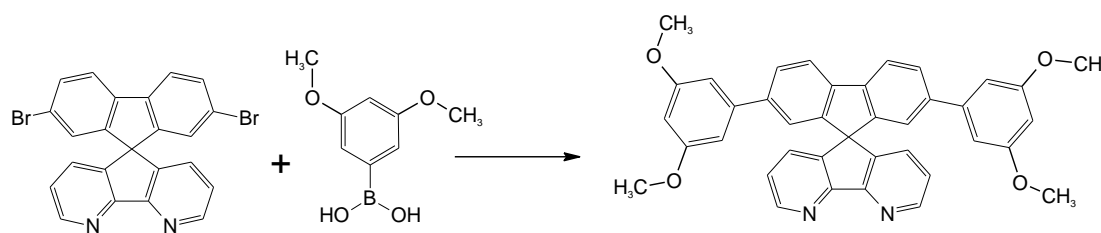

Figure 2.8: Synthetic route for L3.

2.3.2.4 Synthesis of L4 (2'7'-bis(3,4,5-trimethoxyphenyl)spiro(cyclopental(1,2-b:5,4-b')dipyridine-5,9'-fluorene))

Compound L4 was synthesized by the following procedure described above for L1 molecule, by mixing 4,5-diaza-2'7'-dibromo-9,9'-spirobifluorene (300 mg, 0,063 mmol) was dissolved in DME and (3,4,5-trimethoxyphenyl) boronic acid (230mg, 1,151mmol) Pd(dppf)Cl$_2$ (52 mg, 0.063 mmol) was dissolved in DME. Finally, organic solvent was evaporated and the residue was purified by silica gel column chromatography (Ethyl acetate: Hexane 2:1). The synthetic route for L4 is summarized in Figure 2.9.

^{1}H NMR (DMSO, 400 MHz): δ, 8.55-8.52 (d, 2H), 7.82-7.4(d 2H), 7.74-7.64 (m 4H), 7.52 (d, 2H) 7.36-7.20 (m 4H), 3.76 (s 6H), 3.59 (s, 12H)

^{13}C NMR (DMSO, 400 MHz): δ, 158.5, 152.9, 151.9, 151.4, 143.62, 139.8, 139.1, 138.27, 130.7, 127.8, 127.4, 127.3, 123.7, 120.6, 60.9, 56.17, 42.38
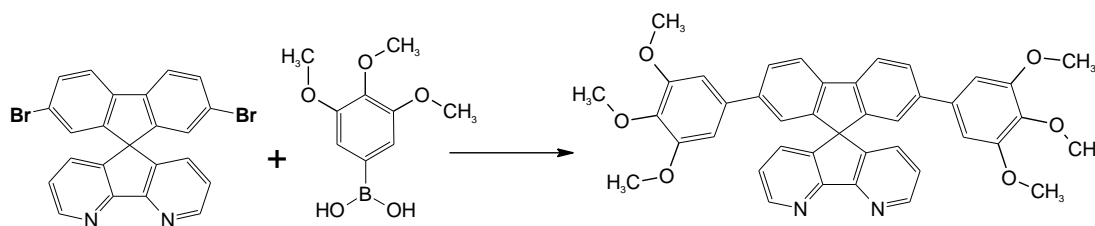

Figure 2.9: Synthetic route for L4.

2.3.3   Synthesis of Light Emitting IR-Based Complexes

Compounds C1-C8 were prepared following literature procedures [109].

2.3.3.1 Synthesis of C1 (2'7'-bis(3,4,5-trimethoxyphenyl)spiro(cyclopental(1,2-b:5,4-b')dipyridine-5,9'-fluorene))

A magnetically stirred suspension of L1 (50 mg, 0.106 mmol) and Di-µ chlorotetrakis[(2-pyridinyl-phenyl-KN)-KC]di-iridium (123 mg, 0.094 mmol) in 10 mL of ethylene glycol under nitrogen was heated to 150 °C. The mixture was maintained at 150 °C for 15 hours. The attached adduct gave a clear yellow solution. At the end of the reaction, the mixture was cooled to room temperature and then 100 mL of water was added. An excess of the bipyridine ligand was removed by two extractions with diethyl ether (40mL). The aqueous layer was again heated to 60-70 °C. NH_4PF_6 (1 g) in 10 mL of water was added and the chromophore PF_6 salt was precipitated. The suspension was then cooled to 5 °C, the yellow solid separated by filtration, dried and recrystallized from acetonitrile / ether by diffusion. The synthetic route for C1 is summarized in Figure 2.10.

1H NMR (ACN-d6, 400 MHz): δ, 8.15-8.07 (m, 6H), 7.95 (t, 2H), 7.85 (m, 4H), 7.76 (m, 2H), 7.54-7.49 (m,6H), 7.45-7.38 (m, 8H), 7.18-7.13 (t, 2H), 7.08-7.05 (t, 4H), 6.99-6.95 (m,2H), 6.46-6.43 (d, 2H)

^{13}C NMR (ACN-d6, 400 MHz): δ, 163.82, 162.12, 150.25, 148.76, 144.58, 143.28, 140.95, 140.07, 138.72, 134.45, 131.76, 130.04, 128.78, 124.57, 123.76, 122.76, 121.65, 119.75, 115.75, 115.78, 66.84
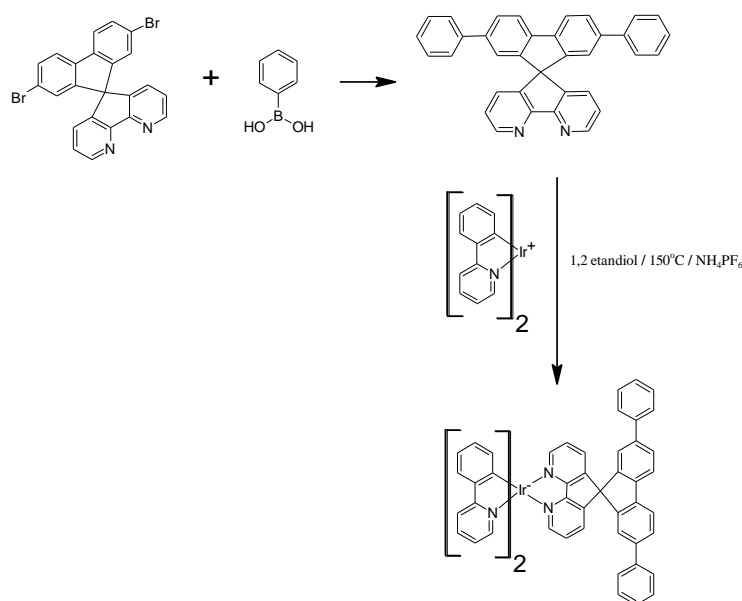

Figure 2.10: Synthetic route for C1.

2.3.3.2 Synthesis of C2 ([2'7'-bis(methoxyphenyl)spiro(cyclopental(2,3-b:5,4-b')dipyridine-5,9'-fluorene)-bis-(2-phenylpyridine-C2′,N)-iridium(III)])

Compound C2 was synthesized by the following procedure described above for C1 molecule, by mixing L2 (50 mg, 0.094 mmol) and Di-µ-chlorotetrakis[(2-pyridinyl-phenyl-KN)-KC]di-iridium (101 mg, 0.094 mmol). The suspension was then cooled to 5 °C, the yellow solid separated by filtration, dried and recrystallized from acetonitrile / ether by diffusion. The synthetic route for C2 is summarized in Figure 2.11.

^{1}H NMR (ACN-d6, 400 MHz): δ, 8.14-8.11 (d, 4H), 8.07 (d, 2H), 7.96 (m, 2H),7.84 (m,4H) 7.76 (m, 2H), 7.56-7.51 (m, 6H),7.43-7.39 (m, 2H), 7.22-7.16 (d, 6H), 7.08 (d, 4H), 6.99-6.97 (t, 2H), 6.43 (d,2H), 2.16 (s, 6H)

^{13}C NMR (ACN-d6, 400 MHz): δ, 168.12, 164.08, 161.62, 159.36, 150.94, 147.61, 143.92, 140.94, 140.70, 136.77, 132.78, 132.34, 131.24, 129.15, 128.90, 128.82, 127.80, 124.21, 122.58, 121.18, 116.11, 115.90, 68.50, 62.07
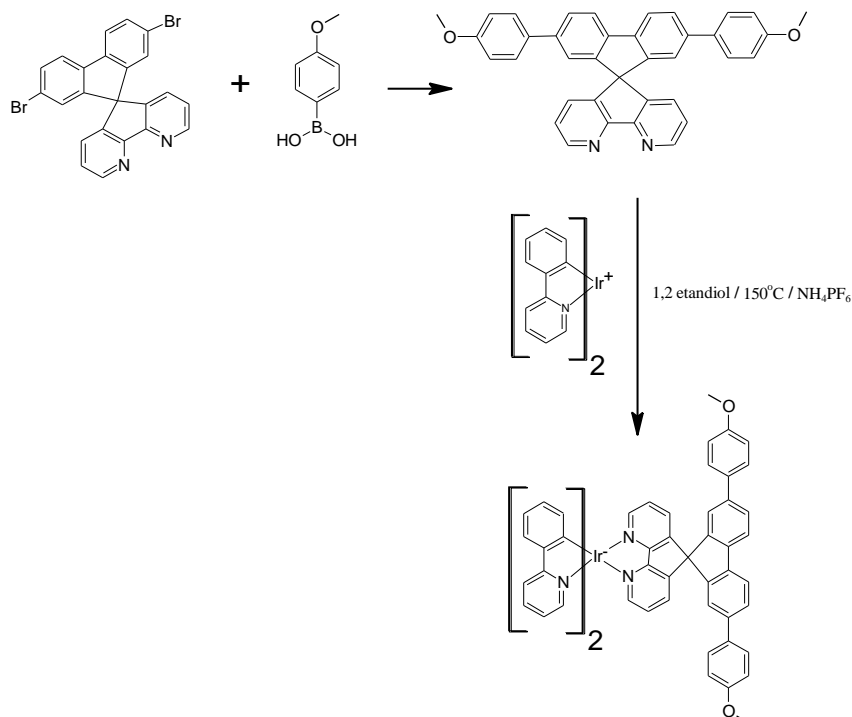

Figure 2.11: Synthetic route for C2.

2.3.3.3 Synthesis of C3 (:[2'7'-bis(3,5-dimethoxyphenyl)spiro(cyclopental(1,2-b:5,4-b')dipyridine-5,9'-fluorene)-bis-(2-phenylpyridine-C2′,N)-iridium(III)])

Compound C3 was synthesized by the following procedure described above for C1 molecule, by mixing L3 (75 mg, 0.126 mmol) and Di-μ-chlorotetrakis[(2-pyridinyl-phenyl-KN)-KC]di-iridium (136 mg, 0.126 mmol). The suspension was then cooled to 5 °C, the yellow solid separated by filtration, dried and recrystallized from acetonitrile / ether by diffusion. The synthetic route for C3 is summarized in Figure 2.12.

^{1}H NMR (ACN-d6, 400 MHz): δ, 8.39-8.37 (d, 2H), 8.13-8.08 (m, 4H), 8.01 (t, 2H), 8.00-7.97 (m,4H), 7.90-7.86 (d, 2H), 7.53-7.50 (d, 2H), 7.44-7.41 (m, 4H), 7.26-7.21 (t, 2H), 7.07 (s, 2H), 6.79-6.67 (m, 6H), 6.53 (s, 2H), 5.93-5.90 (d, 2H), 3.83 (s, 12H)

^{13}C NMR (ACN-d6, 400 MHz): δ, 167.44, 162.15, 161.37, 150.32, 148.75, 144.58, 143.27, 141.97, 140.87, 140.07, 138.70, 134.45, 131.76, 130.04, 128.70, 128.41, 124.57, 123.87, 122.77, 122.49, 119.69, 115.49, 105.17, 99.11, 66.84, 55.24
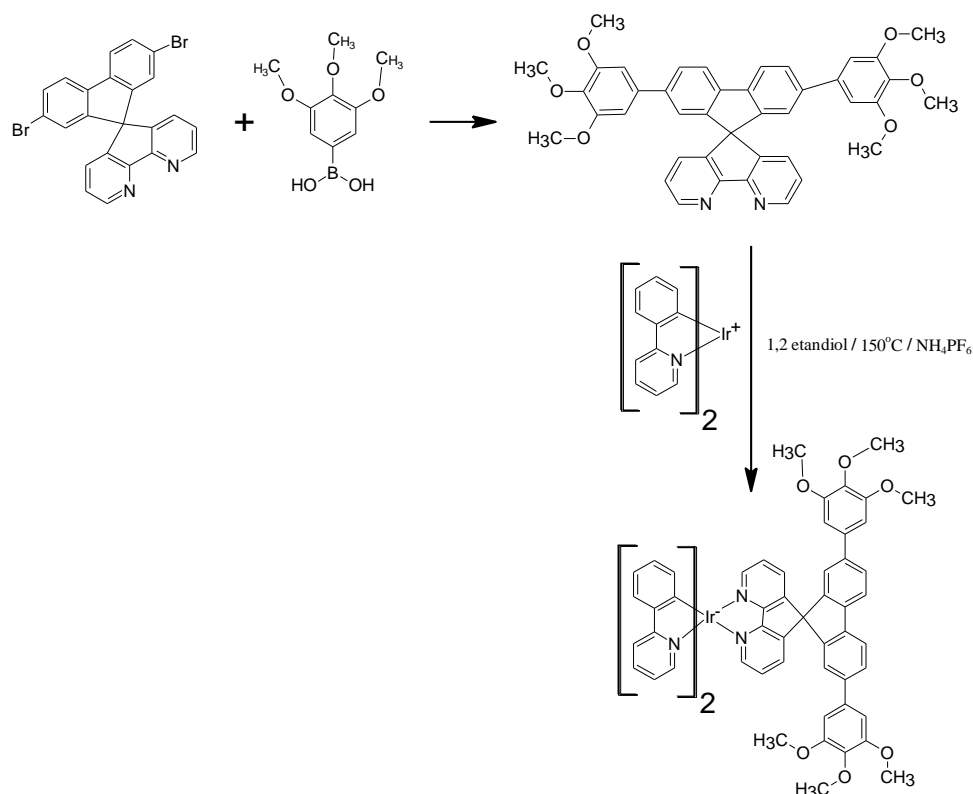

Figure 2.12: Synthetic route for C3.

2.3.3.4 Synthesis of C4 ([2'7'-bis(3,4,5-trimethoxyphenyl)spiro(cyclopental(1,2-b:5,4-b')dipyridine-5,9'-fluorene)-bis-(2-phenylpyridine-C2′,N)-iridium(III)])

Compound C4 was synthesized by the following procedure described above for C1 molecule, by mixing L4 (75 mg, 0.115 mmol) and Di-μ-chlorotetrakis[(2-pyridinyl-phenyl-KN)-KC]di-iridium (123 mg, 0.115 mmol). The suspension was then cooled to 5 °C, the yellow solid separated by filtration, dried and recrystallized from acetonitrile /ether by diffusion. The synthetic route for C4 is summarized in Figure 2.13.

^{1}H NMR (ACN-d6, 400 MHz): δ, 8.12 (d, 4H), 8.07 (d, 2H), 7.94-7.88 (m, 4H), 7.82-7.77 (m, 4H), 7.50-7.48 (d, 2H), 7.44-7.42 (m, 2H), 7.11-7.05 (m, 6H), 6.99-6-94 (m,2H), 6.76 (t, 4H), 6.44-6.41(d, 2H), 3.83 (s,12H), 3.76 (s, 6H)

^{13}C NMR (ACN-d6, 400 MHz): δ, 167.41, 162.21, 153.71, 150.41, 148.72, 144.58, 143.32, 141.06, 138.63, 135.81, 134.46, 131.69, 130.05, 128.47, 124.52, 123.65, 122.76, 122.42, 121.41, 119.69, 104.70, 66.92, 59.97, 56.17
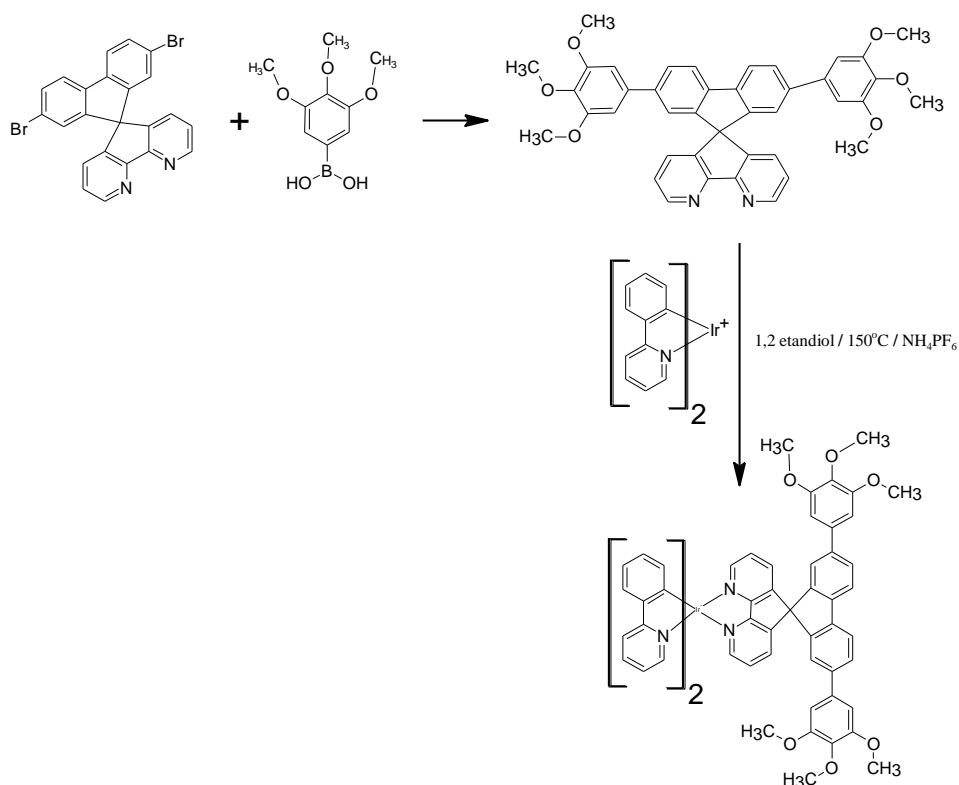

Figure 2.13: Synthetic route for C3.

39

2.3.3.5 Synthesis of C5 (:[2',7'-diphenylspiro(cyclopental(1,2-b')dipyridine-5,9-fluorene) -bis-(2-(2',4'-difluorophenyl)-pyridine-C6',N)-iridium (III)])

Compound C5 was synthesized by the following procedure described above for C1 molecule, by mixing L1 (50 mg, 0.106 mmol) and Di-μ-chlorotetrakis[(3-5-difluoro 2-(2-pyridinyl-KN)phenyl-KC]di-iridium (129 mg, 0.106 mmol). The suspension was then cooled to 5 °C, the red solid separated by filtration, dried and recrystallized from acetonitrile /ether by diffusion. The synthetic route for C5 is summarized in Figure 2.14.

^{1}H NMR (ACN-d6, 400 MHz): δ, 8.14-811 (d, 4H), 8.08-7.98 (m,2H), 7.96-7.93 (t,2H), 7.85-7.80 (m,4H), 7.76 (d,2H),7.56-7.48 (m, 6H), 7.43-7.39 (2H), 7.22-7.13 (m,4H),7.10-7.04 (m, 2H), 7.00-6.97 (m,2H), 6.97-6.95 (m,2H), 6.46-6.43 (d, 2H)

^{13}C NMR (ACN-d6, 400 MHz)**:** δ, 167.45, 164.47, 162.17, 150.34, 148.86, 144.67, 144.60, 143.77, 142.88, 141.90, 138.71, 134.48, 131.74, 130.05, 128.48, 128.44, 124.56, 123.75, 122.69, 121.99, 119.73, 109.92, 102.74, 66.76
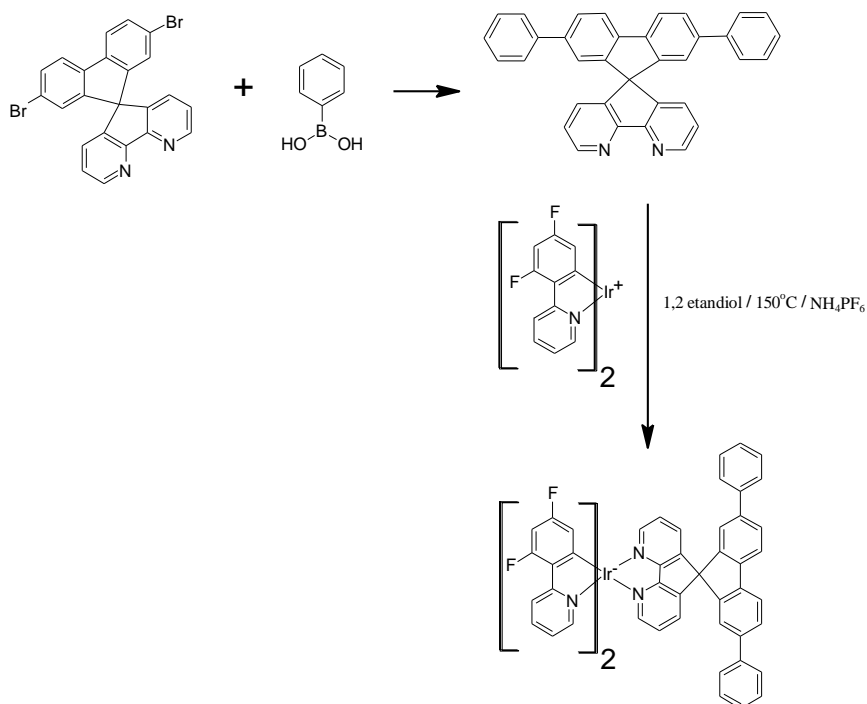

Figure 2.14: Synthetic route for C5.

2.3.3.6 Synthesis of C6 (: [2'7'-bis(methoxyphenyl)spiro(cyclopental(2,3-b:5,4-b')dipyridine-5,9'-fluorene)-bis-(2-(2′,4′-difluorophenyl)-pyridine-C6′,N)-iridium (III)])

Compound C6 was synthesized by the following procedure described above for C1 molecule, by mixing L2 (50 mg, 0.094 mmol) and Di-μ-chlorotetrakis[(3-5-difluoro 2-(2-pyridinyl-KN)phenyl-KC]di-iridium (114 mg, 0.094 mmol). The suspension was then cooled to 5 °C, the red solid separated by filtration, dried and recrystallized from acetonitrile /ether by diffusion. The synthetic route for C6 is summarized in Figure 2.15.

^{1}H NMR (ACN-d6, 400 MHz): δ, 8.40-8,37 (d, 2H), 8.14-8.11 (m, 4H), 8.03-8.00 (m, 2H), 7.88-7.81 (m, 4H), 7.56- 7.52 (m, 6H), 7.46-7.44 (m, 2H), 7.25-7.20 (m, 6H), 7.17-7.04 (m,2H), 6.80-6.6.71 (m, 2H), 5.92-5.89 (d, 2H), 3.52 (s, 6H)

^{13}C NMR (ACN-d6, 400 MHz): δ, 161.91, 150.55, 149.02, 143.45, 143.18, 140.98, 140.05, 139.75, 136.25, 135.05, 128.69, 128.30, 124.22, 123.72, 122.42, 121.92, 121.68, 115.69, 114.03, 108.63, 99.01, 67.02, 63.16
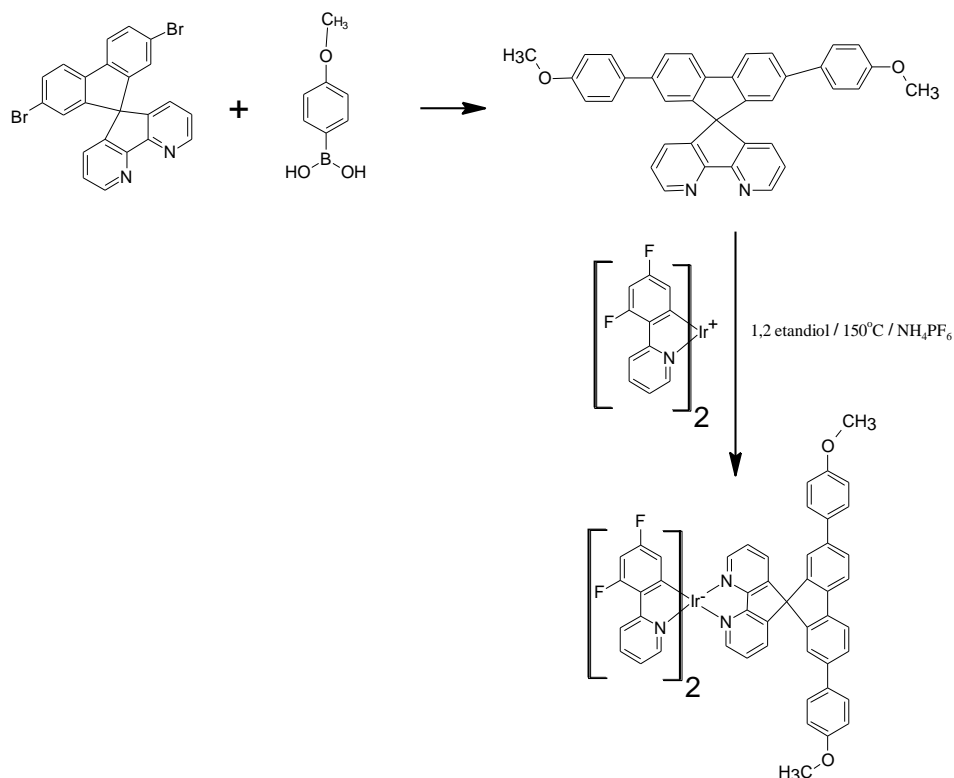

Figure 2.15: Synthetic route for C6.

41

2.3.3.7 Synthesis of C7 (: [2',7'-diphenylspiro(cyclopental(1,2-b')dipyridine-5,9-fluorene)-bis-(2-(2′,4′-difluorophenyl)-pyridine-C6′,N)-iridium (III)])

Compound C7 was synthesized by the following procedure described above for C1 molecule, by mixing L3 (50 mg, 0.084 mmol) and Di-μ-chlorotetrakis[(3-5-difluoro 2-(2-pyridinyl-KN)phenyl-KC]di-iridium (102 mg, 0.084 mmol). The suspension was then cooled to 5 °C, the red solid separated by filtration, dried and recrystallized from acetonitrile /ether by diffusion. The synthetic route for C7 is summarized in Figure 2.16.

^{1}H NMR (ACN-d6, 400 MHz): δ, 8.39-8.37 (d, 2H), 8.13-8.08 (m, 4H), 8.02-7.97 (m, 2H), 7.90 (d, 4H), 7.87-7.86 (d, 2H), 7.53-7.42 (m, 4H), 7.26.7.22 (t, 2H), 7.07 (s, 2H), 6.79-6.67 (m, 6H), 6.53 (d, 2H), 5.93.5.90 (d, 2H), 3.81 (s, 12H)

^{13}C NMR (ACN-d6, 400 MHz): δ, 161.94, 161.38, 157.22, 150.62, 148.97, 143.45, 143.11, 141.93, 141.33, 140.84, 139.72, 135.00, 128.69, 128.44, 122.56, 121.54, 117.29, 105.18, 99.09, 98.58, 63.16, 55.24
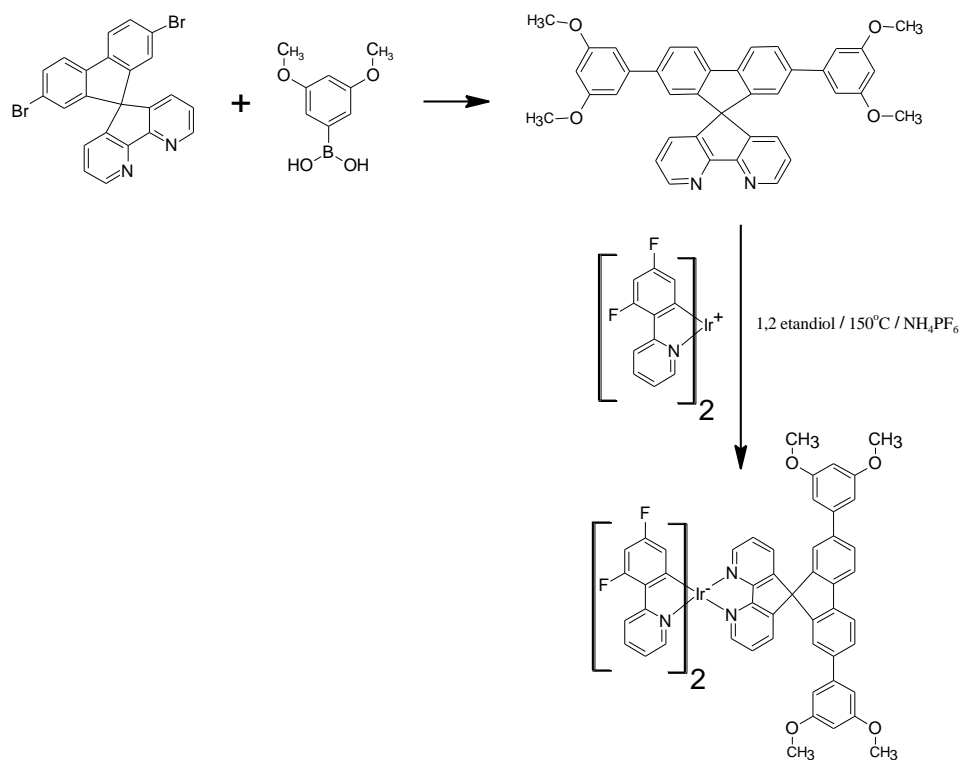

Figure 2.16: Synthetic route for C7.

2.3.3.8 Synthesis of C8 ([2'7'-bis(methoxyphenyl)spiro(cyclopental(2,3-b:5,4-b')dipyridine-5,9'-fluorene)-bis-(2-(2′,4′-difluorophenyl)-pyridine-C6′,N)-iridium (III)])

Compound C8 was synthesized by the following procedure described above for C1 molecule, by mixing L4 (50 mg, 0.076 mmol) and Di-μ-chlorotetrakis[(3-5-difluoro 2-(2-pyridinyl-KN)phenyl-KC]di-iridium (93 mg, 0.076 mmol). The suspension was then cooled to 5 °C, the red solid separated by filtration, dried and recrystallized from acetonitrile /ether by diffusion. The synthetic route for C8 is summarized in Figure 2.17.

^{1}H NMR (ACN-d6, 400 MHz): δ, 8.38 (d, 2H), 8.08 (m, 4H), 8.02-7.97 (m, 2H), 7.89-7.85 (m, 4H), 7.53-7.40 (m, 4H), 7.26-7.22 (d, 2H), 7.07 (s, 2H), 6.79-6.67 (m, 4H), 6.53 (d,2H), 5.90 (d,2H), 3.82 (s, 12H), 3.52 (s, 6H)

^{13}C NMR (ACN-d6, 400 MHz): δ, 167.41, 162.21, 159.63, 153.71, 150.41, 148.72, 144.76, 144.58, 143.32, 141.06, 138.63, 138.18, 135.81, 134.46, 131.69, 130.05, 128.47, 124.52, 123.65, 122.76, 122.42, 121.41, 119.69, 104.70, 66.92, 69.92, 56.17
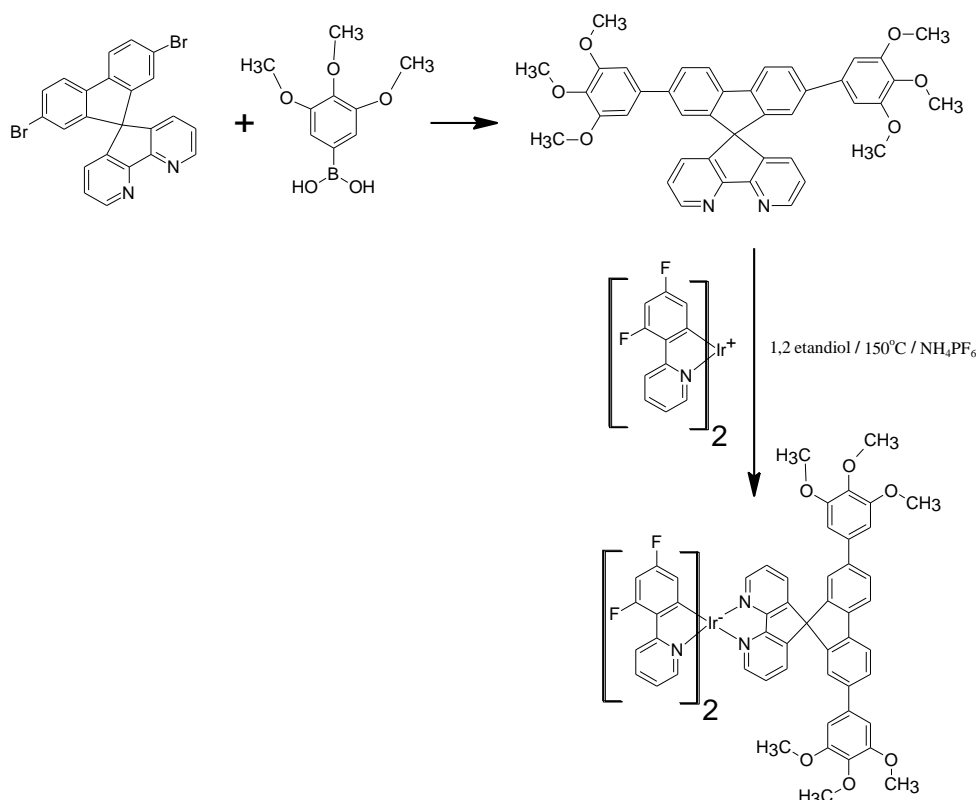

Figure 2.17: Synthetic route for C8.

2.4   Results and Discussion

2.4.1   Photo-physical Properties of Iridium (III) Complexes

The photo-physical properties of the Ir(III) complexes were investigated by UV-vis absorption and PL emission spectroscopy in dilute acetonitrile solution. The absorption and emission peaks indicate that the photo-physical properties of these Ir(III) complexes are finely tuned by the modification of the ligands that bind to the metal core.

The UV-vis absorption spectra are shown in Figure 2.18 and Figure 2.19 for complexes without and with Flor based metal cores respectively. The results of the analysis were summarized in Table 2.1. The observed intense absorption peaks at UV-vis measurement of C1 and C5 that have ligand L1 were occurred at 312 nm, C2 and C6 that have ligand L2 were occurred at 314 nm, C3 and C7 that have ligand L3 were occurred at 316 nm, C4 and C8 that have ligand L4 were occurred at 318 nm (see Figure 2.18 and Figure 2.19). These intense bands which are mostly located in the ultraviolet region below 350 nm, originated from the ligand-based spin-allowed singlet π-π* transitions [110]. Another region is much weaker bands which extends into the visible region above 385 nm [111]. These lower energy absorptions are assigned to spin allowed metal-to-ligand-charge transfer (MLCT) [112-114]. The spin-allowed intra-ligand-charge-transfer ligands causes these intense bands which are observed between 312 and 318. On the other hand, the metal-to-ligand charge-transfer, in which intersystem crossing occurred, and spin-orbit coupling causes the weaker absorption band near 385 nm, i.e. a lower energy band pass occurs. Thus, it appears that the metal core and ligand interaction is causing red shift [115].
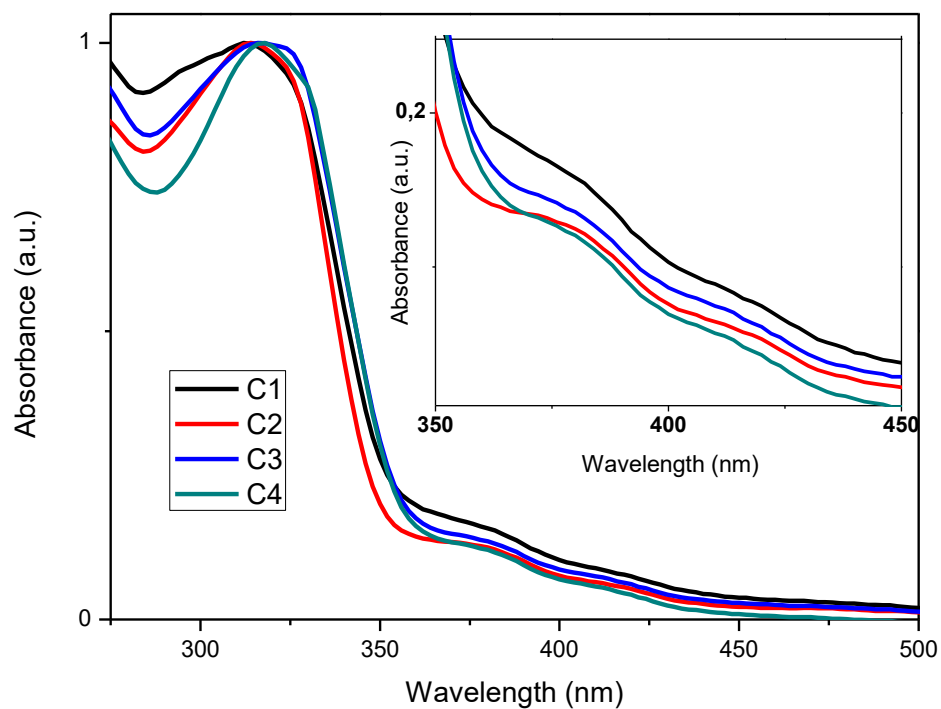
Figure 2.18: Normalized UV-vis absorption spectra of the complexes C1, C2, C3 and C4.
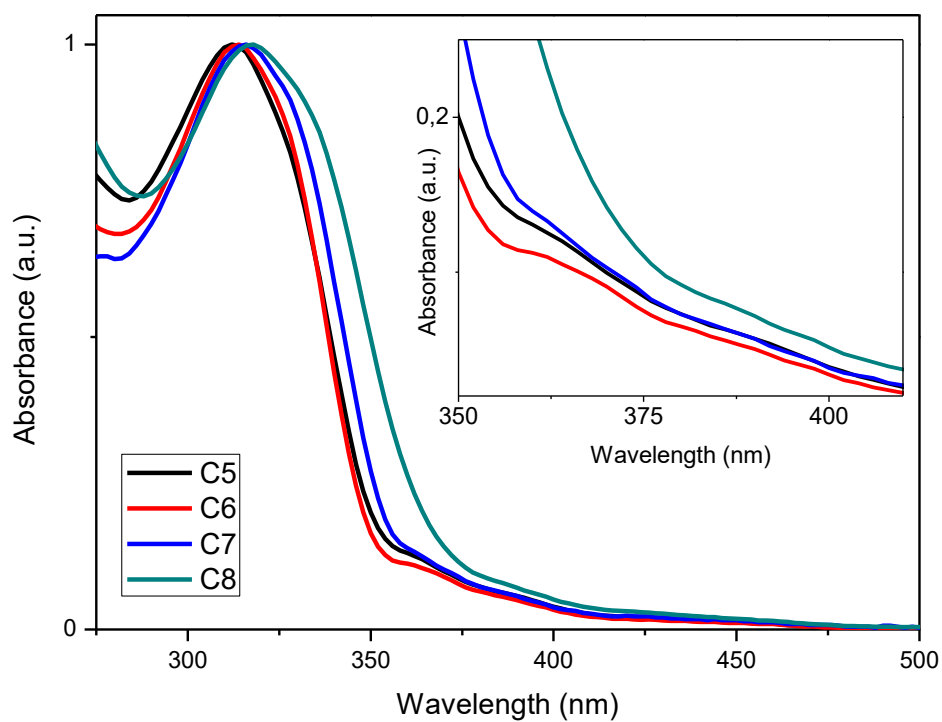

Figure 2.19: Normalized UV-vis absorption spectra of the complexes C5, C6, C7 and C8.

The photoluminescence measurements of the complexes were obtained at room temperature in acetonitrile (MeCN) solution on Luminescence Spectrometer LS50B (Perkin Elmer). The photoluminescence spectra of all the complexes are given in Figure 2.20. The complexes C1-C4 emit orange light, whose peak wavelengths occur in the range of 572-578 nm and the complexes C5-C8 emit green light, whose peak wavelengths occur in the range of 511- 519 nm. These PL peaks were also given in Table 2.1.

According to the light emitting theory by changing the structure of the ligand bonded to the metal core, the light emission of the complexes can be tuned. In the group of C1-C4 complexes, red shifts are observed as adding methoxy groups. The reason is that the methoxy groups bonded to the molecule will increase the electron density in the main structure and increase the tendency of electron-donating. Thus, the HOMO level will shift to the upper energy, the energy band gap will decrease or the wavelength will increase and therefore the red shift will take place. The same is true for the C5-C8 series. However the difference in emission colors between C1-C4 series and C5-C8 series, indicates that electron withdrawing character of fluoro substituents on ppy ligand results in a strong effect on the energy levels of the complexes C5-C8. This effect will shift HOMO level to the lower energy, the energy band gap will increase or the wavelength will decrease so blue shift observed.
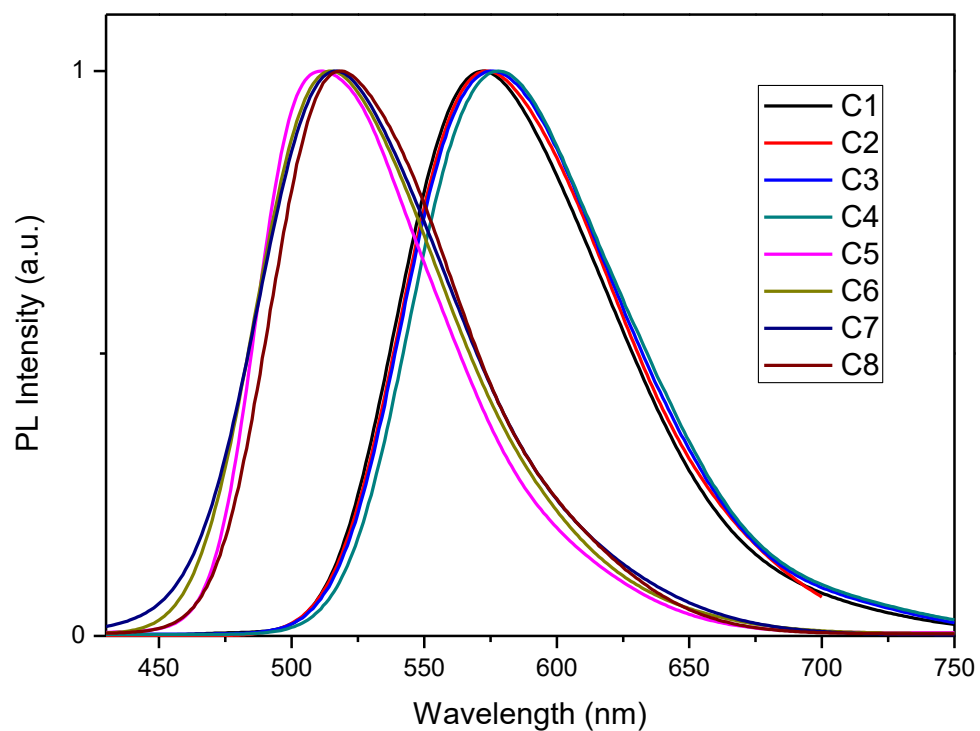
Figure 2.20: Normalized PL spectra of complexes (C1 to C8) in CH_2Cl_2 at 293 K.

Table 2.1: Photo-physical data of complexes 1 to 8.

Compound	UV-vis absorption			PL Emission λ_{em} (nm)	FWHM of PL (nm)
	λ_{abs} (nm)	^{1}MLCT	^{3}MLCT		
C1	312	383	422	572	86
C2	314	382	418	574	92
C3	316	382	420	576	94
C4	318	382	421	578	92
C5	312	367	394	510	78
C6	314	365	393	515	83
C7	316	367	393	517	86
C8	318	368	389	519	82

2.4.2 Electrochemical Properties of Iridium (III) Complexes

The electrochemical properties of Iridium (III) complexes synthesized in this work such as HOMO, LUMO and band gap energies were determined by cyclic voltammetry (CV) measurements. These measurements were taken with CHI440B model CV instrument. There are three different electrodes in this CV system; a glassy carbon was used as the working electrode, Ag/Ag^+ is used as reference electrode and Pt-wire is used as counter electrode. CV measurements were obtained in an acetonitrile solution at a concentration of 0.1 M tetrabutylammonium hexafluorophosphate (TBAPF$_6$). The Ir (III) complexes added into the solution and were coated on the working electrode. CV data for each complex were collected under an N_2 atmosphere at a scan rate of 50 mV/s. In Table 2.2 the experimentally obtained onset oxidation (E_{ox}) potentials and onset reduction (E_{red}) potentials from CV data and also calculated HOMO and LUMO energy levels and band gap energies of these complexes have been given.

It is accepted that it is possible to adjust energy vacancies in Ir(III) complexes by changing their ligand properties [113].The HOMO and LUMO levels of the Ir (C^N)3 or Ir (C^N)2 (acac) complexes generally occur in iridium metal-centered d orbitals and in a fraction of the π-orbitals in the ligands [92]. In addition, for the bis-cyclometal Ir(III) complexes mentioned in this thesis, the LUMO level is mostly on the strong electron attracting ligand N^N, while the HOMO levels depend on the chemical nature of the C^N ligands [116, 117]

Thus, theoretically, by adding electron-withdrawing groups attached to the phenyl moiety in the C^N ligand, the HOMO can be stabilized and the energy gap will increase. In addition, in the Ir (III) complexes, the oxidation usually involves conversion of Ir(III)/Ir(IV) [118]. In other words, an electron emerges from the center of the metal, causing oxidation. That is, electron attracting groups will cause very low electron density around the metal center and a lower HOMO energy level will be created. In contrast to the complex mentioned in the literature [116, 117] LUMO is located on the ligand N^N and can influence the electron density of the metal center by reduction with the addition of an electron to LUMO.

CV data of C1-C8 complexes are shown in Figure 2.21-Figure 2.28. Oxidation (E_{ox})

and reduction (E_{red}) energy values were obtained based on the peak points in these CV graphs. HOMO and LUMO energy levels are calculated by the following formula,

$$LUMO = e \, (E_{1/2(red)} - E_{1/2(Fe)} + 4.8)$$

$$HOMO = -e \, (E_{1/2(ox)} - E_{1/2(Fe)} + 4.8)$$

Where 'e' is electron charge value, equal to $1.6021765 \times 10^{-19}$ coulomb and $E_{1/2(Fe)}$ is Ferrocene potential which was used as an internal standard (0.40 V). HOMO energy levels ranged from -5.71 to -5.85 eV for complexes C1-C4 and from -5.80 to -6.22 eV for complexes C5-C8. LUMO energy levels ranged from -3.18 to -3.20 eV for complexes C1-C4 and from -3.23 to -3.30 eV for complexes C5-C8. The energy gaps between HOMO and LUMO are ranged from 2.51 to 2.92 eV for C1-C4 and from 2.57 to 2.92 eV for C5-C8. The CV analysis results are given in Table 2.2.
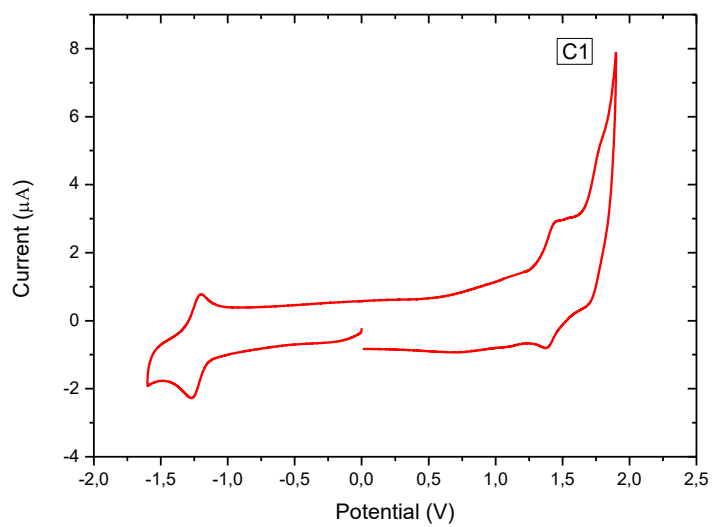
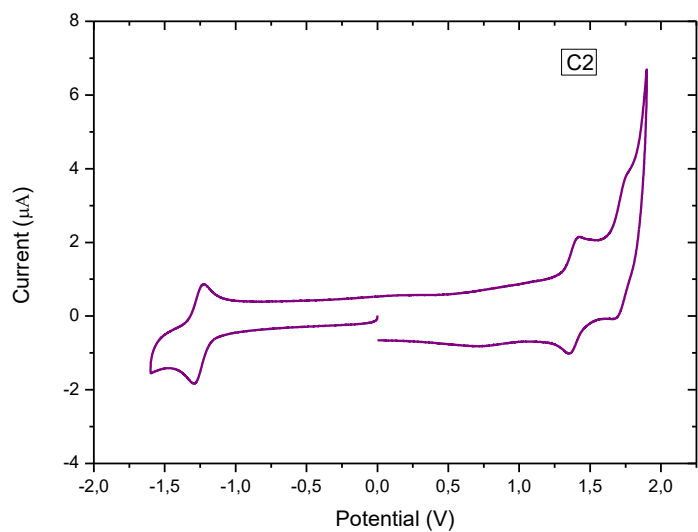**Figure 2.21:** Cyclic voltammogram of C1.

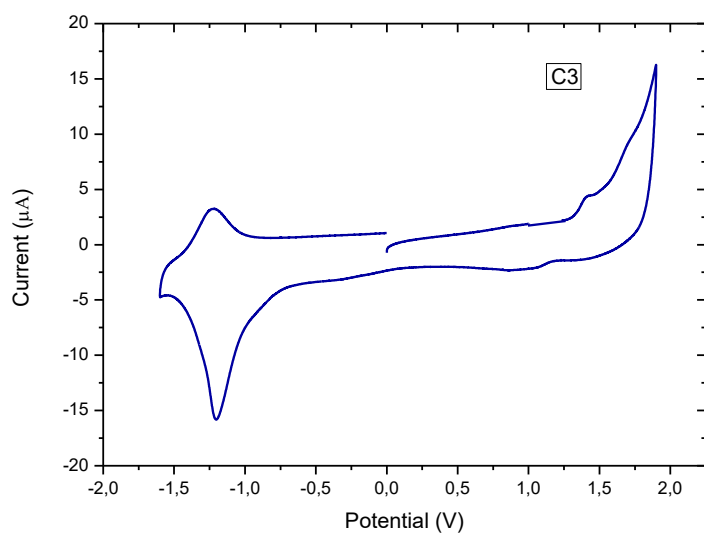**Figure 2.22:** Cyclic voltammogram of C2.

Figure 2.23: Cyclic voltammogram of C3.
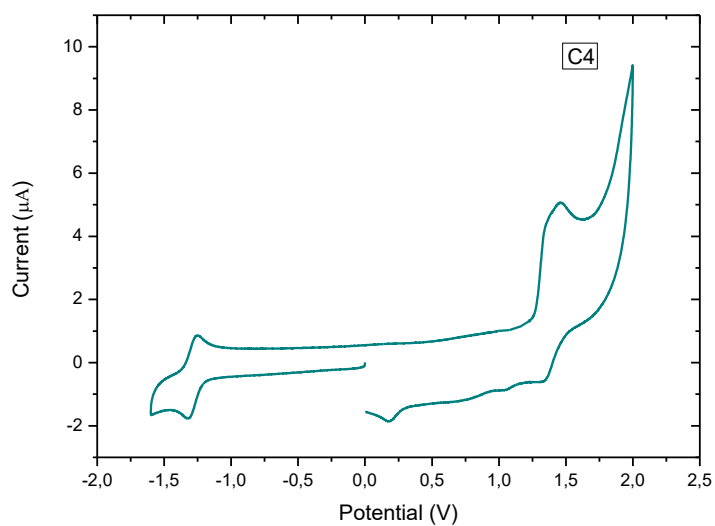

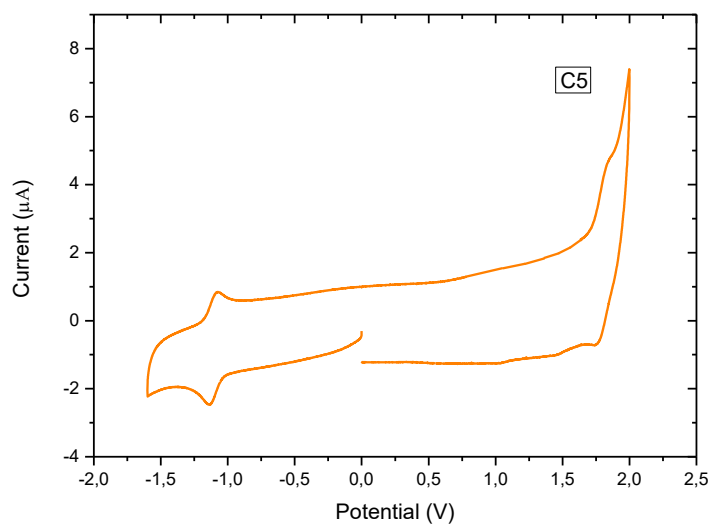**Figure 2.24:** Cyclic voltammogram of C4.

Figure 2.25: Cyclic voltammogram of C5.
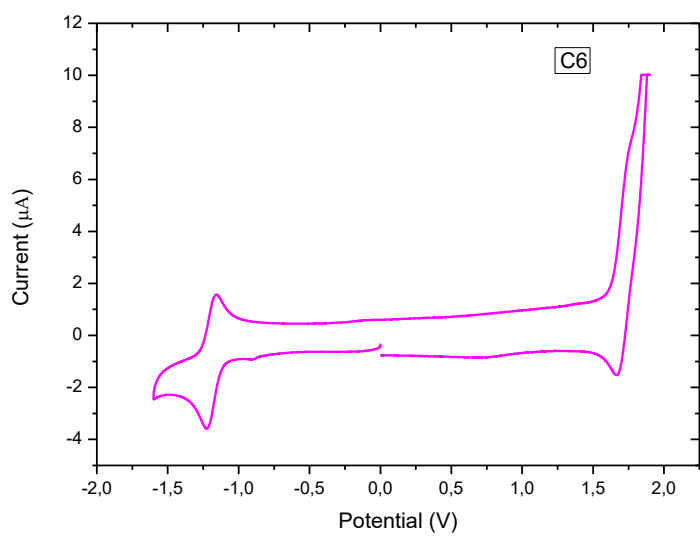

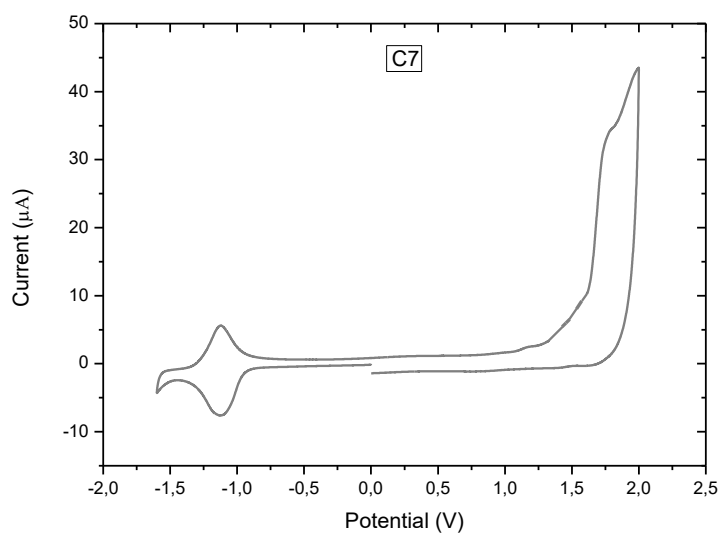**Figure 2.26:** Cyclic voltammogram of C6.
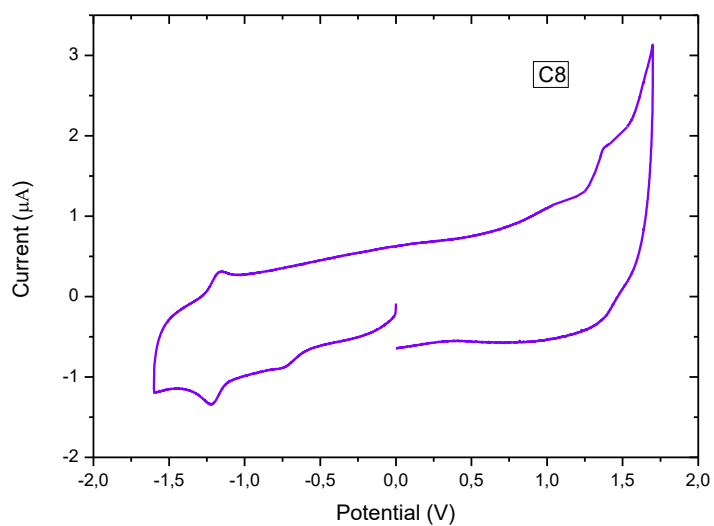
Figure 2.27: Cyclic voltammogram of C7.

Figure 2.28: Cyclic voltammogram of C8.

Table 2.2: Electrochemical properties of complexes 1 to 8.

Compound	E_{ox} (V)	E_{red} (V)	HOMO (eV)	LUMO (eV)	E_g (eV)
C1	1.45	1.20	−5.85	−3.20	2.65
C2	1.41	1.22	−5.81	−3.18	2.63
C3	1.38	1.22	−5.78	−3.18	2.60
C4	1.31	1.20	−5.71	−3.20	2.51
C5	1.82	1.10	−6.22	−3.30	2.92
C6	1.72	1.15	−6.12	−3.25	2.87
C7	1.54	1.14	−5.94	−3.26	2.68
C8	1.40	1.17	−5.80	−3.23	2.57

HOMO and LUMO energy levels of complexes C1, C2, C3 and C4 are (−5.85/ −3.20), (−5.81/−3.18) (−5.78/−3.18) and (−5.71/−3.20) eV respectively. It can be obviously seen that the HOMO energy level of C4 achieves the smallest value which is almost 0.14 eV less than those of C1. As it is mentioned above that by adding electron-donating group (OCH₃) to the spiro part of the molecule, the electron density on Ir metal center can be increased and subsequently HOMO energy level of the whole molecule can be stabilized. Correspondingly, complexes C2, C3 and C4 which contain OCH₃ groups have stabilized HOMO energies which are observed at −5.81, −5.78 and −5.71 eV and therefore energy gaps have been narrowed to 2.63, 2.60 and 2.51 eV.

On the other hands, the complexes C5, C6, C7, and C8 have higher oxidation potentials than that of complexes C1, C2, C3 and C4, which shows that the electron density on the Ir metal center can be reduced by four electron-withdrawing fluoro substituents on the phenyl ring of the ppy ligand and subsequently HOMO level can be stabilized. In the C^N ligand of C5, electron-donating fluoro substitute is involved and thus C5 has a HOMO energy level in the order of −6.22 eV. For complexes C6, C7 and C8, all HOMO energy levels rise to −6.12, −5.94 and −5.80 eV, respectively. This is possibly

explained by the existence of the electron-donating methoxy groups (OCH$_3$) on the molecule, by which the electron density of the HOMO levels can be increased and stabilized to a lower ionization potential. Hence, complexes C5, C6, C7 and C8 have much destabilized, higher HOMO energy levels than that of complexes C1, C2, C3 and C4.

In this study, the LUMO energy levels of the complexes C1-C4 and C5-C8 are found as around −1.20 and −1.15 eV respectively. These are relatively low and only have insignificant modifications because of the addition of particularly strong electron-withdrawing N^N ancillary ligands. The LUMO level of complex C8 is slightly higher than that of complex C5, because of the difference between protons numbers in the methoxy group on the Spiro molecule. The reason can be due to the fact that the increasing of a proton number in N^N ligand can make electron decreasing in the LUMO so electron can be attracted easier from the HOMO.

The schematic demonstration of HOMO and LUMO levels of all complexes is given in Figure 2.29. It can be seen from this figure that the band gap energies are decreased or red shifted by increasing the electron donating methoxy group and it is also seen that due to electron withdrawing fluorine atoms in the Ir metal cores of C5-C8 complexes, dominantly HOMO levels are stabilized therefore, band gap energies are blue shifted.
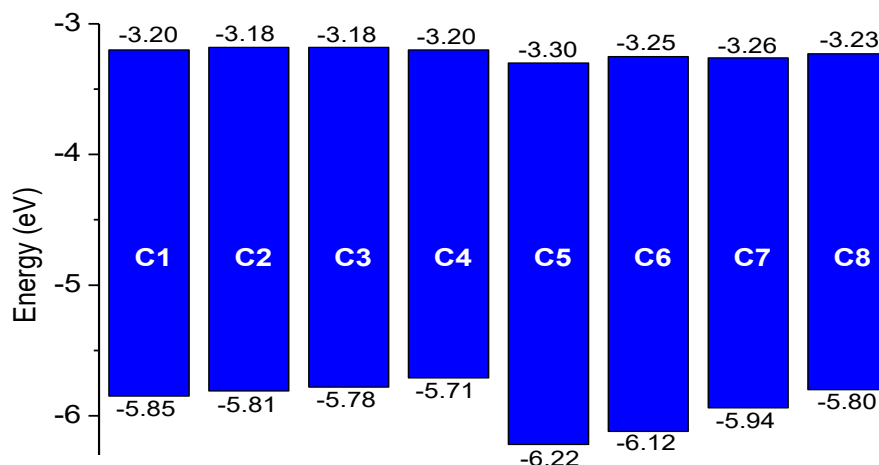

Figure 2.29: HOMO and LUMO energy diagrams of all complexes.

2.5   OLED Fabrication

2.5.1   OLED Fabrication Procedure

This section describes the device manufacturing processes. The spin coating and further drying of the layers anode, PEDOT/PSS and emissive layer was done under room temperature and atmospheric pressure. Coating of the cathode layer was carried out by the vacuum evaporation system. The device configuration studied in this work is ITO/PEDOT:PSS/Ir(III) complex/Al. The OLED structure is also shown in Figure 2.30.
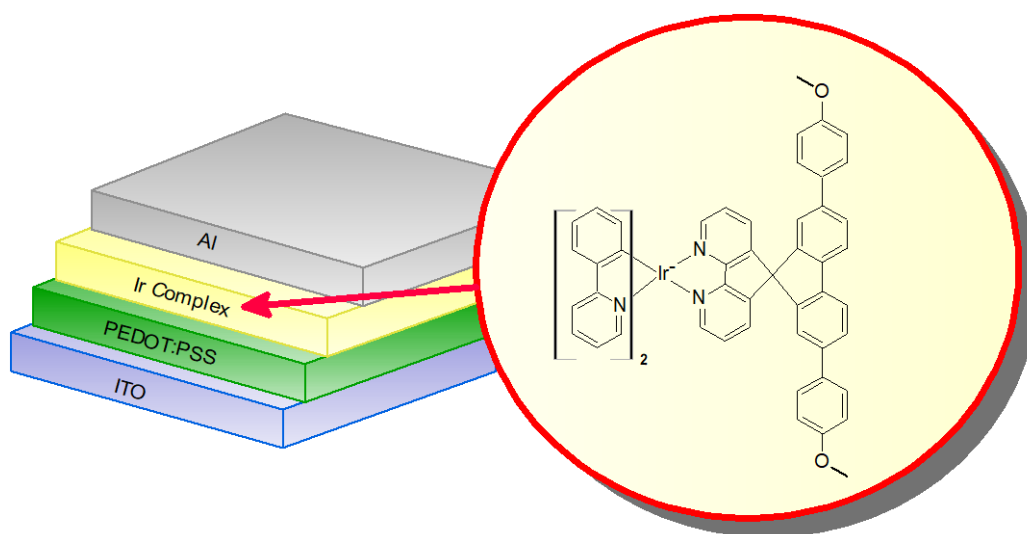

Figure 2.30: The simple two layer OLED structure studied in this work.

The devices were produced as follows: firstly, about a half centimeter of an edge of 3x3 cm^2 ITO-coated glass substrate, (18-24 Ω/sq surface resistivity), was etched by a 3HCl +1HNO$_3$ (aqua regia) acid solution with a production of a tape covered other surfaces. After the tape was removed from the surface, cleaning procedure was applied by toluene, acetone, isopropyl alcohol, and deionized water respectively and dried under N$_2$. PEDOT/PSS was coated over the ITO by spin coater with 3600 rpm for 45 seconds. The purpose of this layer is to flatten the electrode, to assist a better and more reproducible hole injection, and to prevent the formation of pinholes which can cause short circuits. Then about a half centimeter of an edge of the PEDOD/PSS surface was etched by deionized water and then dried at 120°C for 30 min. The Ir(III) complex was coated by spin coater by 1200-1500 rpm for 45 seconds on the surface subsequently. The etching about a half centimeter of an edge of the emissive layer carried out at

dichloromethane. The 2.7 nm Al electrode was thermally evaporated by using a shadow mask under 1.23×10^{-5} Torr with in an Edward Auto 500 evaporator.

2.5.2   Characterization of OLEDs

Electrical characterizations (current density changes under applied voltages) and electroluminescence characterizations (luminance changes under applied voltages) were carried out for the four OLEDs which are constructed by using complexes C2, C4, C6, and C8 as emissive layers. The EL spectra, current density-voltage and luminescence-voltage data were collected by using a Keithley 2400 source unit and calibrated Hamamatsu C9920-12 EQE measurement system. In this thesis the current density, luminance, external quantum efficiency versus voltage characteristics and electroluminescence intensity versus wavelength characteristics have been given for the OLED devices of C2, C4, C6, and C8. The photograph of OLED devices of C6 which emits green light and C2 which emits yellow light is given in the Figure 2.31. The photographs of C6 and C2 solutions with dichloromethane under UV light have ben also demonstrated in Figure 2.32.
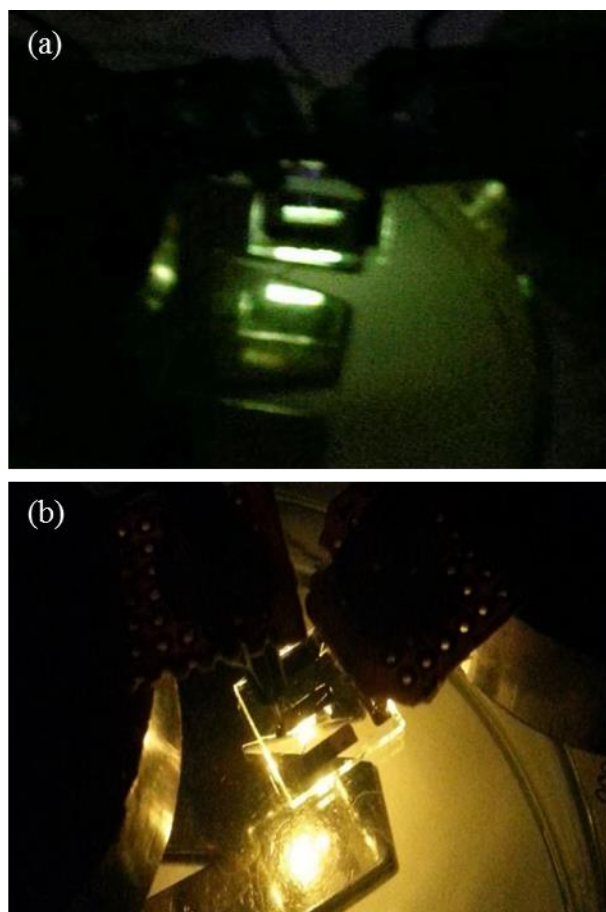
Figure 2.31: Photographs of OLED devices of C6 (a) and C2 (b) when they have been operating.
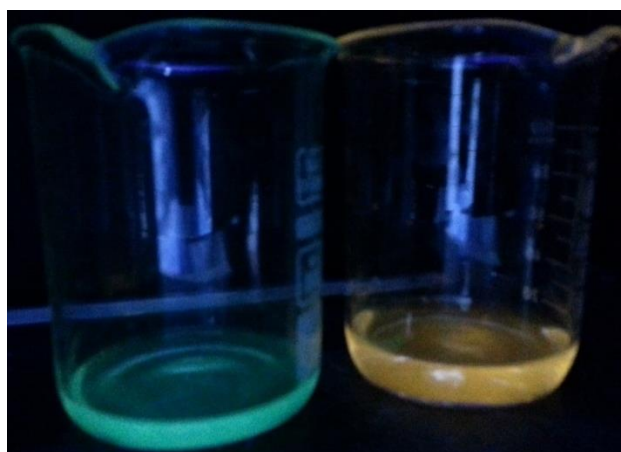

Figure 2.32: C6 (on left) and C2 (on right) materials solved in dichloromethane under UV light.

The typical current density versus voltage characteristics of simple layer (PEDOT:PSS and emissive layer) OLEDs, can be seen in Figure 2.33, Figure 2.34, Figure 2.35 and Figure 2.36 for C2, C4, C6 and C8 respectively. That typical characteristic responses

follow a slow increase and then a rapid increase of current density after a certain voltage over increasing voltage. In these graphs, the current density appears to increase at low voltages. This means that devices made with the novel iridium complexes synthesized in this study can operate at low voltages.
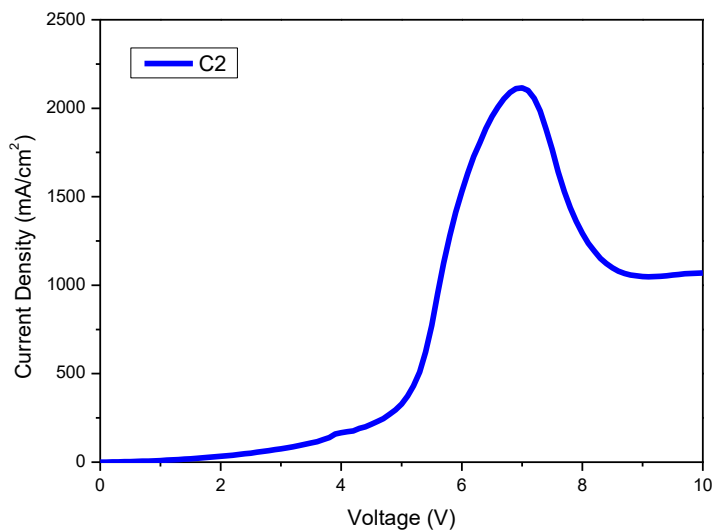

Figure 2.33: Current density- voltage characteristic for the LEC device in which C2 used as emissive layer.
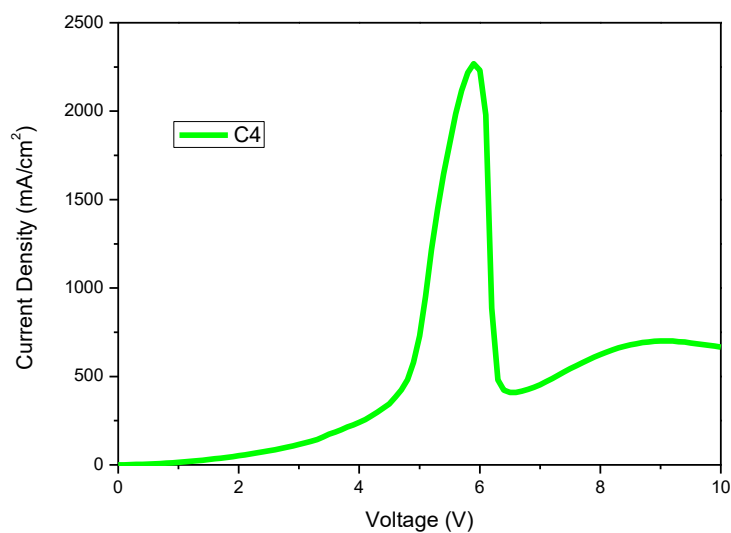

Figure 2.34: Current density- voltage characteristic for the LEC device in which C4 used as emissive layer.
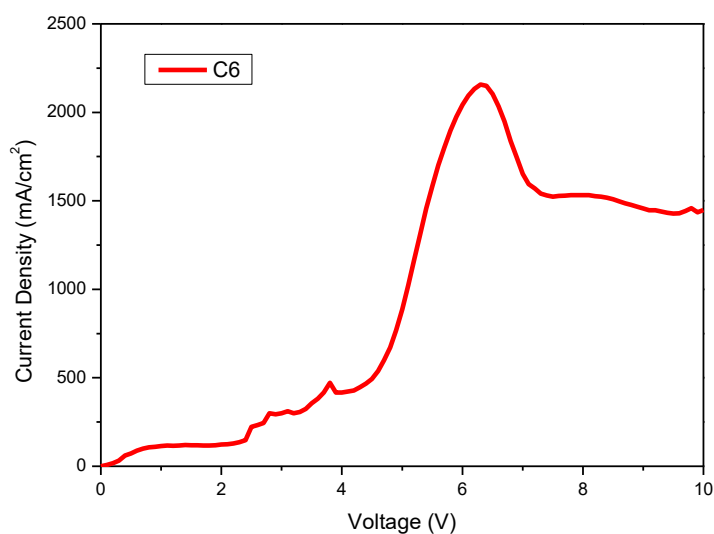
Figure 2.35: Current density- voltage characteristic for the LEC device in which C6 used as emissive layer.
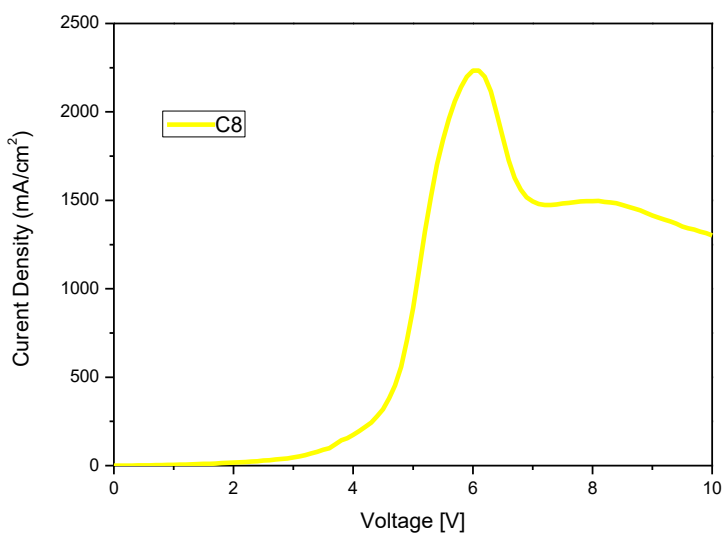

Figure 2.36: Current density- voltage characteristic for the LEC device in which C8 used as emissive layer.

The luminance versus voltage graphs are given in Figure 2.37, Figure 2.38, Figure 2.39, and Figure 2.40 for C2, C4, C6 and C8 respectively. It can be seen from these figures that the turn-on voltages, which defines the voltage required to give a 1 cd/m^2 luminance, are 4.2, 4.1, 4.0, and 4.1 V for C2, C4, C6, and C8 respectively. On the

60

other hand, it has been determined operating voltages of C2, C4, C6 and C8 as 5.8, 5.5, 5.3 and 5.1 V, respectively, when the luminance is maximal. The peak luminance values are obtained as 1107 cd/m^2, 277 cd/m^2, 30 cd/m^2, and 15 cd/m^2 for C2, C4, C6, and C8 respectively.
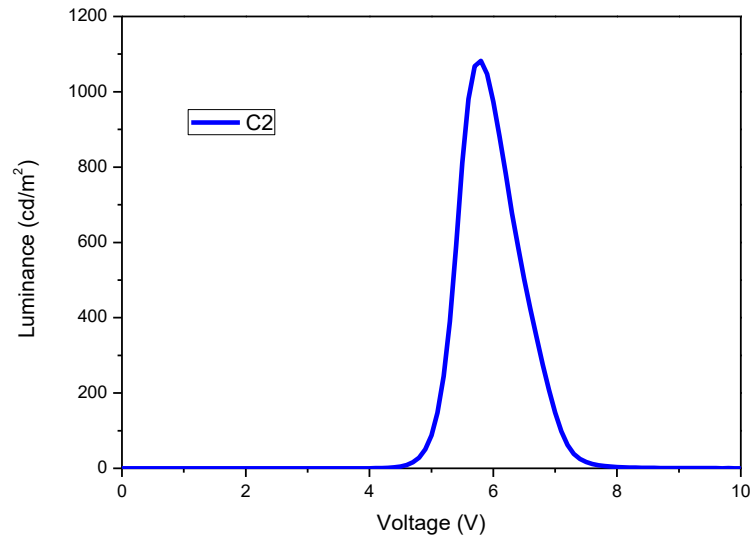

Figure 2.37: Luminance- voltage characteristic for the LEC device in which C2 used as emissive layer.

Figure 2.38: Luminance- voltage characteristic for the LEC device in which C4 used as emissive layer.
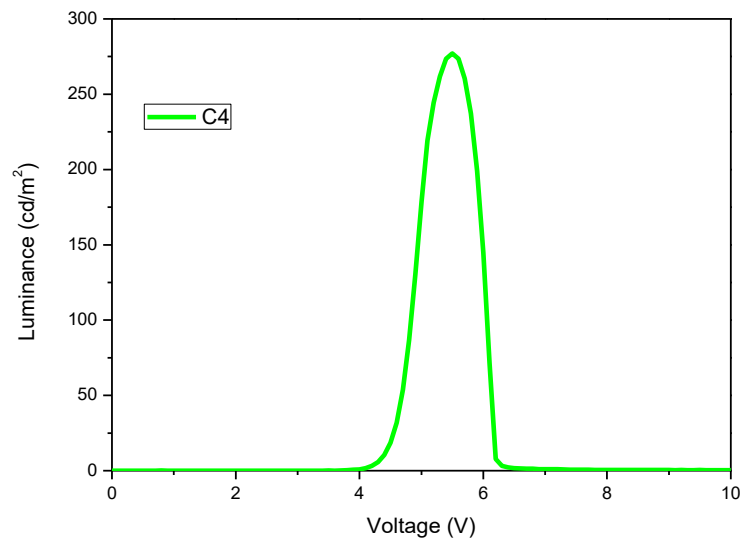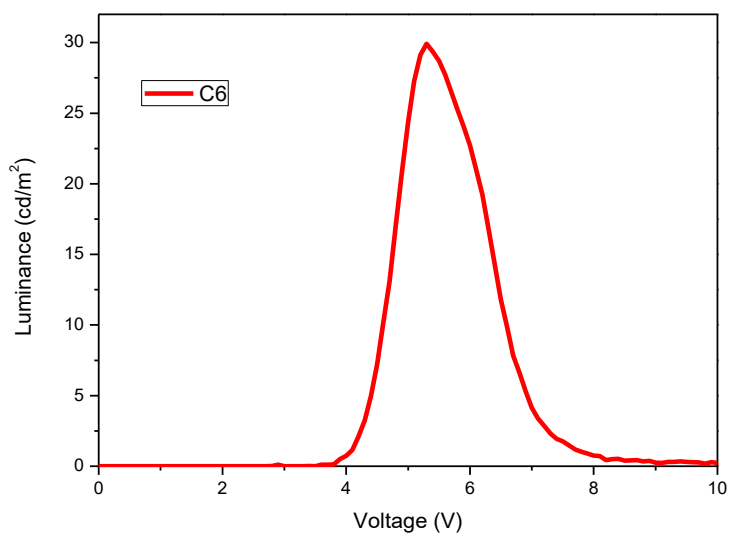
Figure 2.39: Luminance- voltage characteristic for the LEC device in which C6 used as emissive layer.

Figure 2.40: Luminance- voltage characteristic for the LEC device in which C8 used as emissive layer.

The EQE and luminance values of the devices were found to be compatible with each other. The peak EQE values are 4%, 0.1%, 0.1%, and <0.1% for C2, C4, C6, and C8

respectively (Figure 2.41, Figure 2.42, Figure 2.43 and Figure 2.44). The device performance values are summarized in Table 2.3 .

Figure 2.41: EQE- voltage characteristic for the LEC device in which C2 used as emissive layer.

Figure 2.42: EQE- voltage characteristic for the LEC device in which C4 used as emissive layer.

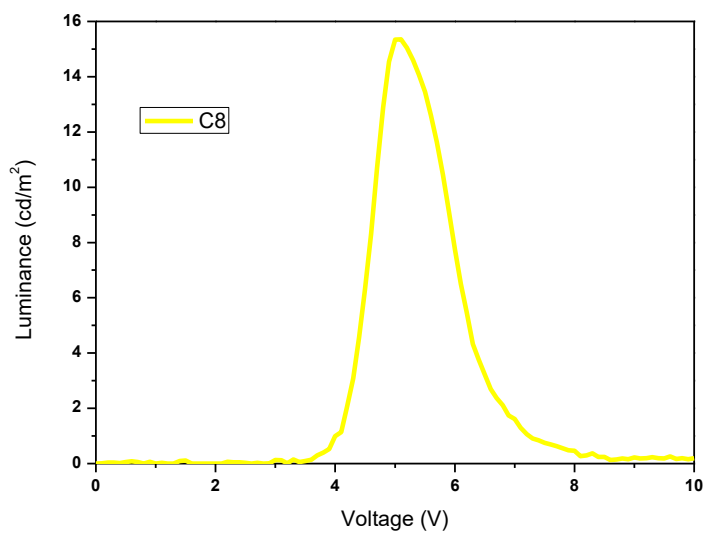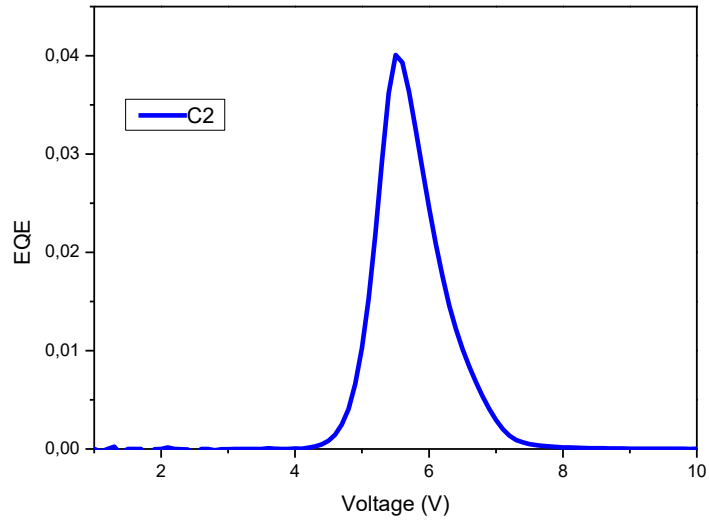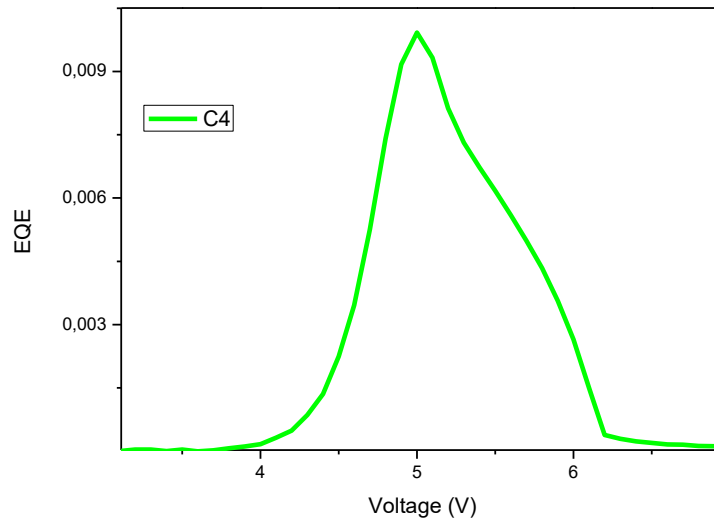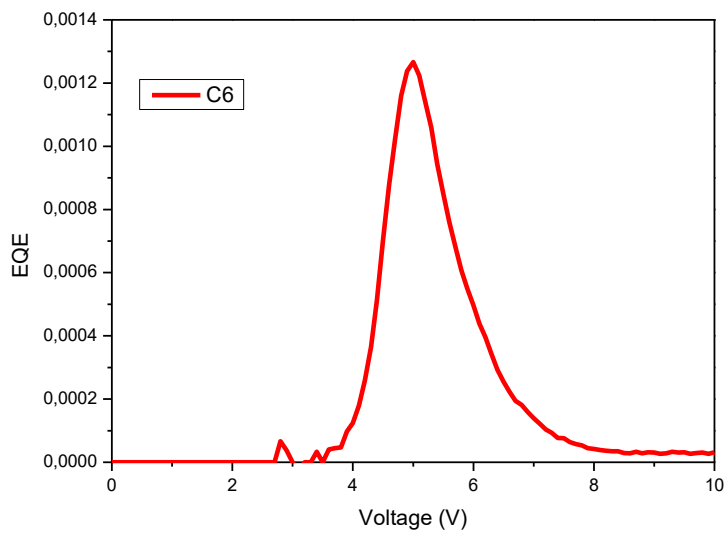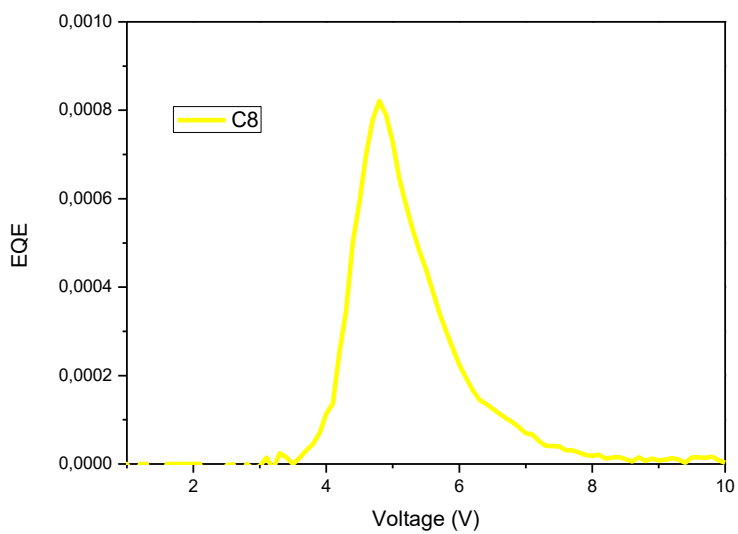**Figure 2.43:** EQE- voltage characteristic for the LEC device in which C6 used as emissive layer.

Figure 2.44: EQE- voltage characteristic for the LEC device in which C8 used as emissive layer.

Table 2.3: Device performance values.

Emitting material of device	EQE (%)	Turn on Voltage (V)	Operating Voltage (V)	Luminance (cd/m^2)
C2	4.6	4.2	5.8	1107
C4	0.1	4.1	5.5	277
C6	0.1	4.0	5.3	30
C8	<0.1	4.1	5.1	15

The electroluminescence spectrum of the devices of C2, C4, C6 and C8 are shown in Figure 2.45, Figure 2.46, and Figure 2.47, Figure 2.48 respectively. The EL spectra obtained for each device contain two intense peaks. In the EL spectrum of the OLED formed using C2 emissive material, two peaks at 561 and 595 nm, corresponding to citrus yellow and orange, were obtained. If the average of these two wavelength values is taken, 578 nm is obtained, which corresponds to the CIE coordinates (0.499, 0.499) and means pure yellow light. In the PL spectrum of the C2 complex 574 nm peak was obtained, which corresponds also to the citrus yellow. That means, a redshift of about 4 nm was observed in the EL emission according to the PL emission for the C2 complex. According to the literature, redshift in these types of iTMC-based OLEDs is achieved between about 20-40 nm [119, 120]. This significant redshift is attributed to optical and electrical carrier excitation of Ir complexes [121]. However, a small redshift occurs in the Ir complexes used in this study.
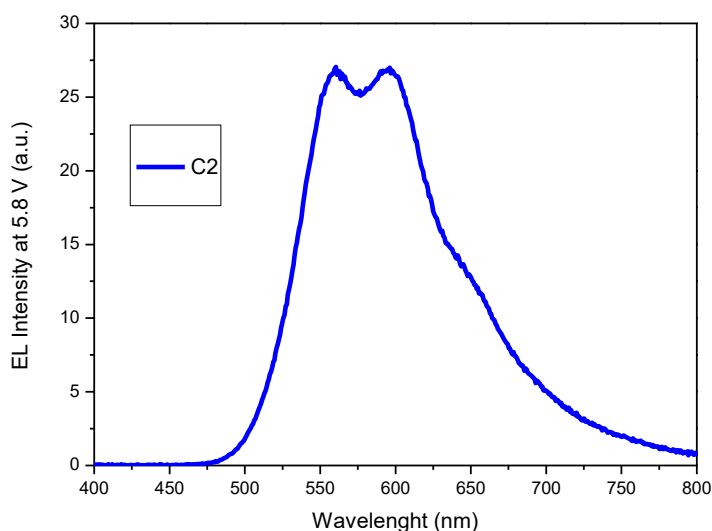
Figure 2.45: EL intensity spectrum of complex C2 at 5.8 V.
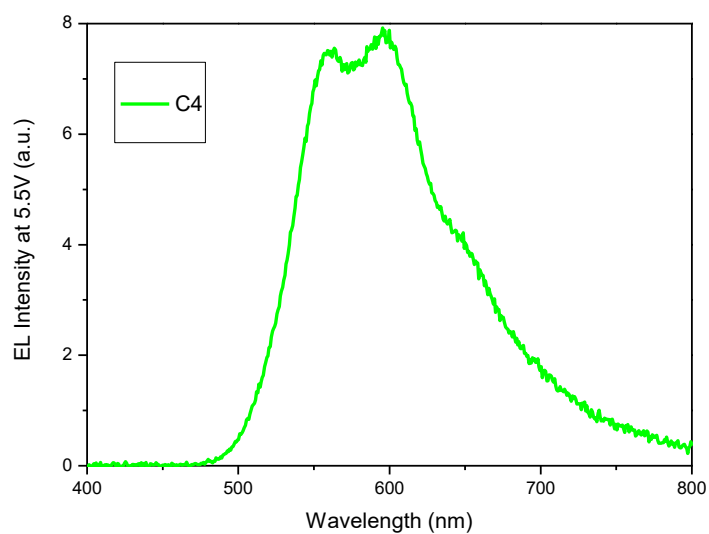
Figure 2.46: EL intensity spectrum of complex C4 at 5.5V.
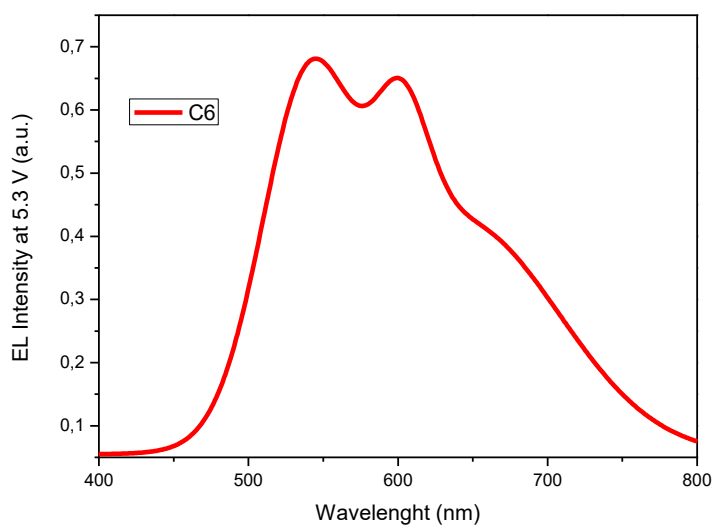
Figure 2.47: EL intensity spectrum of complex C6 at 5.3 V.
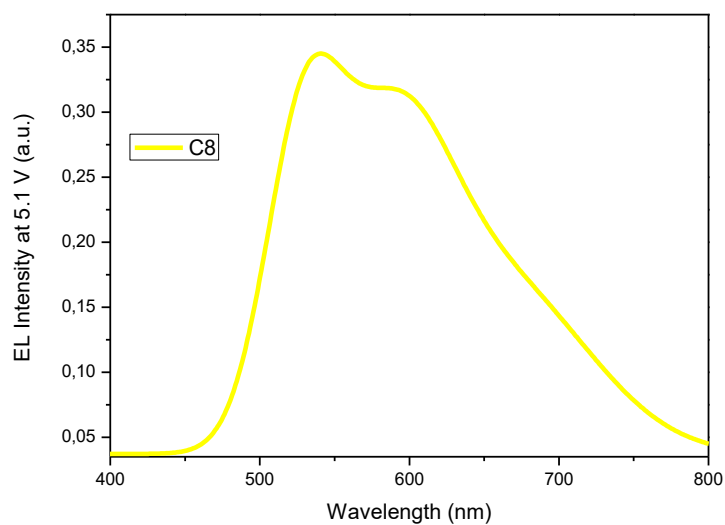
Figure 2.48: EL intensity spectrum of complex C8 at 5.1 V.

For all devices the EL peaks and CIE coordinates were summarized in Table 2.4. The CIE coordinates of C2 and C4 EL emissions corresponds to pure yellow, and also CIE coordinates of C6 and C8 EL emissions corresponds to yellowish green.

Table 2.4: Electroluminescence and photoluminescence comparison.

Emitting material of device	EL peak 1 (nm)	EL peak 2 (nm)	Average EL (nm)	CIE coordinates (x,y)	PL peak (nm)
C2	561	595	578	(0.499, 0.499)	574
C4	563	595	579	(0.506, 0.493)	578
C6	544	599	571	(0.451, 0.547)	515
C8	546	598	572	(0.458, 0.541)	519

3. CONCLUSIONS

Iridium (III) metal-organic complexes have attracted considerable attention due to their easy device process in OLED applications and the possibility of obtaining light in high efficiency.

In this thesis four novel spirobifluorene based ligands have been synthesized by palladium catalyzed Suzuki coupling reaction. These ligands were prepared with well-defined chemical structure and purity. Also eight novel Ir(III) complexes have been synthesized by using these ligands. The synthesis and characterization of functionalized Iridium complexes using these spiro-based ligands was confirmed by ^{1}H NMR, ^{13}C NMR, UV-Vis, PL and CV results.

These new iridium complexes, whose optical properties are determined by UV-Vis and PL spectrometer have realized green and orange color light emission. Absorption measurements revealed that all compounds absorbed in the UV region (between 260 and 430 nm). The absorption spectra of the compounds showed a small amount (~1 nm) of redshift from C1 to C4. Iridium complexes from C5 to C8 are similar in absorbance change as the same ligands are modified to the group N^N. Transitions in the 300 nm region originate from the ligands and it is known that the absorbance between 350-430 nm originates from the complexes. The PL spectrum of complexes C1-C4 emit orange light, whose peak wavelengths occur in the range of 572-578 nm and the complexes C5-C8 emit green light, whose peak wavelengths occur in the range of 511- 519 nm. According to the light emitting theory by changing the structure of the ligand bonded to the metal core, the light emission of the complexes can be tuned. In the group of C1-C4 complexes, red shifts are observed as adding methoxy groups. The reason is that the methoxy groups bonded to the molecule will increase the electron density in the main structure and increase the tendency of electron-donating.

HOMO and LUMO energy levels and energy band gap of all the complexes were determined by cyclic voltammogram analysis. Using the CV measurements, the energy band gaps of these compounds were determined by calculating the oxidation and reduction potentials in the solution. The energy band gaps of the synthesized compounds were found to be 2.65, 2.63, 2.60 and 2.51 eV for C1, C2, C3, C4

complexes, respectively. Similarly, CV measurements of the complexes C5, C6, C7, C8 were obtained and the energy band gaps of these compounds were found to be 2.92, 2.87, 2.68 and 2.57 eV, respectively. The reason for reduction of these band gaps is due to the increase of the electron donating methoxy group in the Spiro molecule, used as an auxiliary ligand. On the other hand, the reason for the blue shift or higher band gap energies observed in C5-C8 relative to C1-C5 is that the Ir metal core of the C5-C8 complexes contain electron withdrawing fluorine atoms.

Four devices were constructed by using C2, C4, C6, and C8 complexes as emissive layer. The device configuration was in the form of simple two layer; ITO/PEDOT:PSS/Ir(III)complex/Al. It has been found that these devices operate at low operating voltages, such as 5.1 to 5.8 V. At these low voltages, luminance values have reached up to 1107 cd /m2, which is a promising value compared to the current literature. The peak luminance values were obtained as 1107, 277, 30, and 15 cd /m^2 for C2, C4, C6, and C8 devices respectively. The peak EQE values were obtained as 4%, 0.1%, 0.1%, and <0.1% for C2, C4, C6, and C8 devices respectively. Decrease in device efficiency appears to be influenced by the presence of methoxy groups. These methoxides are thought to cause a loss of charge by reducing the electron density which are transferred from ligand to the metal. When they are increased, it is believed that the efficiency of the device is reduced due to the decrease of the positive charge on the metal and therefore the decrease of electrons from metal to ligand by charge transition.

The EL spectrum of the OLED device contain two intense peaks for each device. The EL peaks of devices using C2, C4, C6, and C8 emissive materials were obtained as (561, 595 nm), (563, 595 nm), (544, 599 nm), and (546, 598 nm) respectively. The average EL values of devices using C2, C4, C6, and C8 were obtained as 578 nm (yellow), 579 nm (yellow), 571 nm (yellowish) and 572 nm (yellowish) with corresponding CIE coordinates (0.499, 0.499), (0.506, 0.493), (0.451, 0.547), and (0.458, 0.541) respectively.

These complexes used as an emissive layer have achieved device performance in the current literature even without adding any additional material such as ionic liquid. This holds great promise for devices created using these Ir(III) complexes that better results will be achieved by optimizing the processes of OLED devices.

As a result of the studies carried out within the scope of this thesis, valuable information has been obtained for the Ir complexes planned to be used for both OLED and LEC. Due to the fact that the structure of these iridium complexes is in salt form, it is thought that charge transport and electron mobilities are very advantageous to other Ir complexes. Given the results obtained in this thesis, it is considered that the Ir complexes obtained in this salt form may be an alternative for LEC devices.

4. REFERENCES

[1]   **Edison, T.A.**, *Electric lamp*, 1880, Google Patents.

[2]   **Germer, E., F. Meyer, and H.-J. Spanner**, *Metal vapor lamp*, 1939, Google Patents.

[3]   **West, R.S**., et al. *43.4: High Brightness Direct LED Backlight for LCD-TV*. in *SID Symposium Digest of Technical Papers*. 2003. Wiley Online Library.

[4]   **Round, H.**, *The electroluminescence of inorganic materials.* Electrical World, 1907. 9: p. 309.

[5]   **Destriau, G**., *Recherches sur les scintillations des sulfures de zinc aux rayons α.* Journal de Chimie Physique, 1936. 33: p. 587-625.

[6]   **M. Pope, H.P.K., and P. Magnante,** *Electroluminescence in Organic Crystals.* J. Chem. Phys. , 1963.

[7]   **Tang, C.W. and S.A. VanSlyke,** *Organic electroluminescent diodes.* Applied physics letters, 1987. 51(12): p. 913-915.

[8]   **Burroughes, J.**, et al., *Light-emitting diodes based on conjugated polymers.* nature, 1990. 347(6293): p. 539-541.

[9]   25/02/2017; http://pioneer.jp/en/info/history/.

[10]   N.o.N.M.A. *The Nobel Prize in Chemistry 2000*. 22 Nov 2017; http://www.nobelprize.org/nobel_prizes/chemistry/laureates/2000/.

[11]   25/02/2017; http://www.oled-info.com/history-page-2.

[12]   25/02/2017; http://globonsomeday.blogspot.com.tr/2010/02/oled-wallpapers-could-make-light-bulbs.html.

[13]   25/02/2017; http://gadget-demo.blogspot.com.tr/2010/01/rolltop-laptop-from-future.html.

[14]   25/02/2017;https://tr.pinterest.com/netizenpros/flexible-oled-gadgets/.

[15]   25/02/2017;http://www.printedelectronicsworld.com/articles/4497/data-eye-glasses-based-on-bidirectional-oled-microdisplays.

[16]   **de Gans, B.J. and U.S. Schubert**, *Inkjet Printing of Polymer Micro-Arrays and Libraries: Instrumentation, Requirements, and Perspectives.* Macromolecular Rapid Communications, 2003. 24(11): p. 659-666.

[17]   **Shi, J. and C.W. Tang**, *Doped organic electroluminescent devices with improved stability.* Applied physics letters, 1997. 70(13): p. 1665-1667.

[18]   **Kido, J.**, et al., *1, 2, 4-triazole derivative as an electron transport layer in organic electroluminescent devices.* Japanese journal of applied physics, 1993. 32(7A): p. L917.

[19]   **Yang, Y. and Q. Pei**, *Light-emitting electrochemical cells from a blend of p- and n-type luminescent conjugated polymers.* Applied physics letters, 1997. 70(15): p. 1926-1928.

[20]   **Noh, Y.-Y.**, et al., *Energy transfer and device performance in phosphorescent dye doped polymer light emitting diodes.* The Journal of chemical physics, 2003. 118(6): p. 2853-2864.

[21]   **Sudhakar, M.**, et al., *Phosphorescence quenching by conjugated polymers.* Journal of the American Chemical Society, 2003. 125(26): p. 7796-7797.

[22]   **Baldo, M.A.**, et al., *Highly efficient phosphorescent emission from organic electroluminescent devices.* Nature, 1998. 395(6698): p. 151-154.

[23]   **Adachi, C.**, et al., *High-efficiency organic electrophosphorescent devices with tris (2-phenylpyridine) iridium doped into electron-transporting materials.* Applied Physics Letters, 2000. 77(6): p. 904-906.

[24]   **Adachi, C.**, et al., *Nearly 100% internal phosphorescence efficiency in an organic light-emitting device.* Journal of Applied Physics, 2001. 90(10): p. 5048-5051.

[25]   **de Bettencourt-Dias, A**., *Lanthanide-based emitting materials in light-emitting diodes.* Dalton Transactions, 2007(22): p. 2229-2241.

[26]   **Ma, B., P.I. Djurovich, and M.E. Thompson,** *Excimer and electron transfer quenching studies of a cyclometalated platinum complex.* Coordination chemistry reviews, 2005. 249(13): p. 1501-1510.

[27]   **Slinker, J.,** et al., *Solid-state electroluminescent devices based on transition metal complexes.* Chemical Communications, 2003(19): p. 2392-2399.

[28]   **Holder, E., B.M. Langeveld, and U.S. Schubert**, *New trends in the use of transition metal–ligand complexes for applications in electroluminescent devices.* Advanced Materials, 2005. 17(9): p. 1109-1121.

[29]   **Jung, S.**, et al., *Surface treatment effects of indium–tin oxide in organic light-emitting diodes.* Optical Materials, 2003. 21(1): p. 235-241.

[30]   **Zhong, Z. and Y. Jiang**, *The surface properties of treated ITO substrates effect on the performance of OLEDs.* The European Physical Journal-Applied Physics, 2006. 34(3): p. 173-177.

[31]   **Chen, F.-C.**, et al., *Copper phthalocyanine buffer layer to enhance the charge injection in organic thin-film transistors.* Applied physics letters, 2007. 90(7): p. 073504.

[32]   **Yu, W.-L.**, et al., *Hole-injection enhancement by copper phthalocyanine (CuPc) in blue polymer light-emitting diodes.* Journal of Applied Physics, 2001. 89(4): p. 2343-2350.

[33]   **Ho, P.K.**, et al., *Molecular-scale interface engineering for polymer light-emitting diodes.* Nature, 2000. 404(6777): p. 481-484.

[34]   **De Kok, M.**, et al., *Modification of PEDOT: PSS as hole injection layer in polymer LEDs.* physica status solidi (a), 2004. 201(6): p. 1342-1359.

[35]   **Agarwal, N. and P.K. Nayak**, *Synthesis, characterization, photophysical and electrochemical properties of new phosphorescent dopants for OLEDs.* Tetrahedron Letters, 2008. 49(17): p. 2710-2713.

[36]   **Qiu, C.**, et al., *Dopant emission mechanism and the effects of host materials on the behavior of doped organic light-emitting diodes.* IEEE Transactions on Electron Devices, 2002. 49(9): p. 1540-1544.

[37]   **Duan, J.-P., P.-P. Sun, and C.-H. Cheng**, *New iridium complexes as highly efficient Orange–Red emitters in organic Light-Emitting diodes.* Advanced Materials, 2003. 15(3): p. 224-228.

[38]   **Baldo, M.**, et al., *Very high-efficiency green organic light-emitting devices based on electrophosphorescence.* Applied Physics Letters, 1999. 75(1): p. 4-6.

[39]   **Le, Q.T.,** et al., *Photoemission study of the interface between phenyl diamine and treated indium–tin–oxide.* Applied physics letters, 1999. 75(10): p. 1357-1359.

[40]   **Smith, L.,** J. Wasey, and W.L. Barnes, *Light outcoupling efficiency of top-emitting organic light-emitting diodes.* Applied Physics Letters, 2004. 84(16): p. 2986-2988.

[41]   **Wu, F.-I.,** et al., *Highly efficient red-electrophosphorescent devices based on polyfluorene copolymers containing charge-transporting pendant units.* The Journal of Physical Chemistry B, 2005. 109(29): p. 14000-14005.

[42]	**Chang, B.J.,** et al., *Characteristics of emissive bilayers in electrophosphorescent organic light-emitting diodes.* Current Applied Physics, 2006. 6(4): p. 658-662.

[43]	**Yu, X.-M**., et al., *High-efficiency white organic light-emitting devices based on a highly amorphous iridium (III) orange phosphor.* Chemistry of materials, 2006. 18(21): p. 5097-5103.

[44]	**Ragni, R.,** et al., *Blue emitting iridium complexes: synthesis, photophysics and phosphorescent devices.* Journal of Materials Chemistry, 2006. 16(12): p. 1161-1170.

[45]	**Kim, Y. and W. Im**, *Effect of hole-blocking layer doped with electron-transport molecules on the performance of blue organic light-emitting device.* physica status solidi (a), 2004. 201(9): p. 2148-2153.

[46]	**Kulkarni, A.P.**, et al., *Electron transport materials for organic light-emitting diodes.* Chemistry of materials, 2004. 16(23): p. 4556-4573.

[47]	**Bettenhausen, J.**, et al., *Electron transport in a starburst oxadiazole.* Journal of applied physics, 1997. 82(10): p. 4957-4961.

[48]	**Beeby, A.**, et al., *Tuning the emission of cyclometalated iridium complexes by simple ligand modification.* Journal of Materials Chemistry, 2003. 13(1): p. 80-83.

[49]	**Choudhury, B.**, *Organic light emitting devices (OLEDs) and structurally integrated photoluminescence based chemical and biological sensors excited by OLEDs.* 2005.

[50]	**Zheludev, N.**, *The life and times of the LED—a 100-year history.* Nature Photonics, 2007. 1(4): p. 189-192.

[51]	**Moore, T**., *Cyclometallated iridium-carbazole complexes for OLED applications*, 2008, Durham University.

[52]	**Baldo, M.**, et al., *Excitonic singlet-triplet ratio in a semiconducting organic thin film.* Physical Review B, 1999. 60(20): p. 14422.

[53]	**Rothe, C., S. King, and A. Monkman**, *Direct measurement of the singlet generation yield in polymer light-emitting diodes.* Physical review letters, 2006. 97(7): p. 076602.

[54]	**Baldo, M.A., M. Thompson, and S. Forrest**, *Phosphorescent materials for application to organic light emitting devices.* Pure and Applied Chemistry, 1999. 71(11): p. 2095-2106.

[55]   **Haskins-Glusac, K.**, et al., *Luminescence quenching of a phosphorescent conjugated polyelectrolyte.* Journal of the American Chemical Society, 2004. 126(45): p. 14964-14971.

[56]   **Chen, C. and J. Shi**, *Metal chelates as emitting materials for organic electroluminescence.* Coordination chemistry reviews, 1998. 171: p. 161-174.

[57]   **Okumoto, K.**, et al., *Green fluorescent organic light-emitting device with external quantum efficiency of nearly 10%.* Applied physics letters, 2006. 89(6): p. 063504.

[58]   **Dini, D.**, *Electrochemiluminescence from organic emitters.* Chemistry of materials, 2005. 17(8): p. 1933-1945.

[59]   **Rees, I.D.**, et al., *Recent developments in light-emitting polymers.* MRS bulletin, 2002. 27(6): p. 451-455.

[60]   **Berggren, M**., et al., *White light from an electroluminescent diode made from poly [3 (4-octylphenyl)-2, 2'-bithiophene] and an oxadiazole derivative.* Journal of Applied Physics, 1994. 76(11): p. 7530-7534.

[61]   **Bundgaard, E. and F.C. Krebs**, *Low-band-gap conjugated polymers based on thiophene, benzothiadiazole, and benzobis (thiadiazole).* Macromolecules, 2006. 39(8): p. 2823-2831.

[62]   **Jing, W.-X.**, et al., *Synthesis of a polyphenylene light-emitting polymer.* Synthetic Metals, 1994. 67(1-3): p. 161-163.

[63]   **Chen, F.-C., Q. Xu, and Y. Yang**, *Enhanced efficiency of plastic photovoltaic devices by blending with ionic solid electrolytes.* Applied physics letters, 2004. 84(16): p. 3181-3183.

[64]   **Mitschke, U. and P. Bäuerle**, *The electroluminescence of organic materials.* Journal of Materials Chemistry, 2000. 10(7): p. 1471-1507.

[65]   **Kraft, A., A.C. Grimsdale, and A.B. Holmes**, *Electroluminescent conjugated polymersÐseeing polymers in a new light.* Angew. Chem. Int. End Engl, 1998. 37: p. 402-428.

[66]   **Hotta, S. and K. Waragai**, *Crystal structures of oligothiophenes and their relevance to charge transport.* Advanced materials, 1993. 5(12): p. 896-908.

[67]   **Klärner, G.**, et al., *Colorfast blue-light-emitting random copolymers derived from di-n-hexylfluorene and anthracene.* Advanced Materials, 1998. 10(13): p. 993-997.

[68] **Rathnayake, H.P.**, et al., *Optimizing OLED Efficacy of 2, 7-Diconjugated 9, 9-Dialkylfluorenes by Variation of Periphery Substitution and Conjugation Length.* Advanced Functional Materials, 2007. 17(1): p. 115-122.

[69] **Zhou, X.-H.**, et al., *Effect of Fluorenone Units on the Property of Polyfluorene and Oligofluorene Derivatives: Synthesis, Structure− Properties Relationship, and Electroluminescence.* Macromolecules, 2006. 39(11): p. 3830-3840.

[70] **Tang, K.-C., K.L. Liu, and I.-C. Chen**, *Rapid intersystem crossing in highly phosphorescent iridium complexes.* Chemical physics letters, 2004. 386(4): p. 437-441.

[71] **Kido, J.**, et al., *Bright red light-emitting organic electroluminescent devices having a europium complex as an emitter.* Applied physics letters, 1994. 65(17): p. 2124-2126.

[72] **O'brien, D.**, et al., *Improved energy transfer in electrophosphorescent devices.* Applied Physics Letters, 1999. 74(3): p. 442-444.

[73] **Adachi, C.**, et al., *Endothermic energy transfer: A mechanism for generating very efficient high-energy phosphorescent emission in organic materials.* Applied Physics Letters, 2001. 79(13): p. 2082-2084.

[74] **Xia, H.**, et al., *Ruthenium (II) complex as phosphorescent dopant for highly efficient red polymers light-emitting diodes.* The Journal of Physical Chemistry B, 2004. 108(10): p. 3185-3190.

[75] **Tung, Y.L.**, et al., *Orange and Red Organic Light-Emitting Devices Employing Neutral Ru (II) Emitters: Rational Design and Prospects for Color Tuning.* Advanced Functional Materials, 2006. 16(12): p. 1615-1626.

[76] **Tung, Y.-L.**, et al., *Highly efficient red phosphorescent osmium (II) complexes for OLED applications.* Organometallics, 2004. 23(15): p. 3745-3748.

[77] **Liu, T.-H. and C.H. Chen**, *Organic light-emitting devices based on a highly robust osmium (II) complex.* Journal of applied physics, 2006. 100(9): p. 094508.

[78] **Wang, Y.**, et al., *Highly efficient electroluminescent materials based on fluorinated organometallic iridium compounds.* Applied Physics Letters, 2001. 79(4): p. 449-451.

[79] **Chen, F.-C.**, et al., *High-performance polymer light-emitting diodes doped with a red phosphorescent iridium complex.* Applied Physics Letters, 2002. 80(13): p. 2308-2310.

[80]   **Ikai, M.**, et al., *Highly efficient phosphorescence from organic light-emitting devices with an exciton-block layer.* Applied Physics Letters, 2001. 79(2): p. 156-158.

[81]   **He, G.**, et al., *High-efficiency and low-voltage p-i-n electrophosphorescent organic light-emitting diodes with double-emission layers.* Applied Physics Letters, 2004. 85(17): p. 3911-3913.

[82]   **Holmes, R.**, et al., *Blue organic electrophosphorescence using exothermic host–guest energy transfer.* Applied Physics Letters, 2003. 82(15): p. 2422-2424.

[83]   **Holmes, R.**, et al., *Efficient, deep-blue organic electrophosphorescence by guest charge trapping.* Applied Physics Letters, 2003. 83(18): p. 3818-3820.

[84]   **Pei, Q.**, et al., *Polymer light-emitting electrochemical cells.* Science, 1995. 269(5227): p. 1086.

[85]   **Lee, J.K.**, et al., *Thin film light emitting devices from an electroluminescent ruthenium complex.* Applied physics letters, 1996. 69(12): p. 1686-1688.

[86]   **Gao, F.G. and A.J. Bard**, *Solid-state organic light-emitting diodes based on tris (2, 2 ‘-bipyridine) ruthenium (II) complexes.* Journal of the American Chemical Society, 2000. 122(30): p. 7426-7427.

[87]   **Slinker, J.D.**, et al., *Efficient yellow electroluminescence from a single layer of a cyclometalated iridium complex.* Journal of the american chemical society, 2004. 126(9): p. 2763-2767.

[88]   **Slinker, J.D.**, et al., *Direct measurement of the electric-field distribution in a light-emitting electrochemical cell.* Nature materials, 2007. 6(11): p. 894-899.

[89]   **Bernhard, S.**, et al., *Efficient electroluminescent devices based on a chelated osmium (II) complex.* Advanced Materials, 2002. 14(6): p. 433.

[90]   **Hu, T.**, et al., *Solid-state light-emitting electrochemical cells based on ionic iridium (iii) complexes.* Journal of Materials Chemistry, 2012. 22(10): p. 4206-4215.

[91]   **Lowry, M.S.**, et al., *Single-Layer Electroluminescent Devices and Photoinduced Hydrogen Production from an Ionic Iridium(III) Complex.* Chemistry of Materials, 2005. 17(23): p. 5712-5719.

[92]   **Nazeeruddin, M.K.**, et al., *Efficient green-blue-light-emitting cationic iridium complex for light-emitting electrochemical cells.* Inorganic chemistry, 2006. 45(23): p. 9245-9250.

[93]   **Hsieh, C.H.**, et al., *Design and synthesis of iridium bis (carbene) complexes for efficient blue electrophosphorescence.* Chemistry-A European Journal, 2011. 17(33): p. 9180-9187.

[94]   **He, L.**, et al., *Toward Highly Efficient Solid-State White Light-Emitting Electrochemical Cells: Blue-Green to Red Emitting Cationic Iridium Complexes with Imidazole-Type Ancillary Ligands.* Advanced Functional Materials, 2009. 19(18): p. 2950-2960.

[95]   **Costa, R.D.**, et al., *Efficient deep-red light-emitting electrochemical cells based on a perylenediimide-iridium-complex dyad.* Chemical Communications, 2009(26): p. 3886-3888.

[96]   **Su, H.-C.**, et al., *Solid-state white light-emitting electrochemical cells using iridium-based cationic transition metal complexes.* Journal of the American Chemical Society, 2008. 130(11): p. 3413-3419.

[97]   **Baranoff, E.**, et al., *Tuning the photophysical properties of cationic iridium (iii) complexes containing cyclometallated 1-(2, 4-difluorophenyl)-1 H-pyrazole through functionalized 2, 2'-bipyridine ligands: blue but not blue enough.* Dalton Transactions, 2013. 42(4): p. 1073-1087.

[98]   **Lawrence, C.**, *The mechanics of spin coating of polymer films.* The Physics of fluids, 1988. 31(10): p. 2786-2795.

[99]   **Gil, T.H.**, et al., *Origin of damages in OLED from Al top electrode deposition by DC magnetron sputtering.* Organic Electronics, 2010. 11(2): p. 322-331.

[100]   **Yang, J.-S. and T.M. Swager**, *Porous shape persistent fluorescent polymer films: an approach to TNT sensory materials.* Journal of the American Chemical Society, 1998. 120(21): p. 5321-5322.

[101]   **Johansson, N.**, et al., *Electronic structure and optical properties of electroluminescent spiro-type molecules.* The Journal of chemical physics, 1997. 107(7): p. 2542-2549.

[102]   **Kim, J.**, *Assemblies of conjugated polymers: intermolecular and intramolecular effects on the photophysical properties of conjugated polymers.* Pure and applied chemistry, 2002. 74(11): p. 2031-2044.

[103]   **Miyaura, N., K. Yamada, and A. Suzuki**, *A new stereospecific cross-coupling by the palladium-catalyzed reaction of 1-alkenylboranes with 1-alkenyl or 1-alkynyl halides.* Tetrahedron Letters, 1979. 20(36): p. 3437-3440.

[104] **Miyaura, N. and A. Suzuki**, *Stereoselective synthesis of arylated (E)-alkenes by the reaction of alk-1-enylboranes with aryl halides in the presence of palladium catalyst.* Journal of the Chemical Society, Chemical Communications, 1979(19): p. 866-867.

[105] **Suzuki, A., R.F. Heck, and E.-i. Negishi**, *The Nobel Prize in Chemistry 2010.* 2010.

[106] **Heck, R.F., E.-i. Negishi, and A. Suzuki**, *For palladium-catalyzed cross couplings in organic synthesis*, 2010, Nobel Prize in Chemistry.

[107] **Miyaura, N. and A. Suzuki**, *Palladium-catalyzed cross-coupling reactions of organoboron compounds.* Chemical reviews, 1995. 95(7): p. 2457-2483.

[108] **Stanforth, S.P.**, *Catalytic cross-coupling reactions in biaryl synthesis.* Tetrahedron, 1998. 54(3): p. 263-303.

[109] **Su, H.C.**, et al., *Highly Efficient Orange and Green Solid-State Light-Emitting Electrochemical Cells Based on Cationic IrIII Complexes with Enhanced Steric Hindrance.* Advanced Functional Materials, 2007. 17(6): p. 1019-1027.

[110] **Wu, H.**, *Metal-organic compounds of iridium (III) and platinum (II): synthesis, characterization and optoelectronic applications.* 2014.

[111] **Nonoyama, M.**, *Benzo [h] quinolin-10-yl-N Iridium (III) Complexes.* Bulletin of the Chemical Society of Japan, 1974. 47(3): p. 767-768.

[112] **Garand, E.**, et al., *Characterization of an activated iridium water splitting catalyst using infrared photodissociation of H 2 tagged ions.* Physical Chemistry Chemical Physics, 2012. 14(29): p. 10109-10113.

[113] **Lowry, M.S. and S. Bernhard**, *Synthetically tailored excited states: phosphorescent, cyclometalated iridium (III) complexes and their applications.* Chemistry-A European Journal, 2006. 12(31): p. 7970-7977.

[114] **Arm, K.J., W. Leslie, and J.G. Williams**, *Synthesis and pH-sensitive luminescence of bis-terpyridyl iridium (III) complexes incorporating pendent pyridyl groups.* Inorganica chimica acta, 2006. 359(4): p. 1222-1232.

[115] **Schneider, G.E.**, *Ionic transition metal complexes containing iridium (III) for lighting applications*, 2013, University_of_Basel.

[116] **Yuan, Y.-J.**, et al., *Impact of ligand modification on hydrogen photogeneration and light-harvesting applications using cyclometalated iridium complexes.* Inorganic chemistry, 2012. 51(7): p. 4123-4133.

[117] **Jiang, W.**, et al., *Zwitterionic iridium complexes: synthesis, luminescent properties, and their application in cell imaging.* Inorganic chemistry, 2010. 49(7): p. 3252-3260.

[118] **Chen, T.-R., H.-P. Lee, and J.-D. Chen**, *Water Attack Umpolung Aromatic Systems To Release Hydrogen.* Inorganic chemistry, 2011. 50(8): p. 3645-3650.

[119] **Costa, R.D**., et al., *Archetype Cationic Iridium Complexes and Their Use in Solid-State Light-Emitting Electrochemical Cells.* Advanced Functional Materials, 2009. 19(21): p. 3456-3463.

[120] **Frohleiks, J**., et al., *Quantum Dot/Light-Emitting Electrochemical Cell Hybrid Device and Mechanism of Its Operation.* ACS applied materials & interfaces, 2016. 8(37): p. 24692-24698.

[121] **Bolink, H.J**., et al., *Origin of the large spectral shift in electroluminescence in a blue light emitting cationic iridium (III) complex.* Journal of Materials Chemistry, 2007. 17(48): p. 5032-5041.

A. APPENDIX

A.1. NMR Measurements of the Ligands

L1 H·NMR
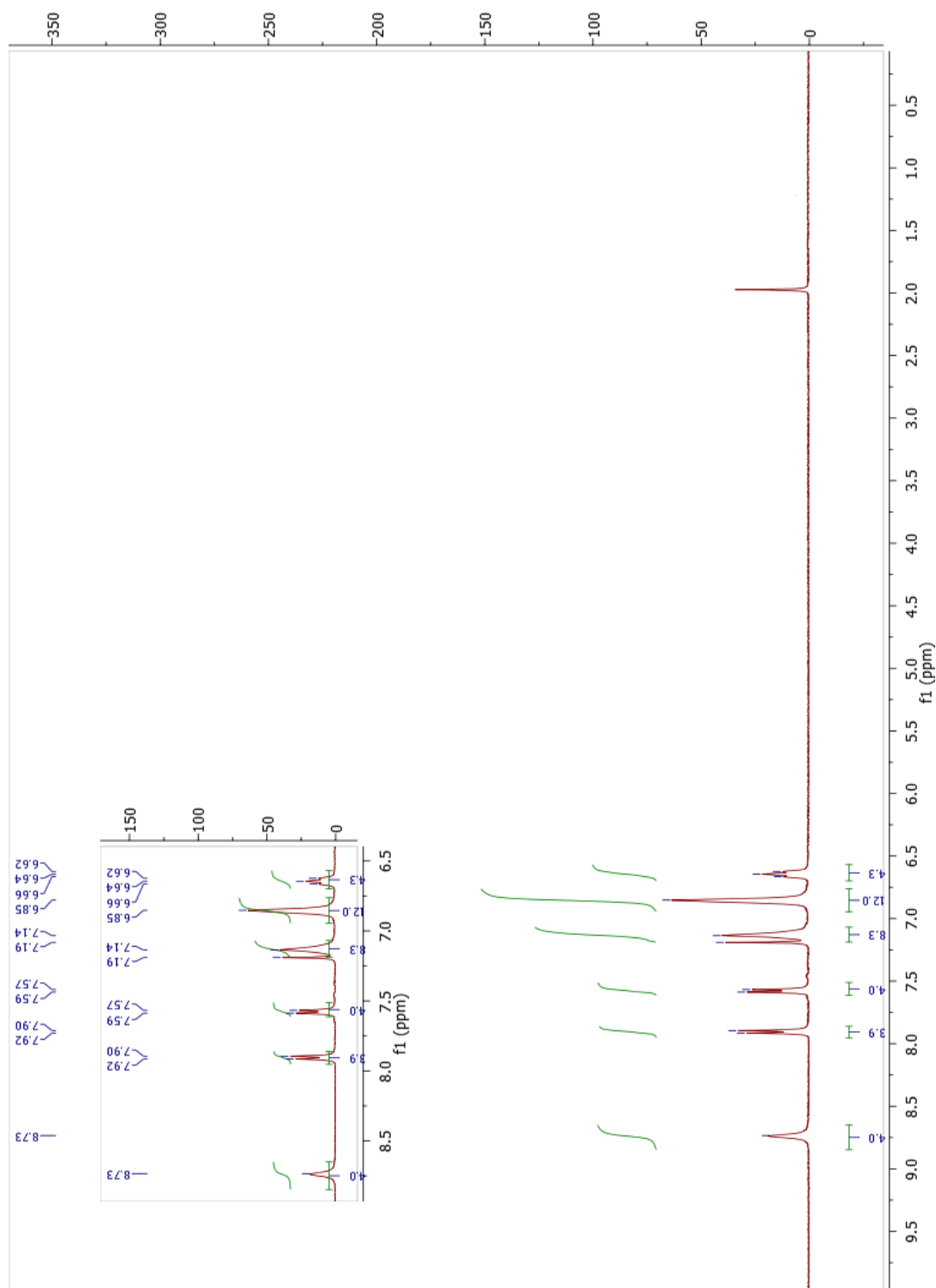
Figure A.1: ^{1}H'NMR spectrum of L1

L1 C·NMR
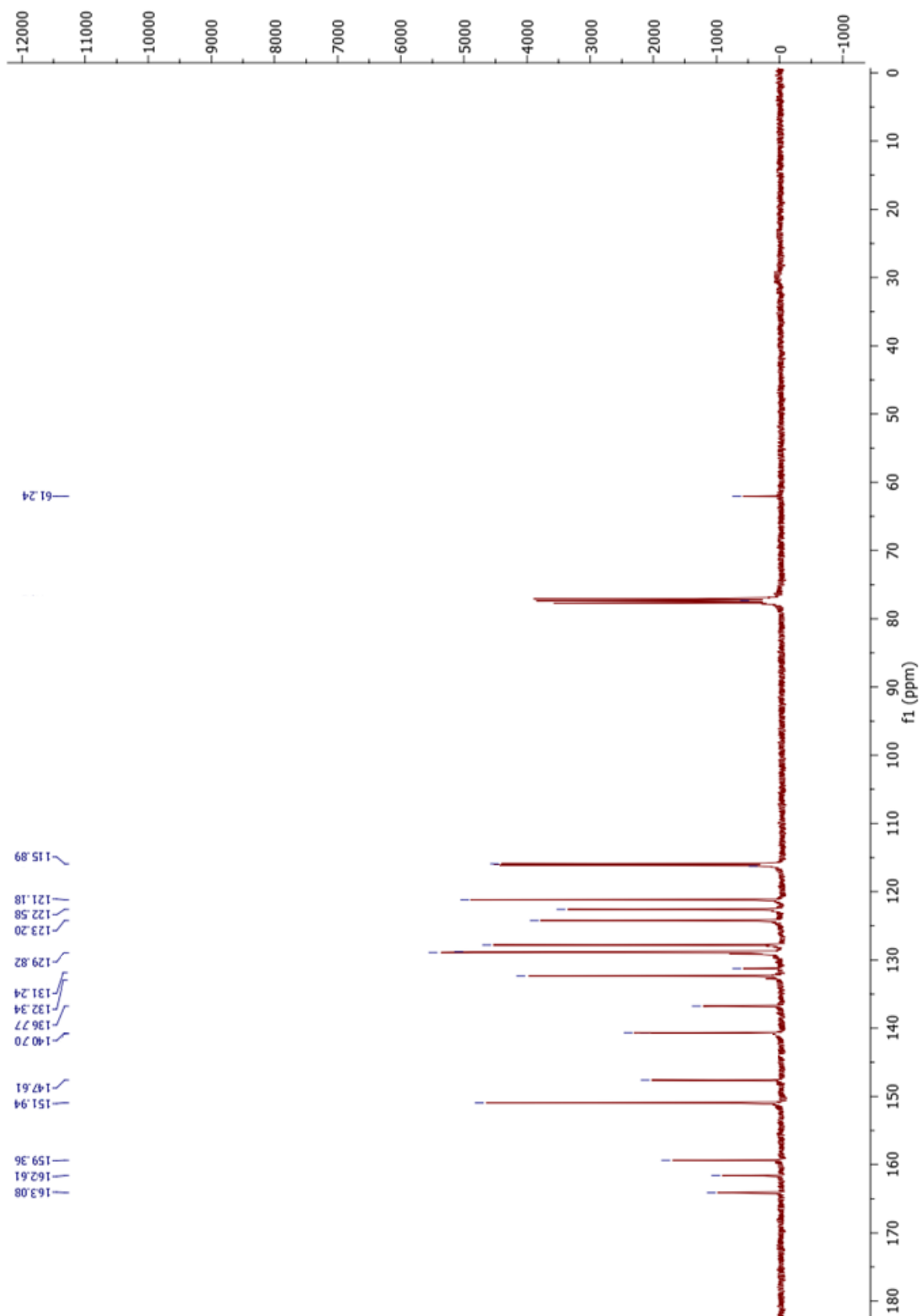
Figure A.2: ^{13}C'NMR spectrum of L1

L2 H·NMR
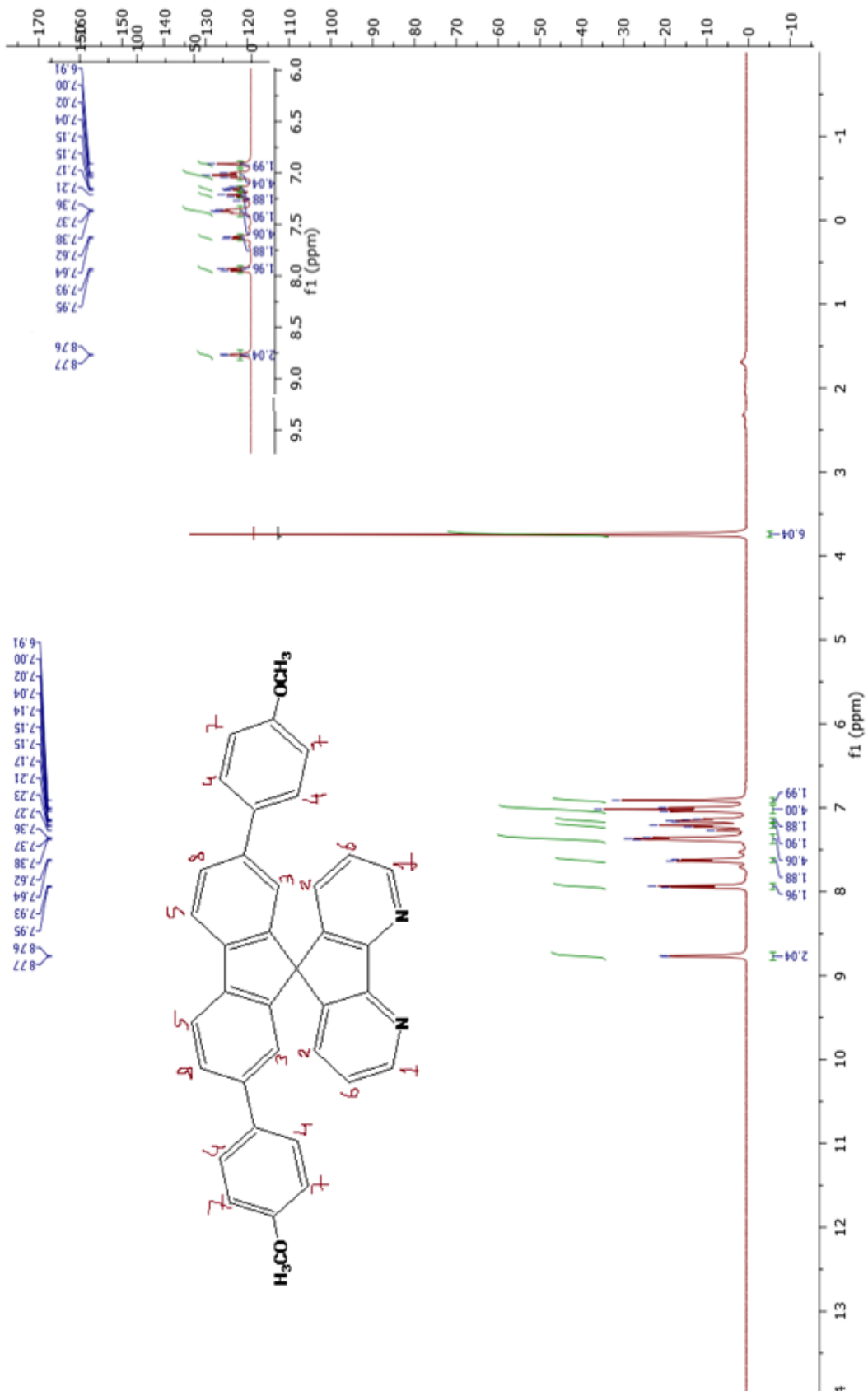
Figure A.3: [1]H'NMR spectrum of L2

L2 C·NMR
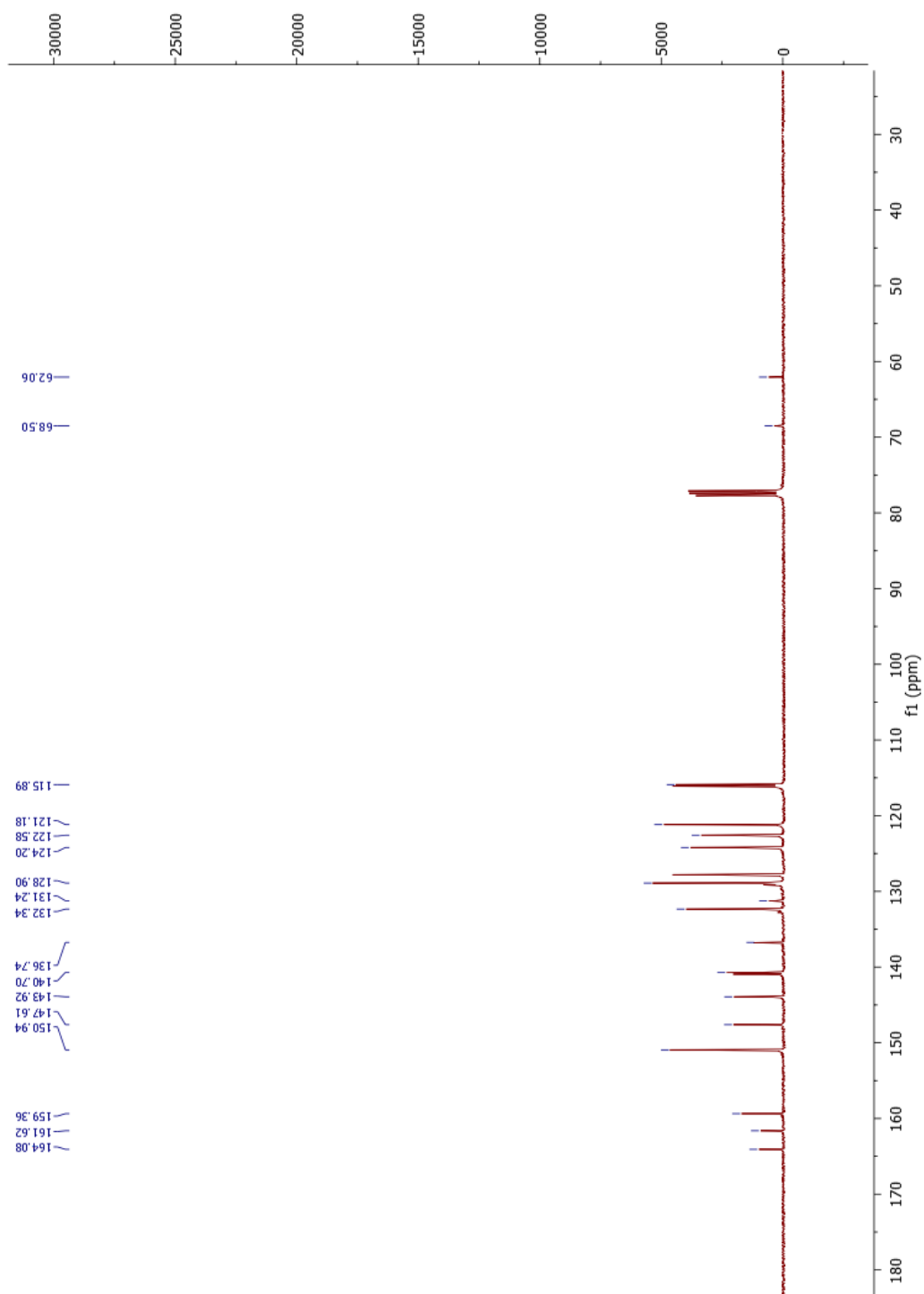
Figure A.4: ^{13}C'NMR spectrum of L2

L3 H·NMR
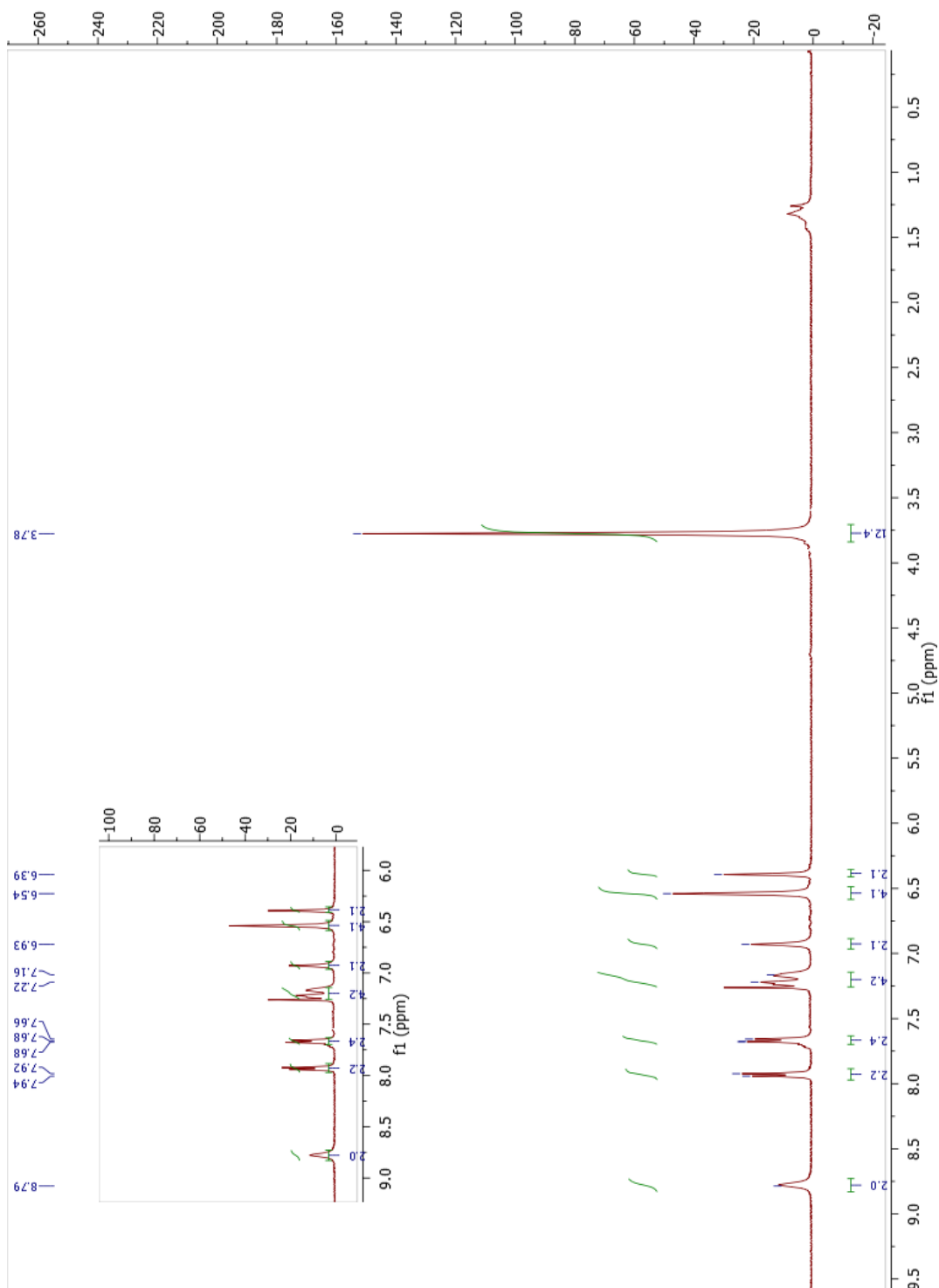
Figure A.5: [1]H'NMR spectrum of L3

L3 C·NMR

Peak labels (ppm): 55.46, 61.75, 99.40, 105.32, 120.69, 122.44, 123.82, 127.71, 132.07, 140.97, 141.30, 142.60, 143.57, 147.18, 150.52, 159.03, 161.07
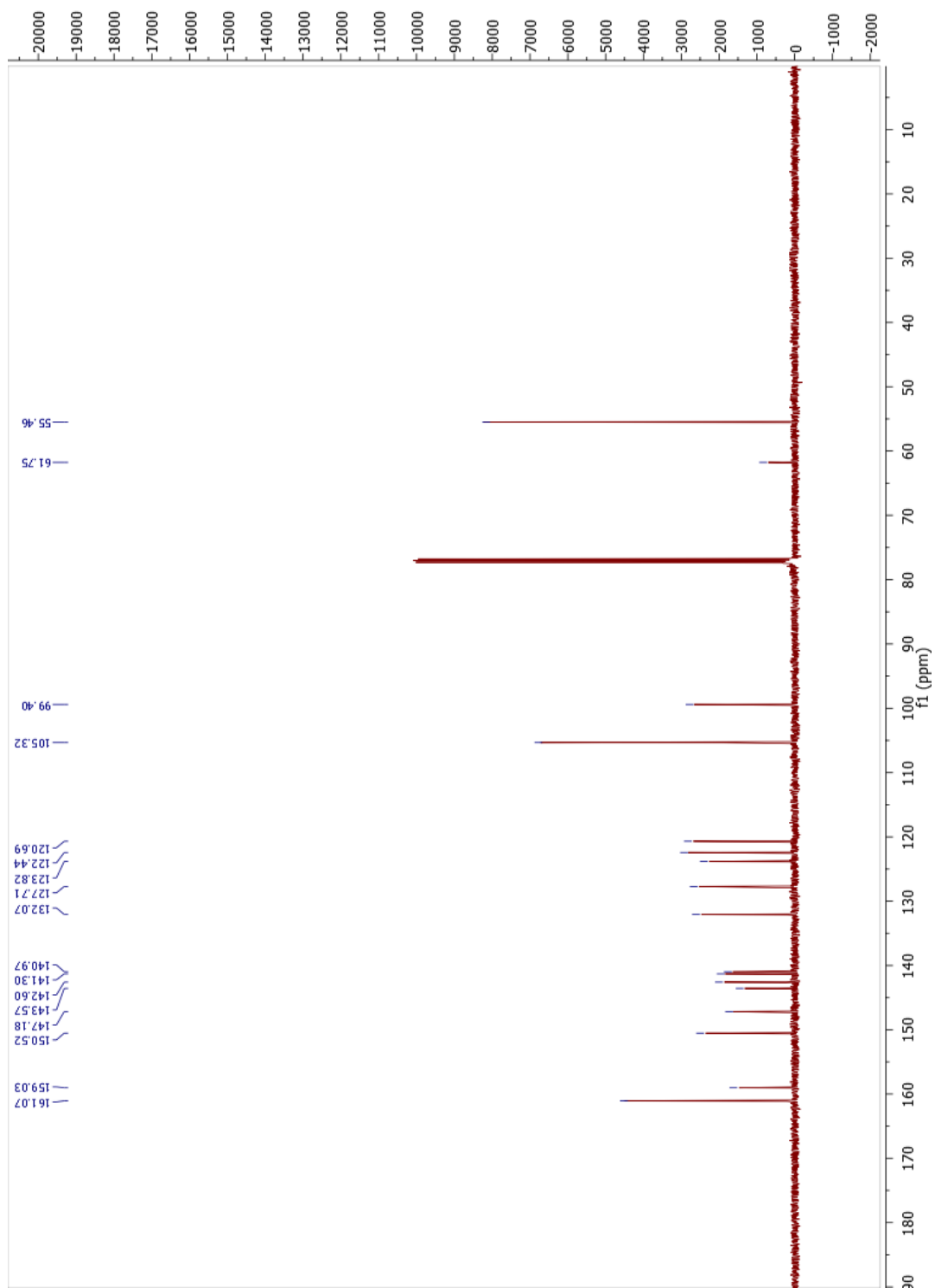
Figure A.6: [13]C'NMR spectrum of L3

L4 H·NMR
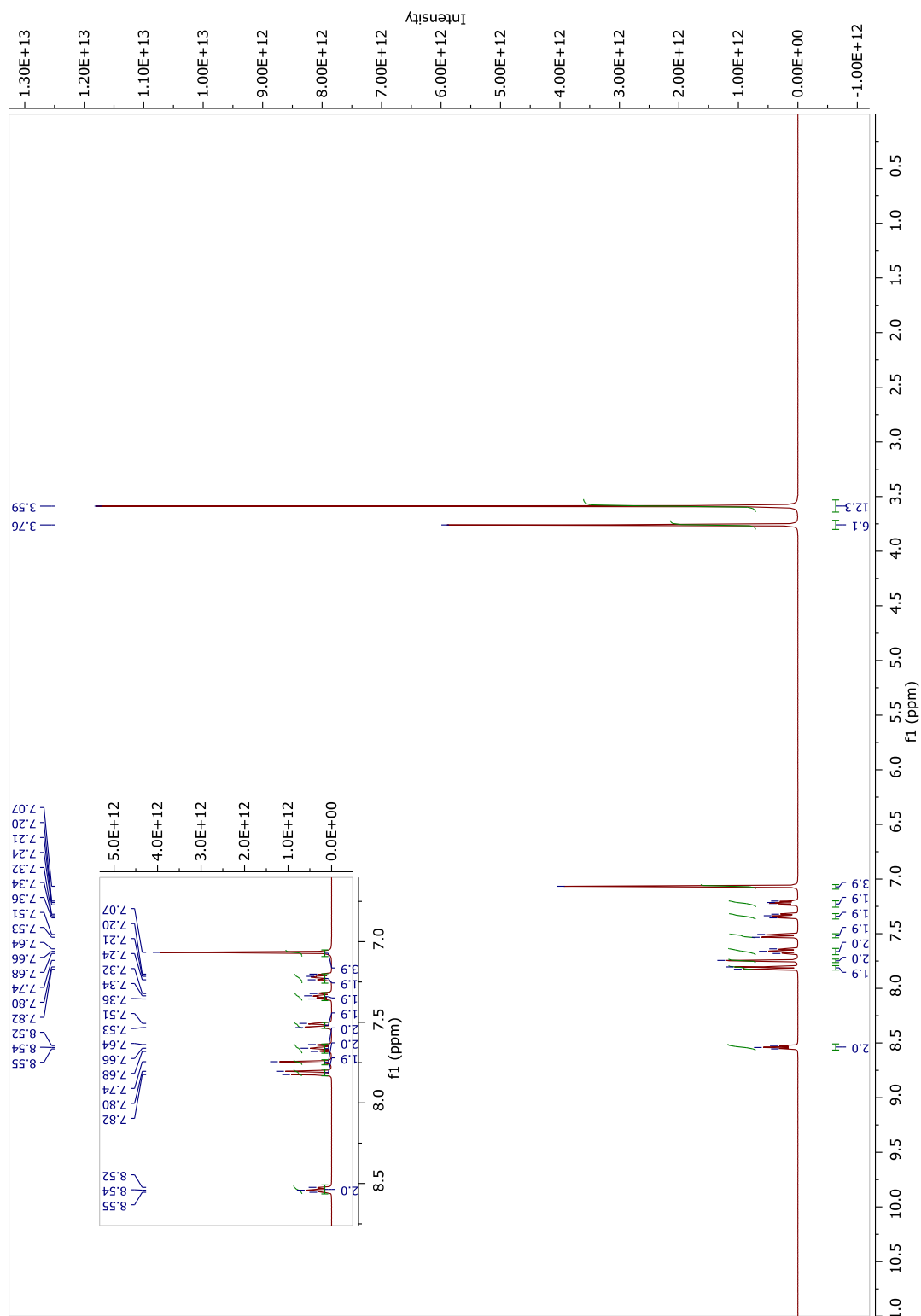
Figure A.7: [1]H'NMR spectrum of L4

L4- C·NMR
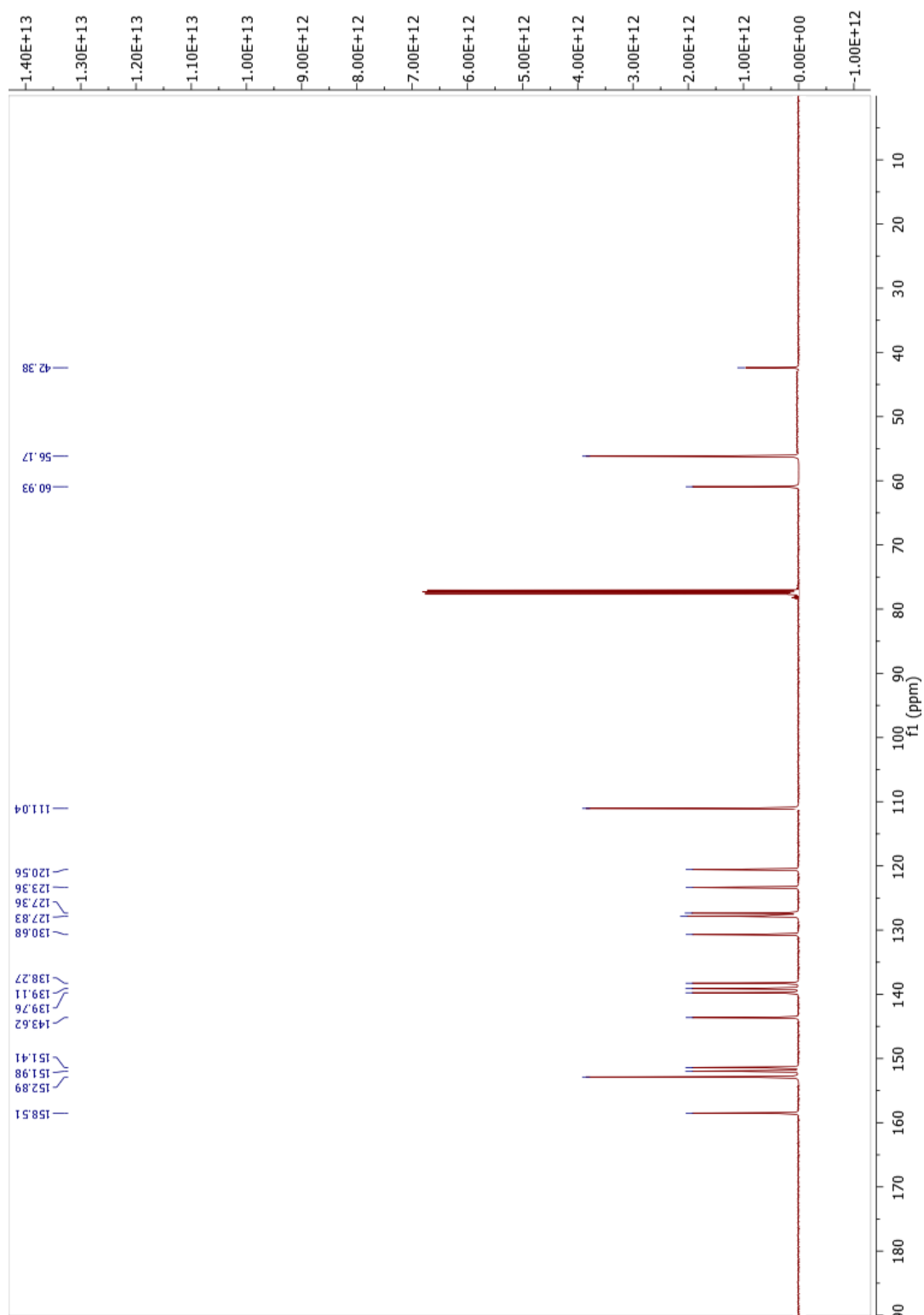
Figure A.8: $^{13}C'NMR$ spectrum of L4

A.2. NMR Measurements of the Complexes

C1-H'NMR

Figure A.9: ^{1}H'NMR spectrum of C1

C1-C'NMR
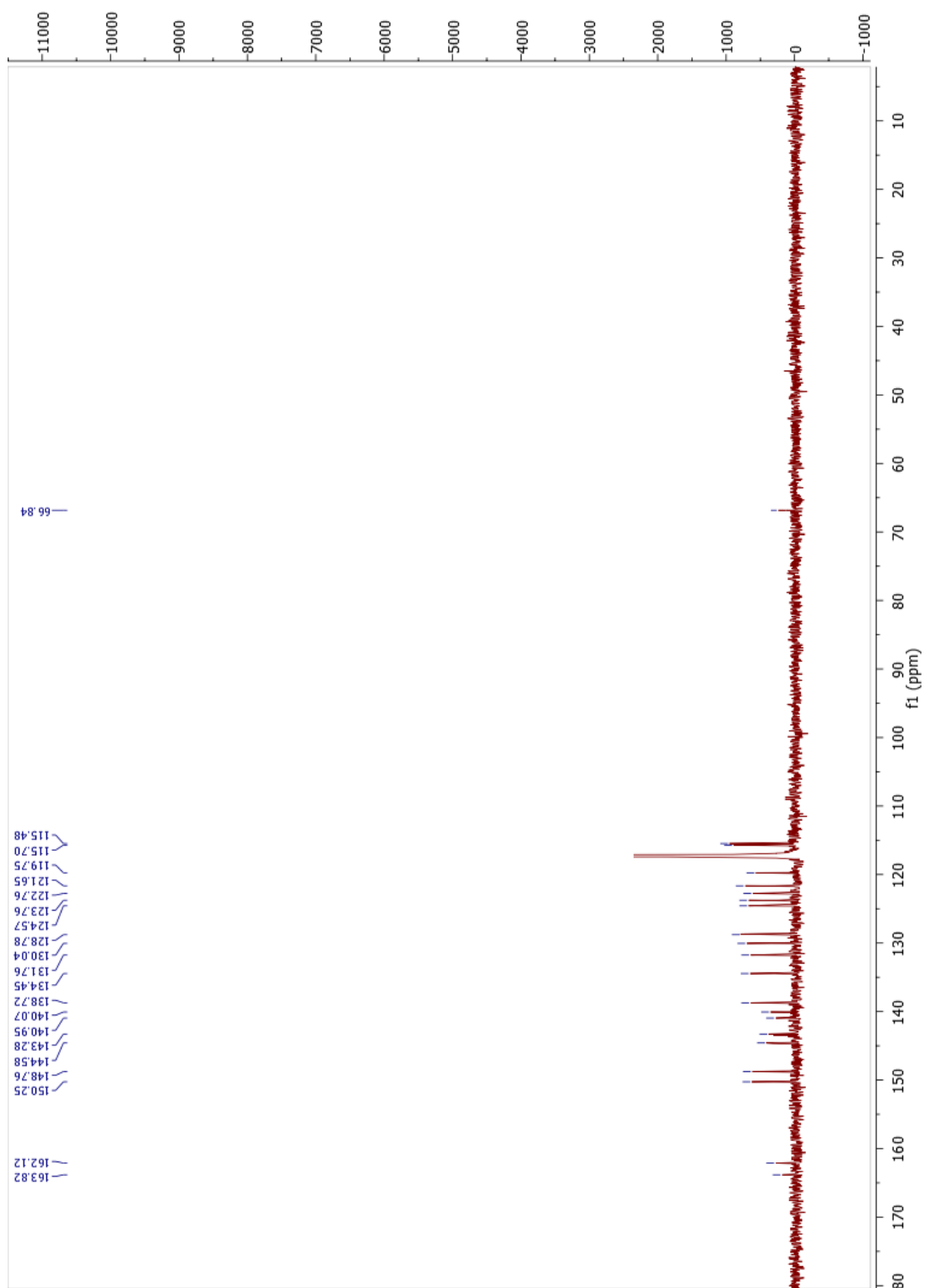
Figure A.10: ^{13}C'NMR spectrum of C1

C2-H'NMR
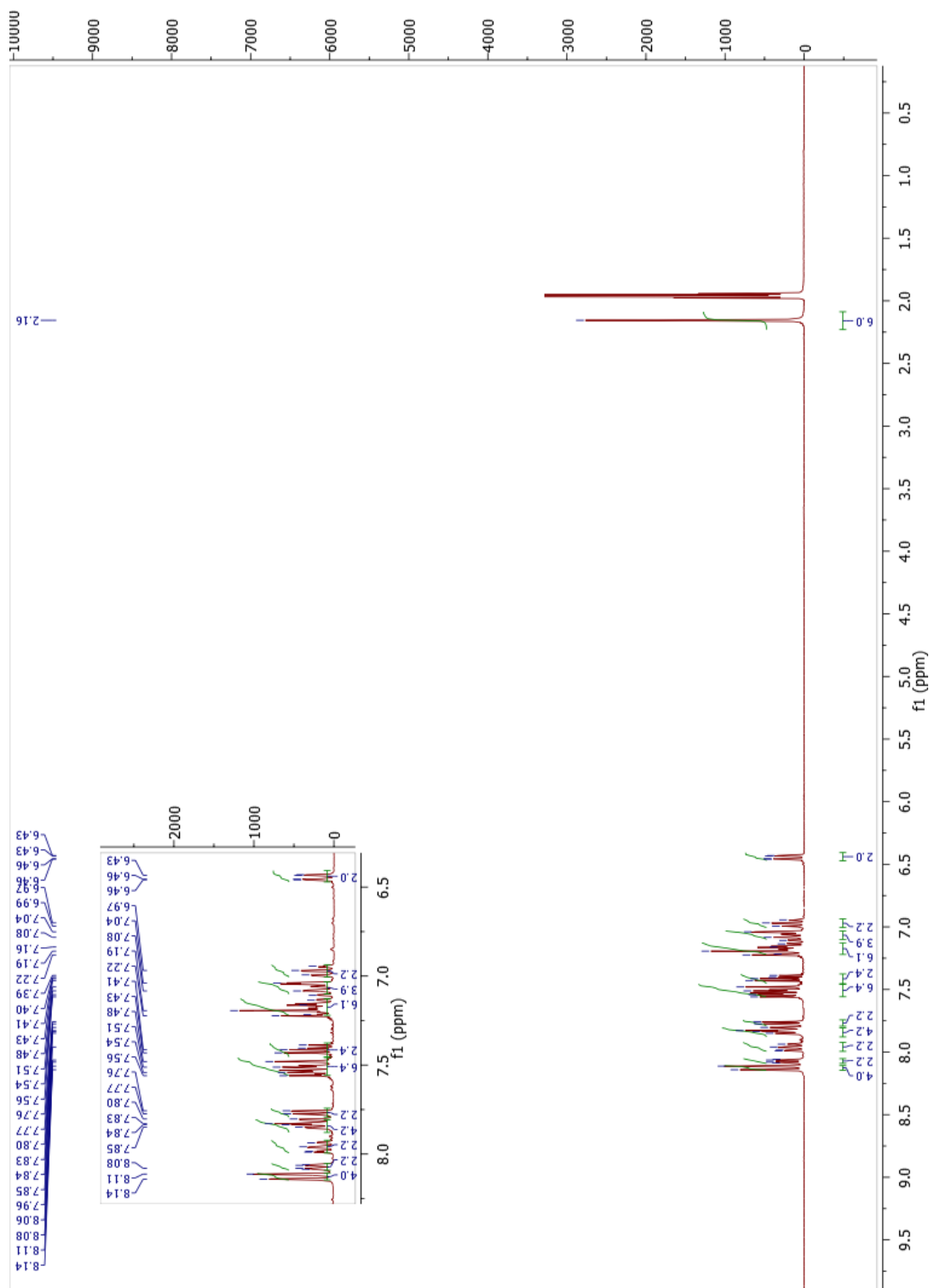
Figure A.11: ^{1}H'NMR spectrum of C2

C2-C'NMR
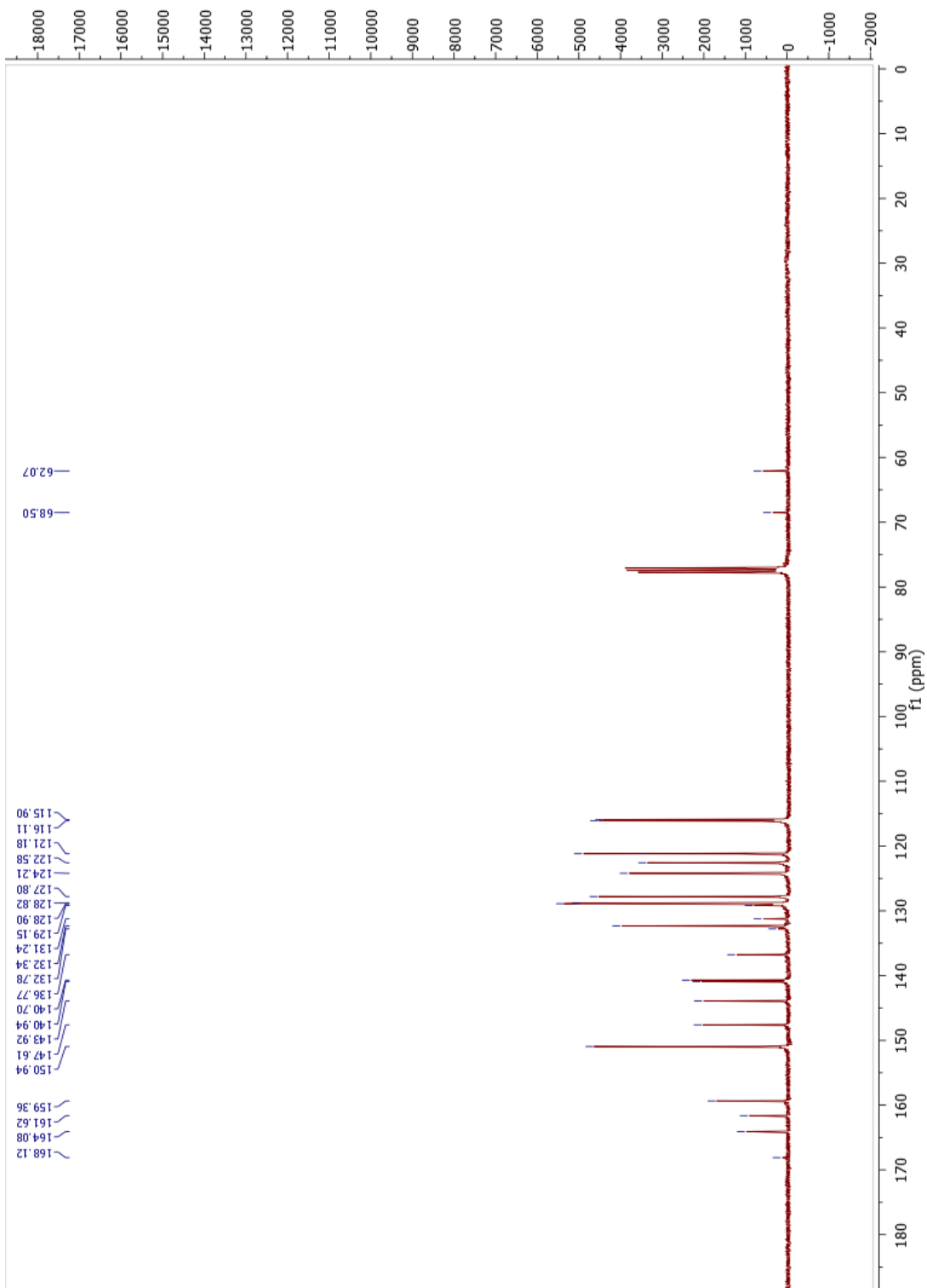
Figure A.12: ^{13}C'NMR spectrum of C2

C3-H'NMR
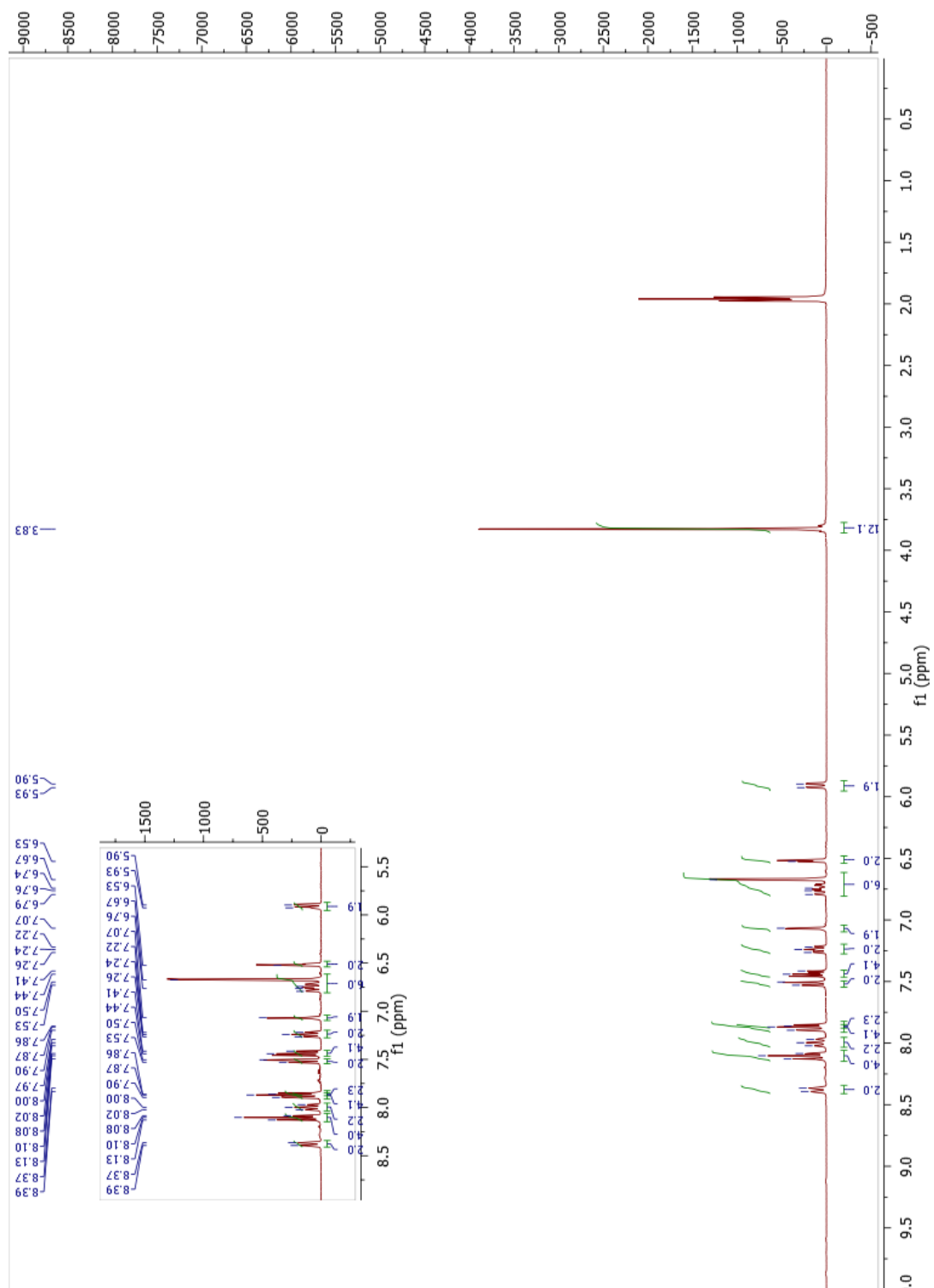
Figure A.13: ^{1}H'NMR spectrum of C3

C3-C'NMR
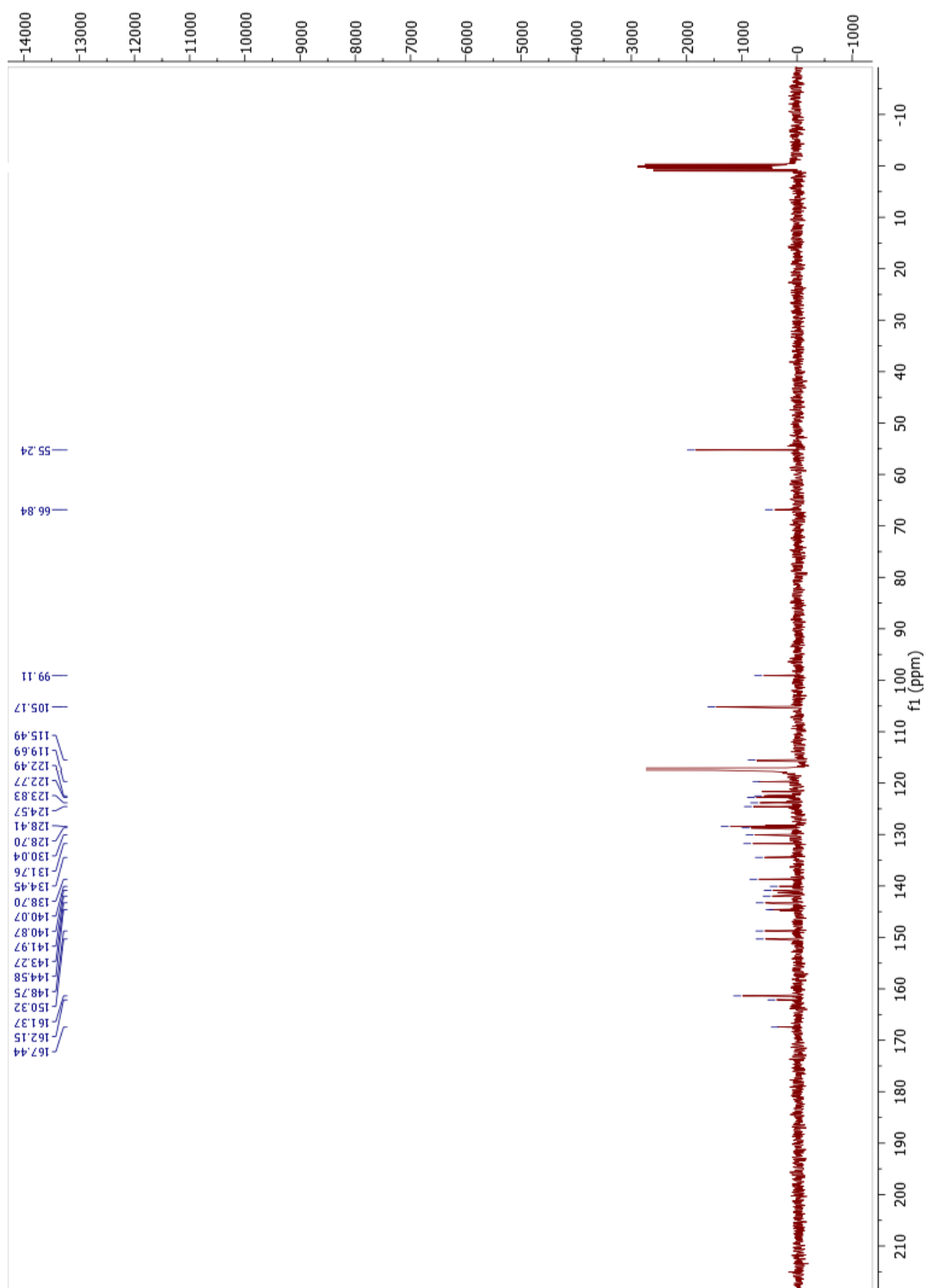
Figure A.14: ^{13}C'NMR spectrum of C3

C4-H'NMR
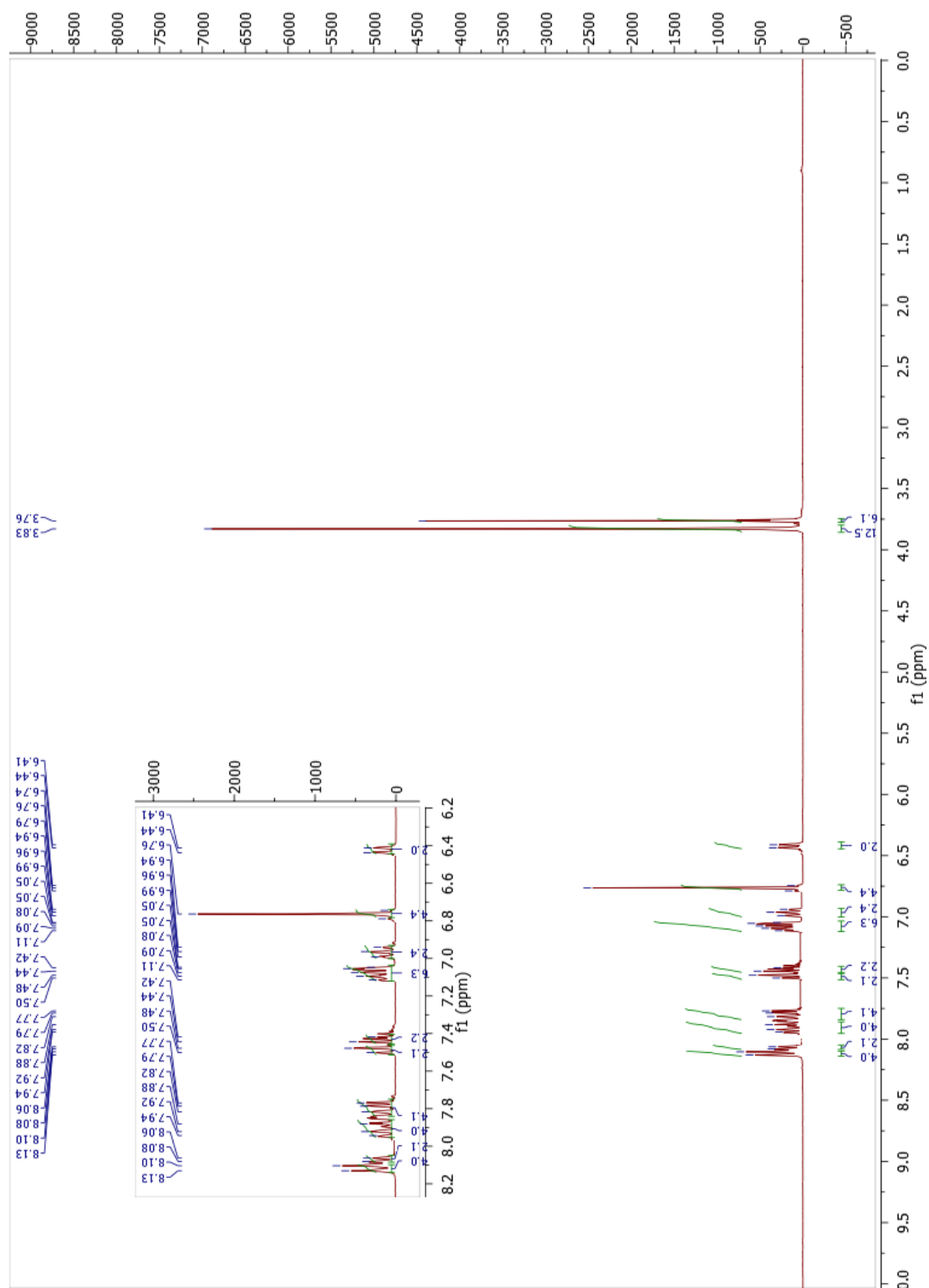
Figure A.15: ^{1}H'NMR spectrum of C4

C4-C'NMR
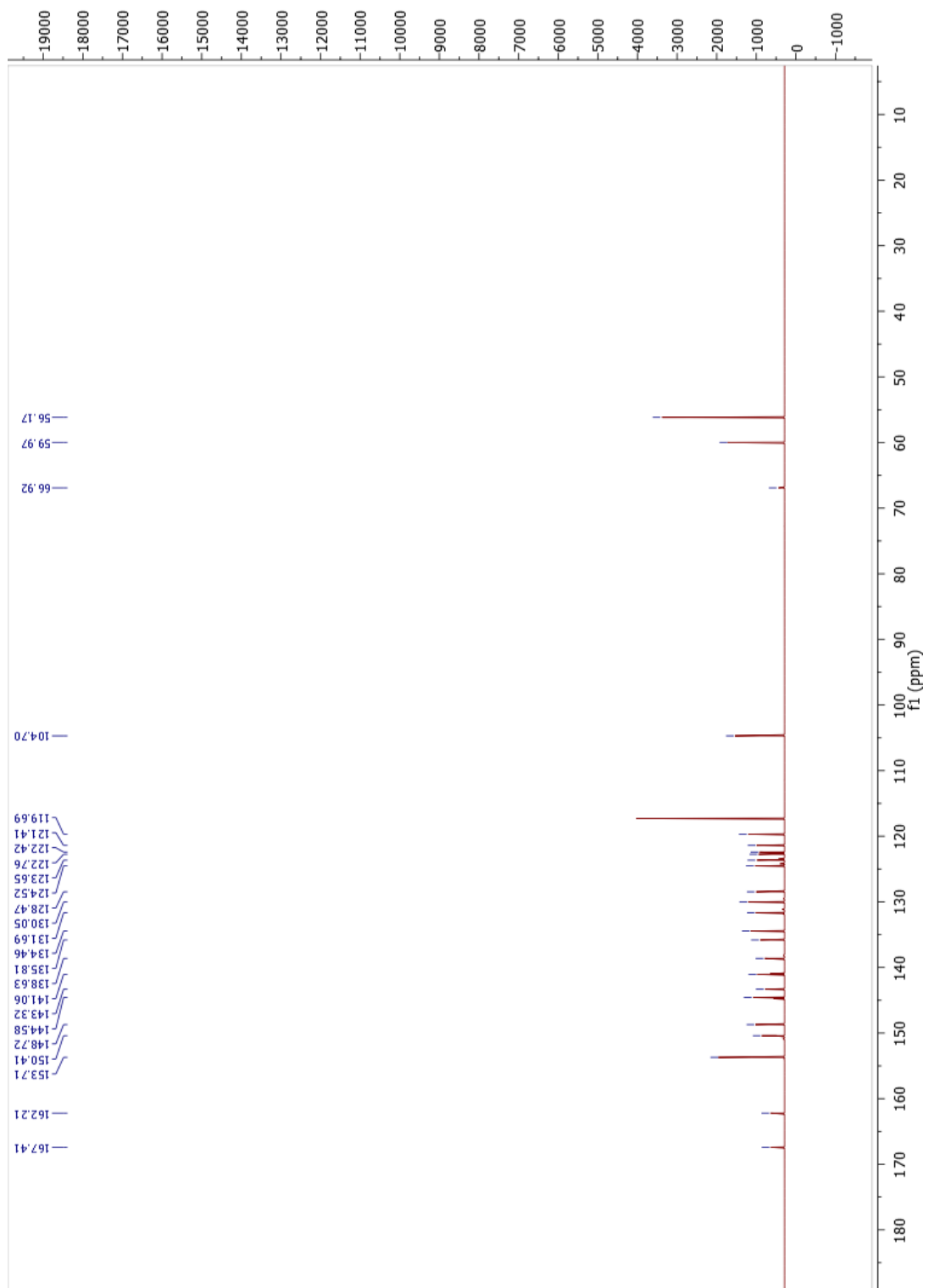
Figure A.16: ^{13}C'NMR spectrum of C4

C5-H'NMR
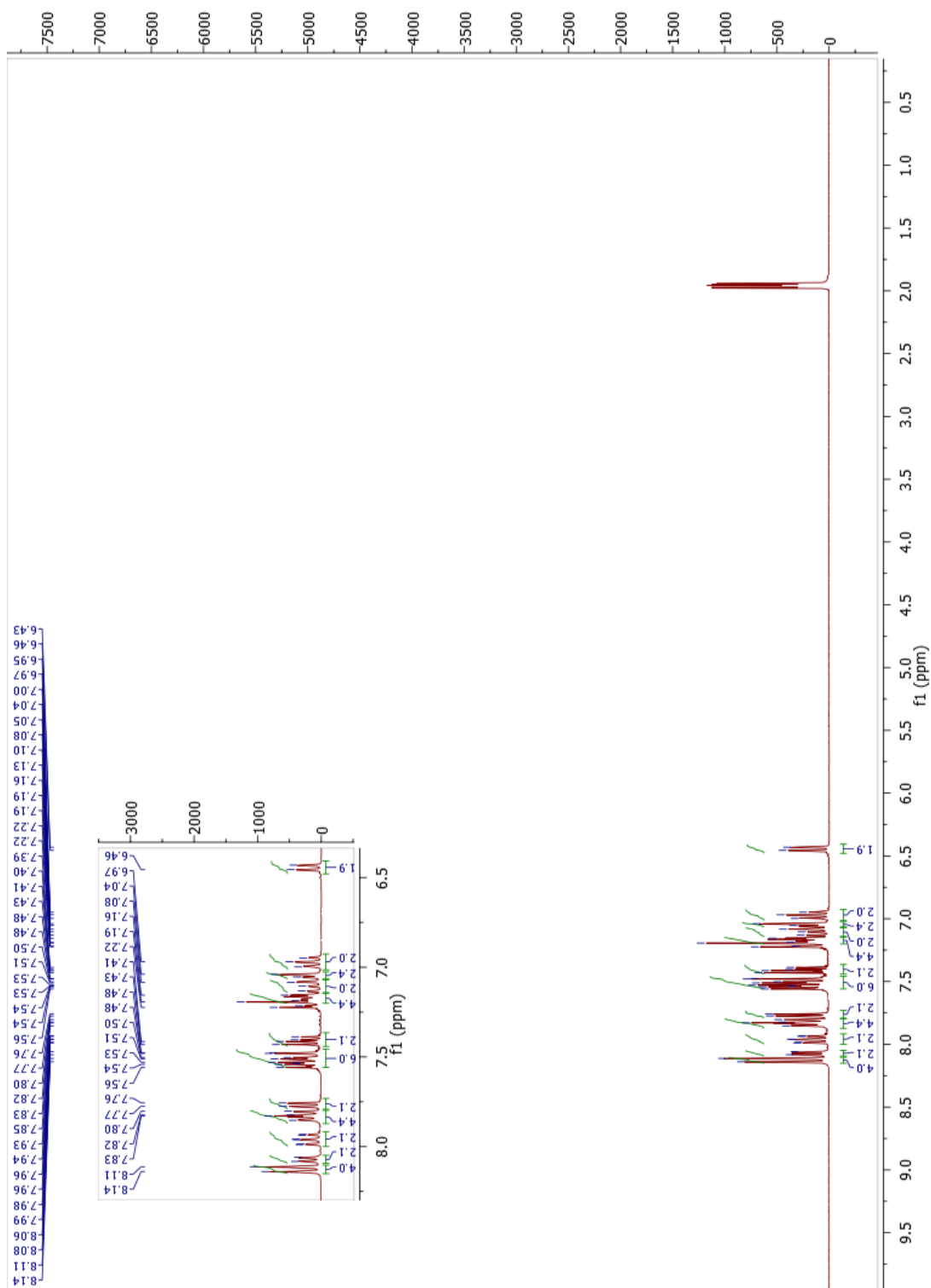
Figure A.17: ^{1}H'NMR spectrum of C5

C5-C'NMR
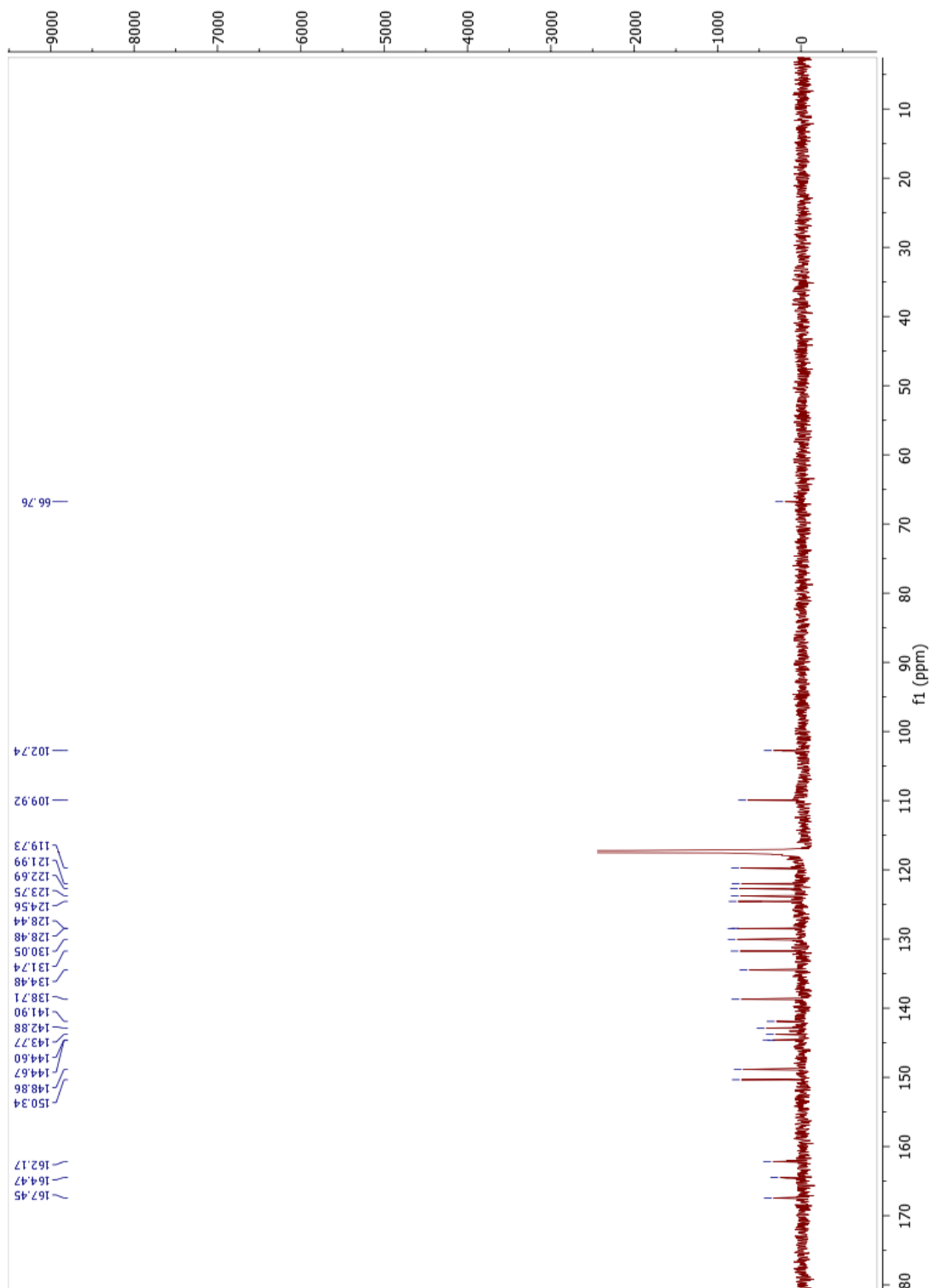
Figure A.18: ^{13}C'NMR spectrum of C5

Peaks (ppm): 66.76, 102.74, 109.92, 119.73, 121.99, 122.69, 123.75, 124.56, 128.44, 128.48, 130.05, 131.74, 134.48, 138.71, 141.90, 142.88, 143.77, 144.60, 144.67, 148.86, 150.34, 162.17, 164.47, 167.45

C6-H'NMR
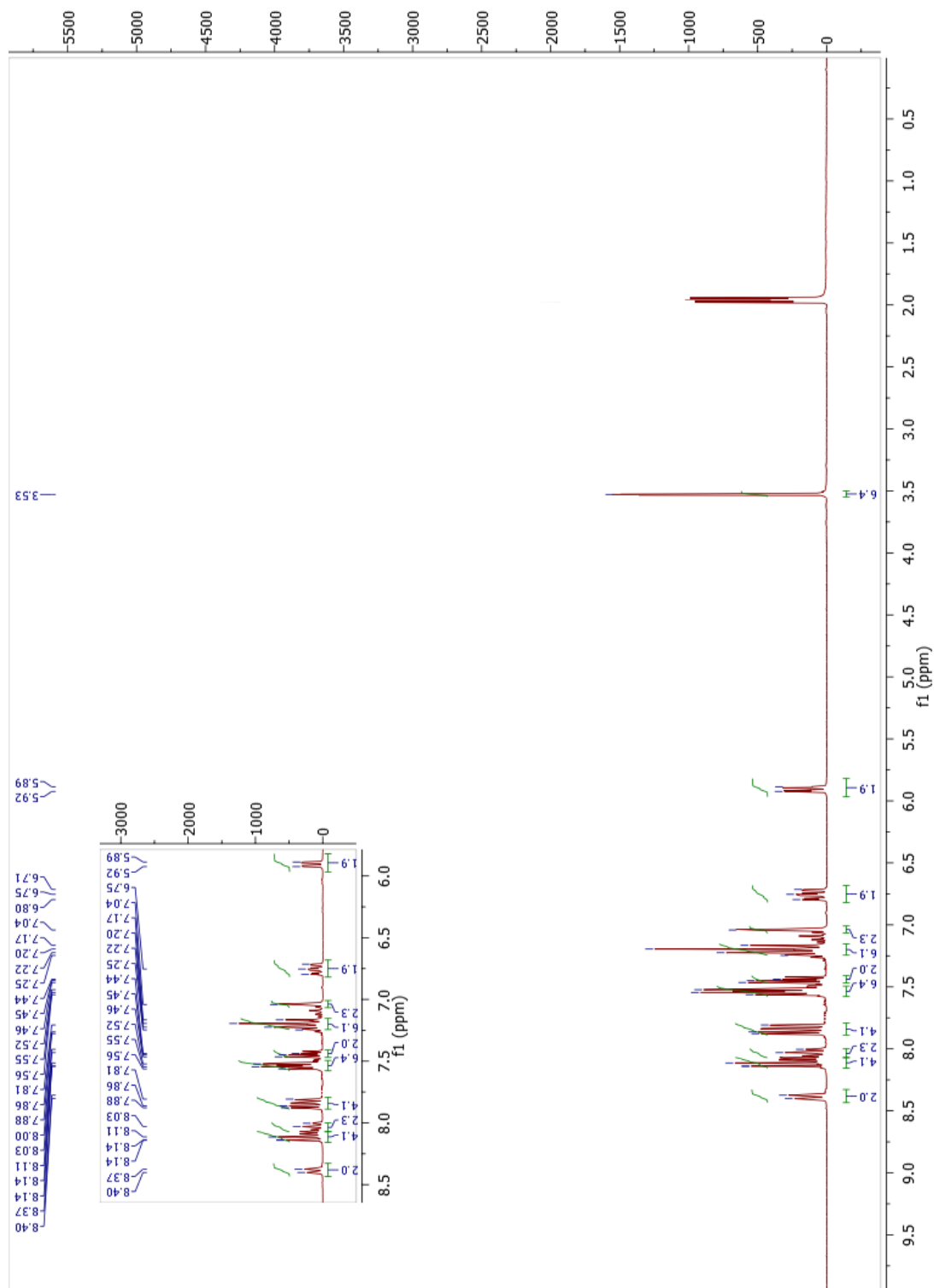
Figure A.19: ^{1}H'NMR spectrum of C6

C6-C'NMR
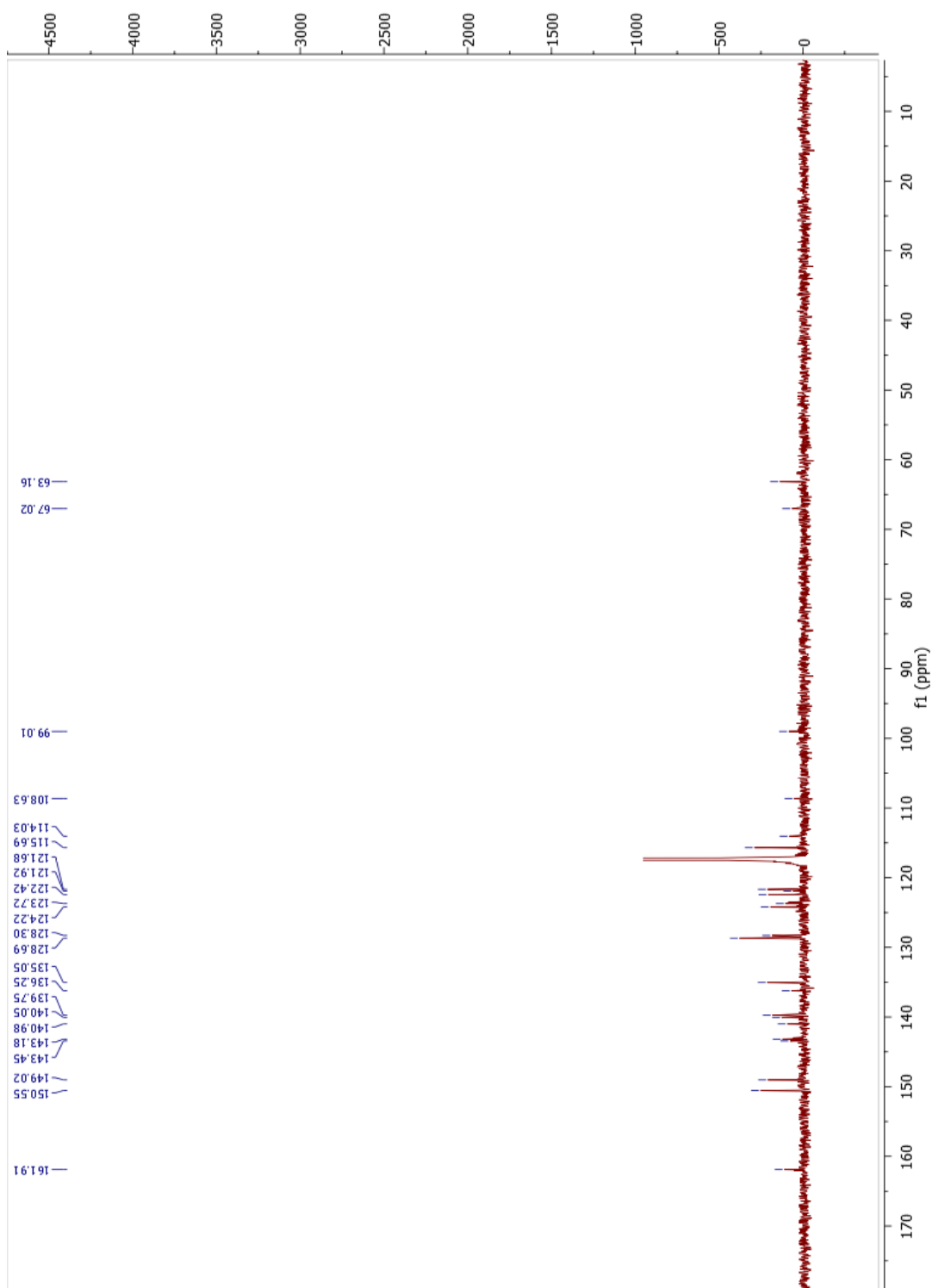
Figure A.20: ^{13}C'NMR spectrum of C6

C7-H'NMR
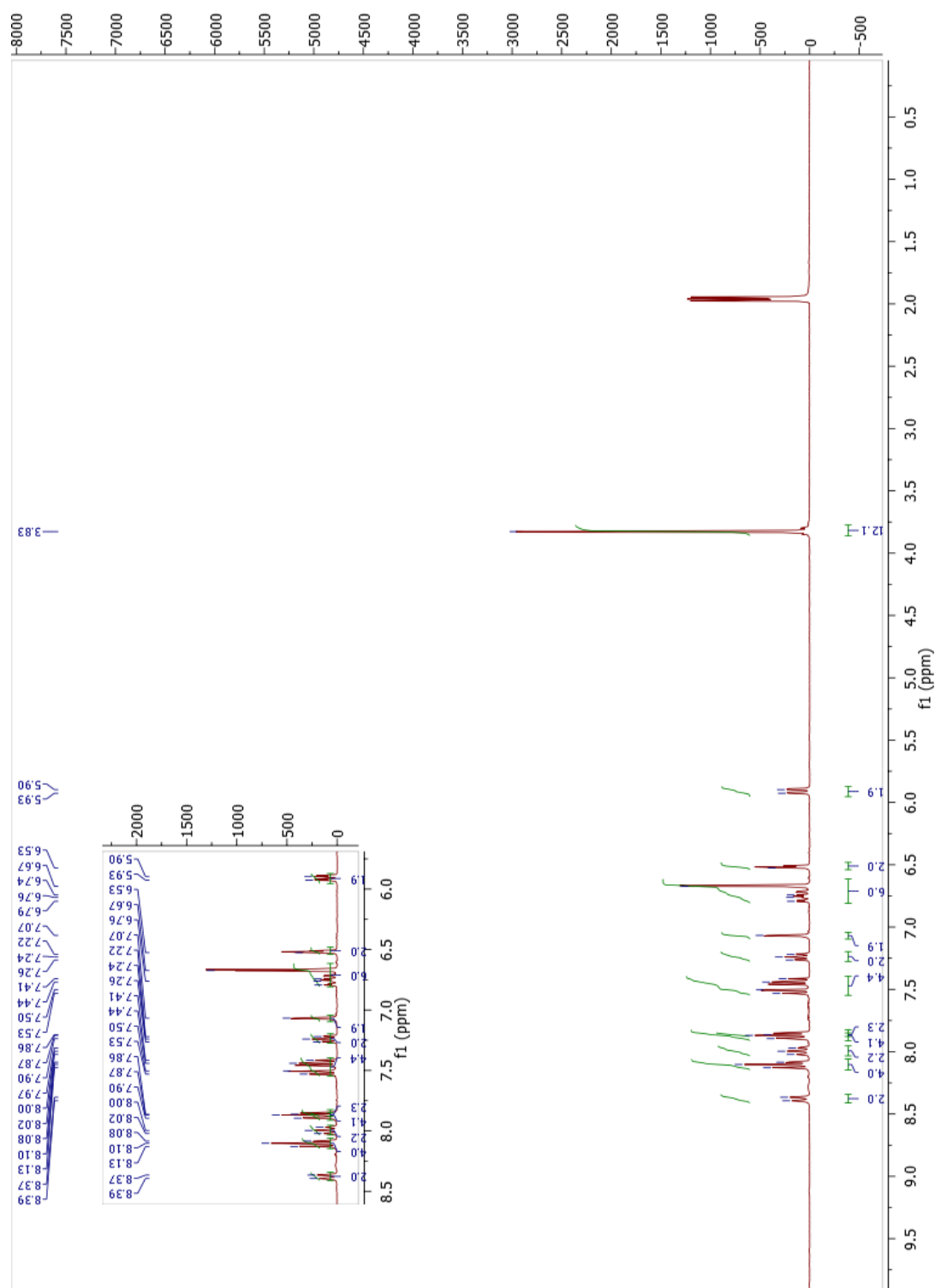
Figure A.21: ¹H'NMR spectrum of C7

C7-C'NMR
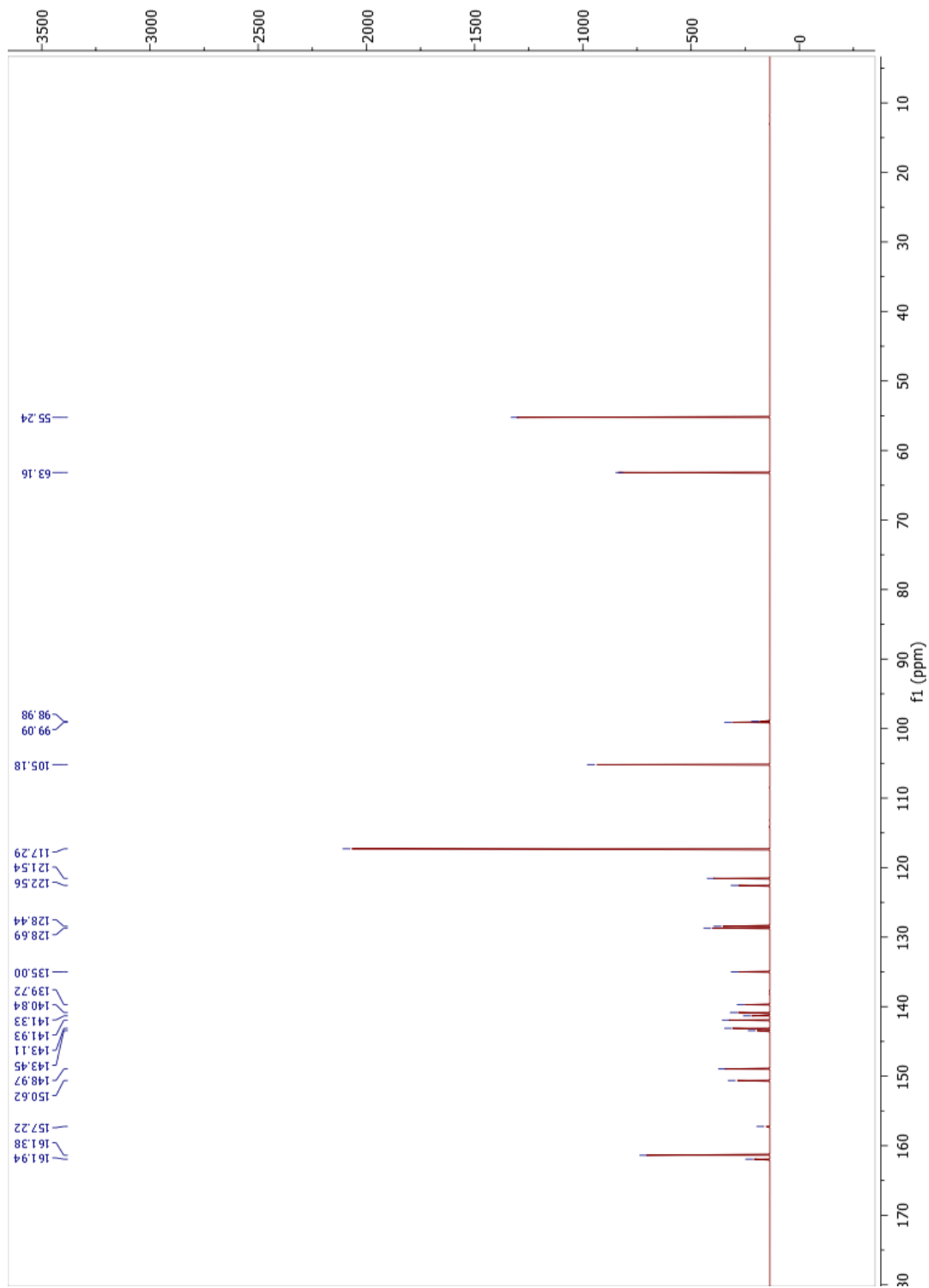
Figure A.22: ^{13}C'NMR spectrum of C7

C8-H'NMR
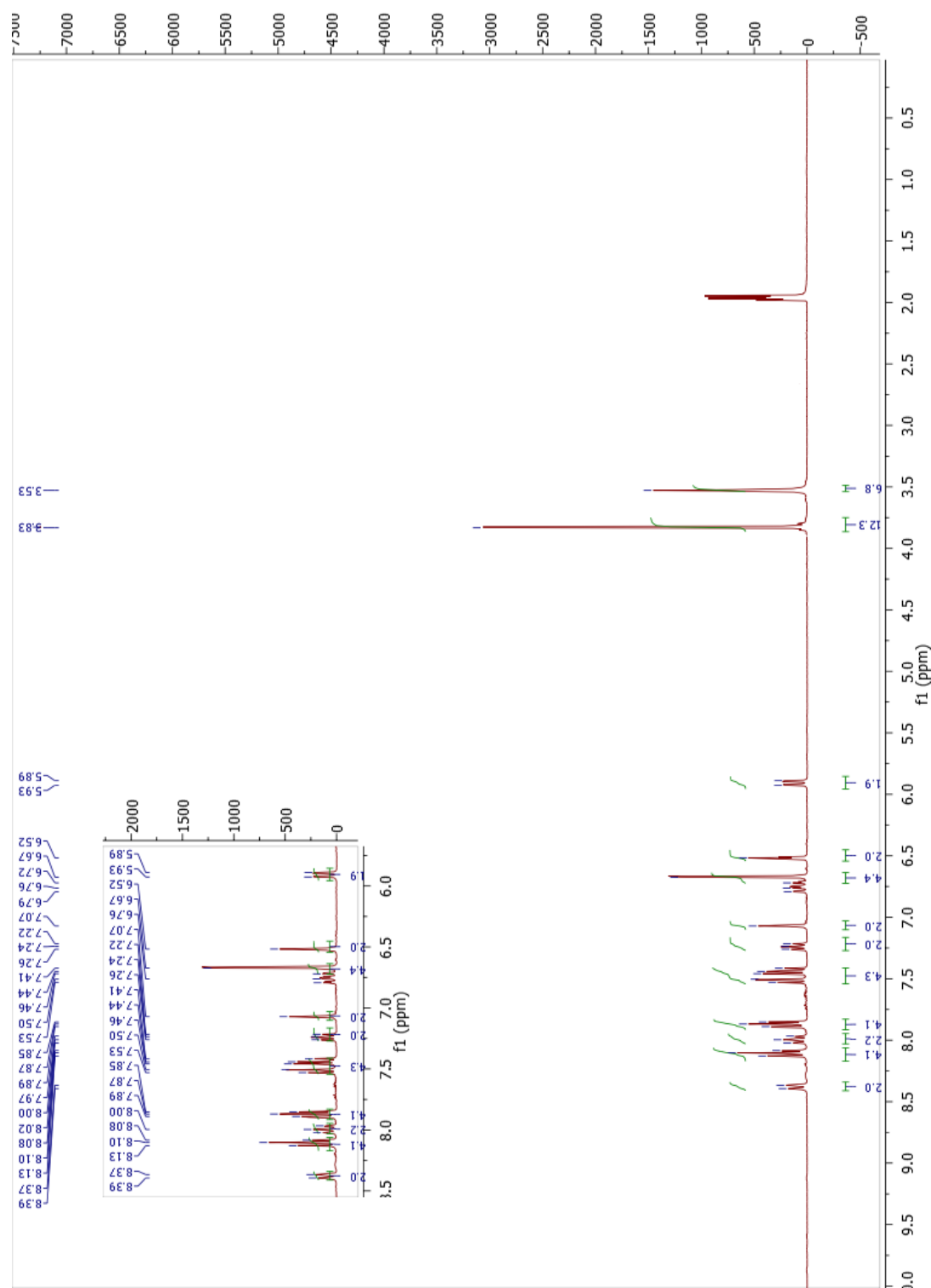
Figure A.23: [1]H'NMR spectrum of C8

C8-C'NMR

Peaks (from top to bottom): 56.17, 59.97, 66.92, 104.70, 119.69, 121.41, 122.42, 122.76, 123.65, 124.52, 128.47, 130.05, 131.69, 134.46, 135.81, 138.18, 138.63, 141.06, 143.32, 144.58, 144.76, 148.72, 150.41, 153.71, 159.63, 162.21, 167.41
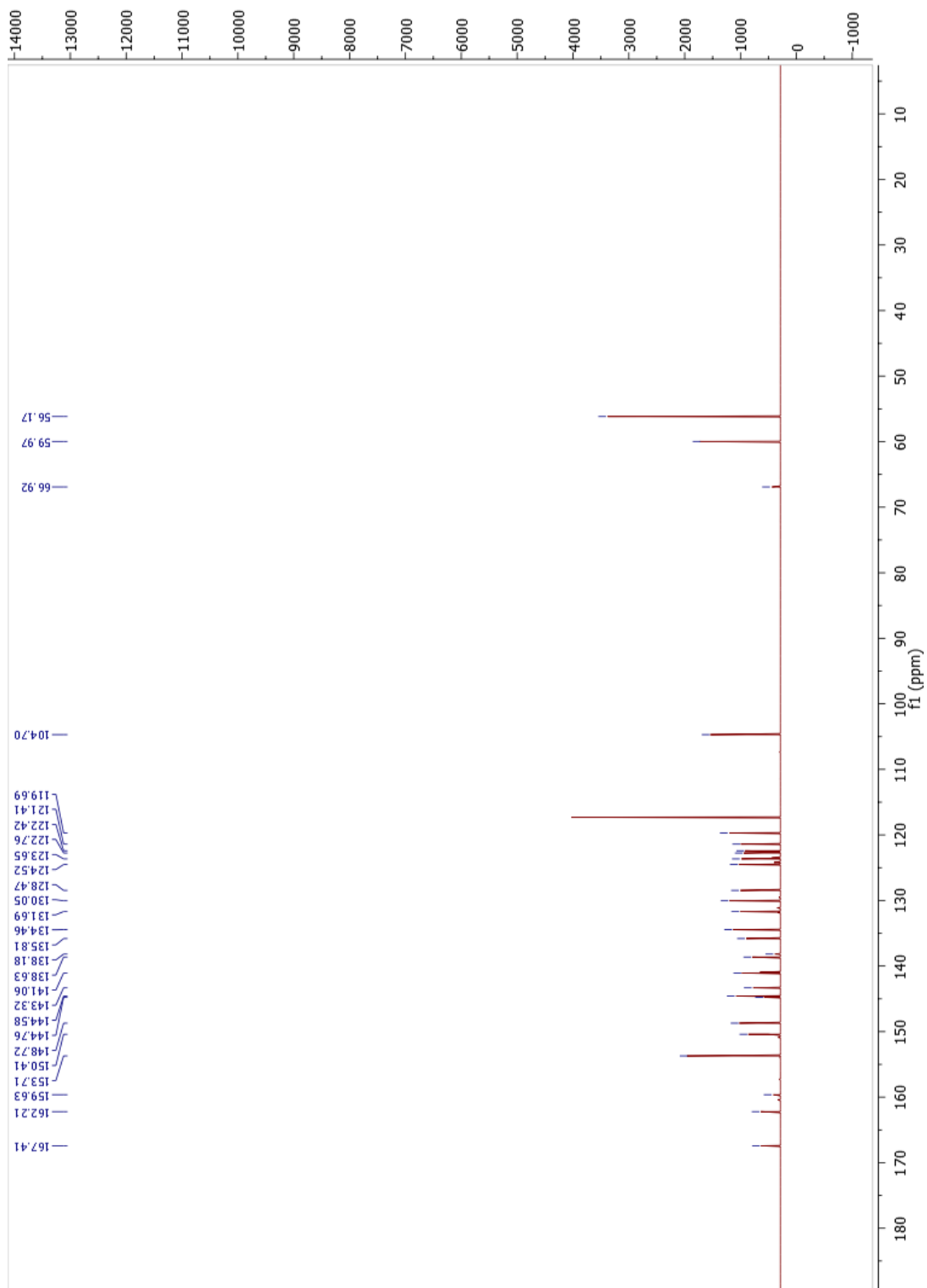
Figure A.24: ^{13}C'NMR spectrum of C8

A.3. FTIR Measurements
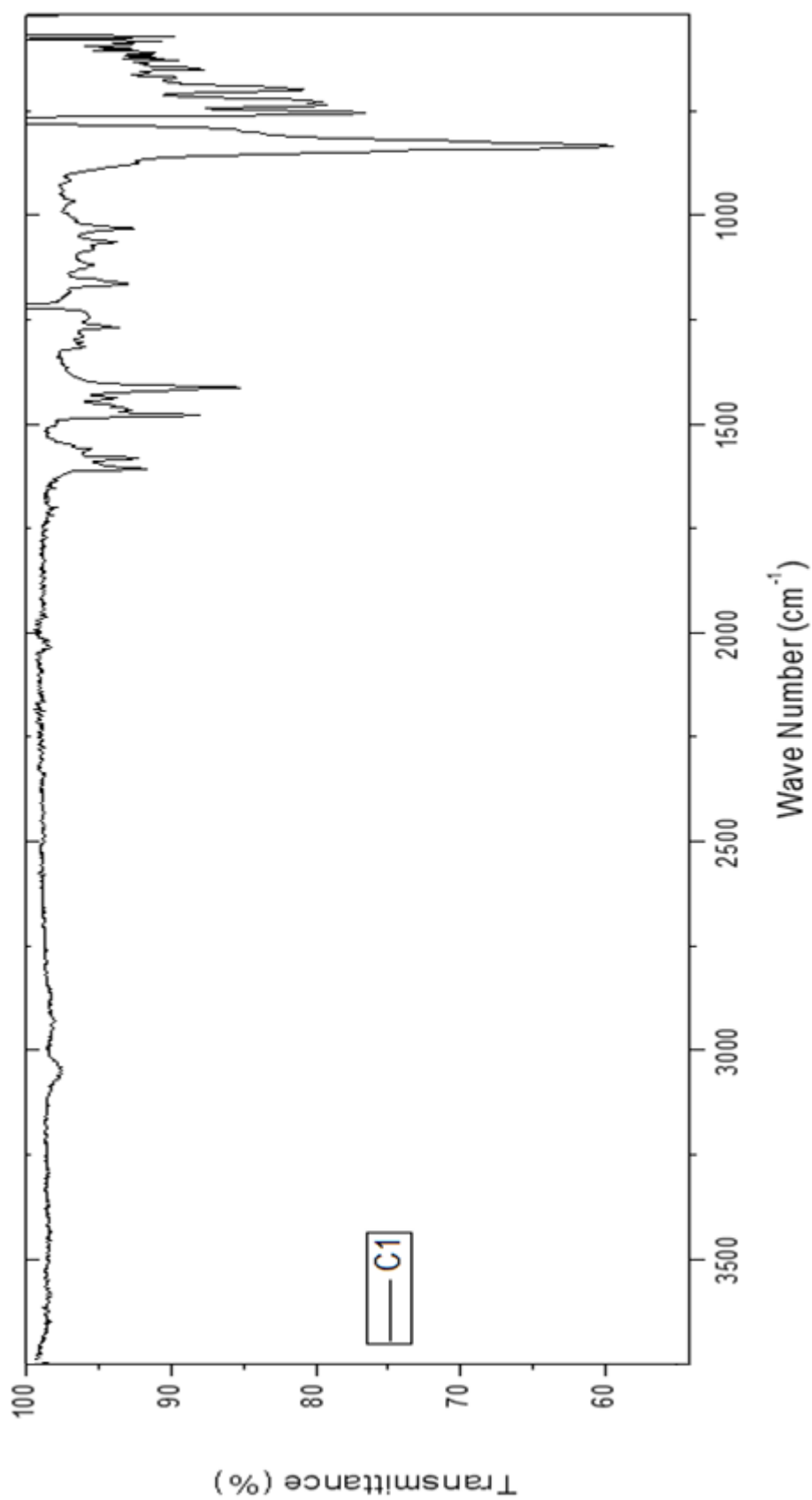
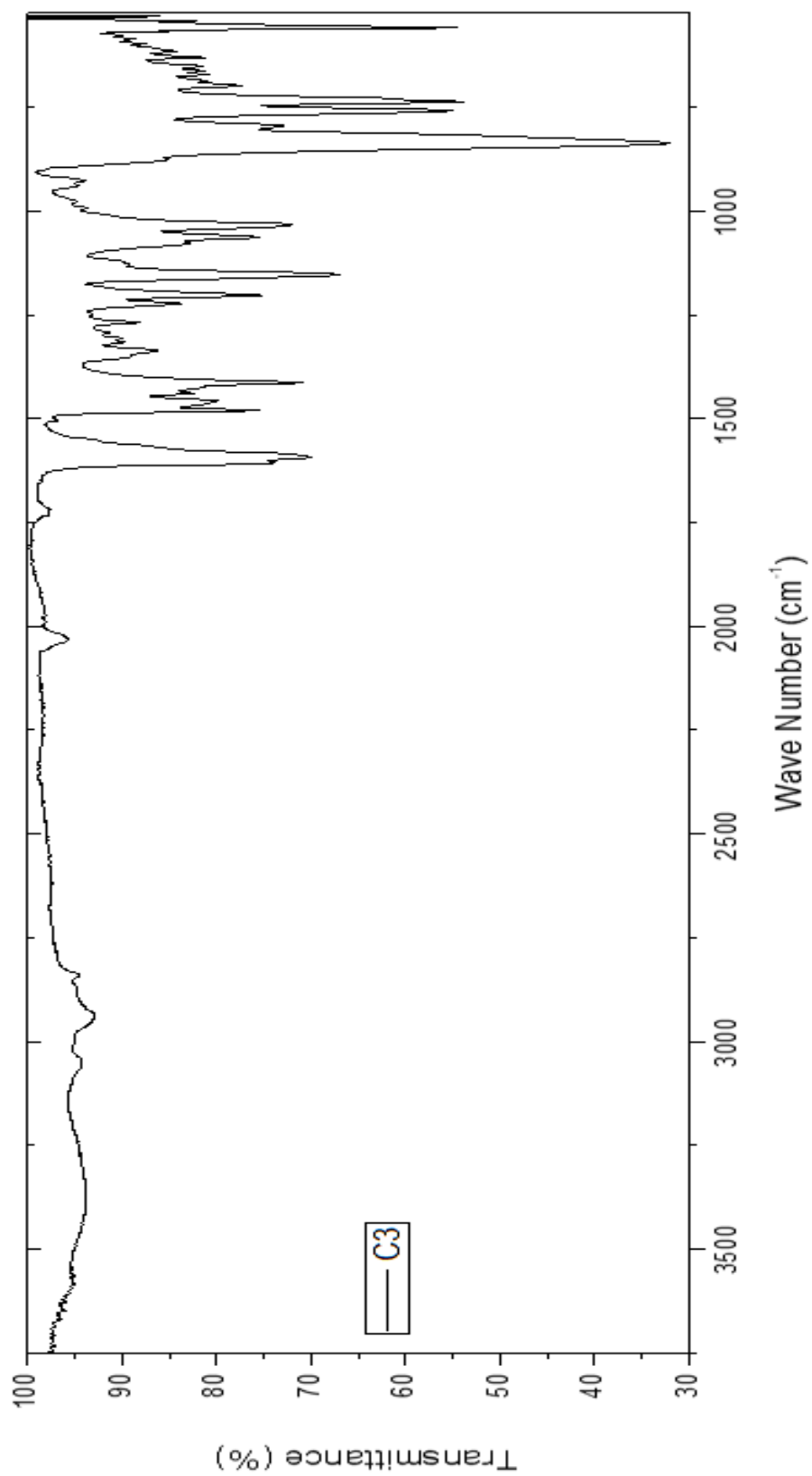**Figure A.25:** FTIR spectrum of C1.
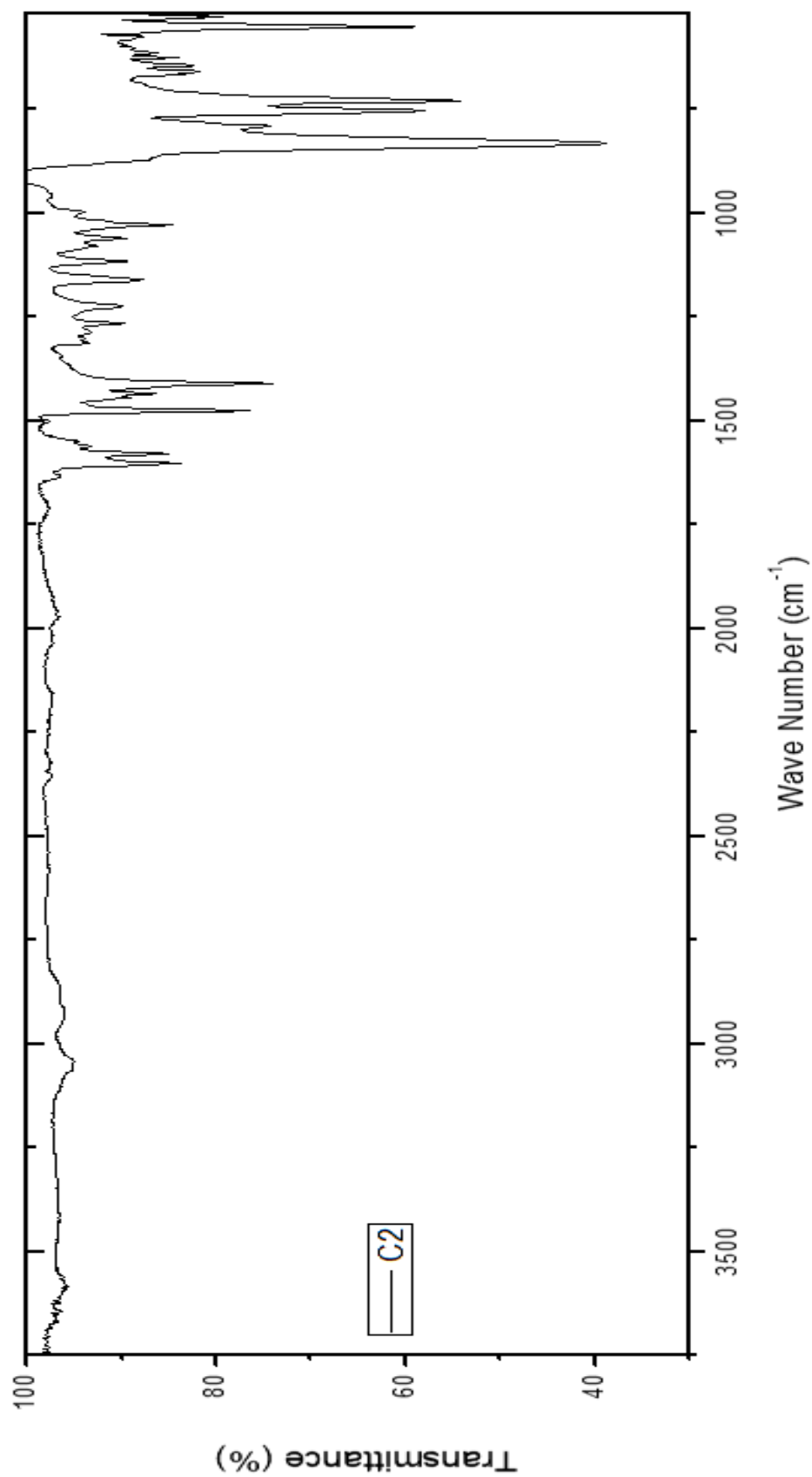
Figure A.26: FTIR spectrum of C2.

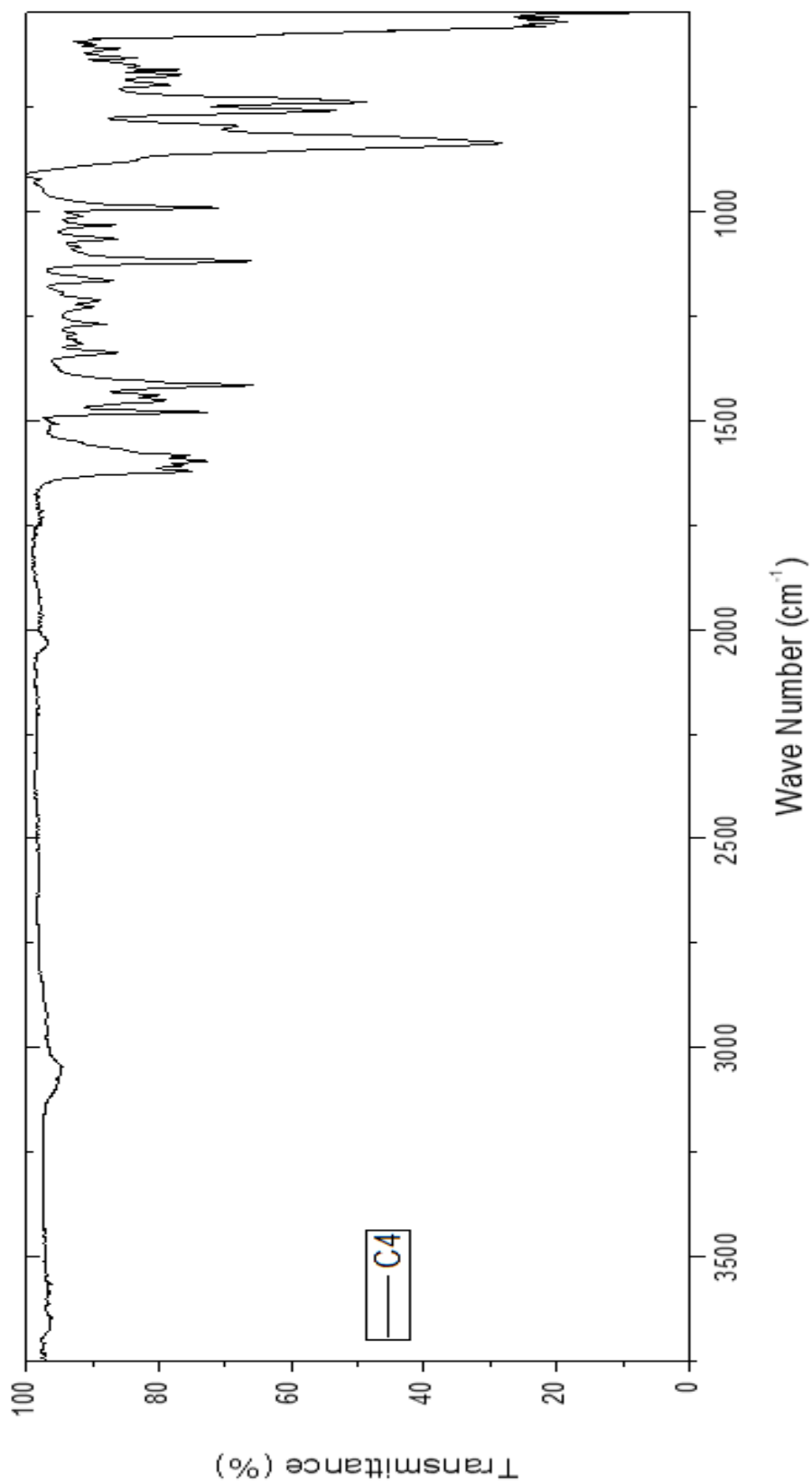**Figure A.27:** FTIR spectrum of C3.
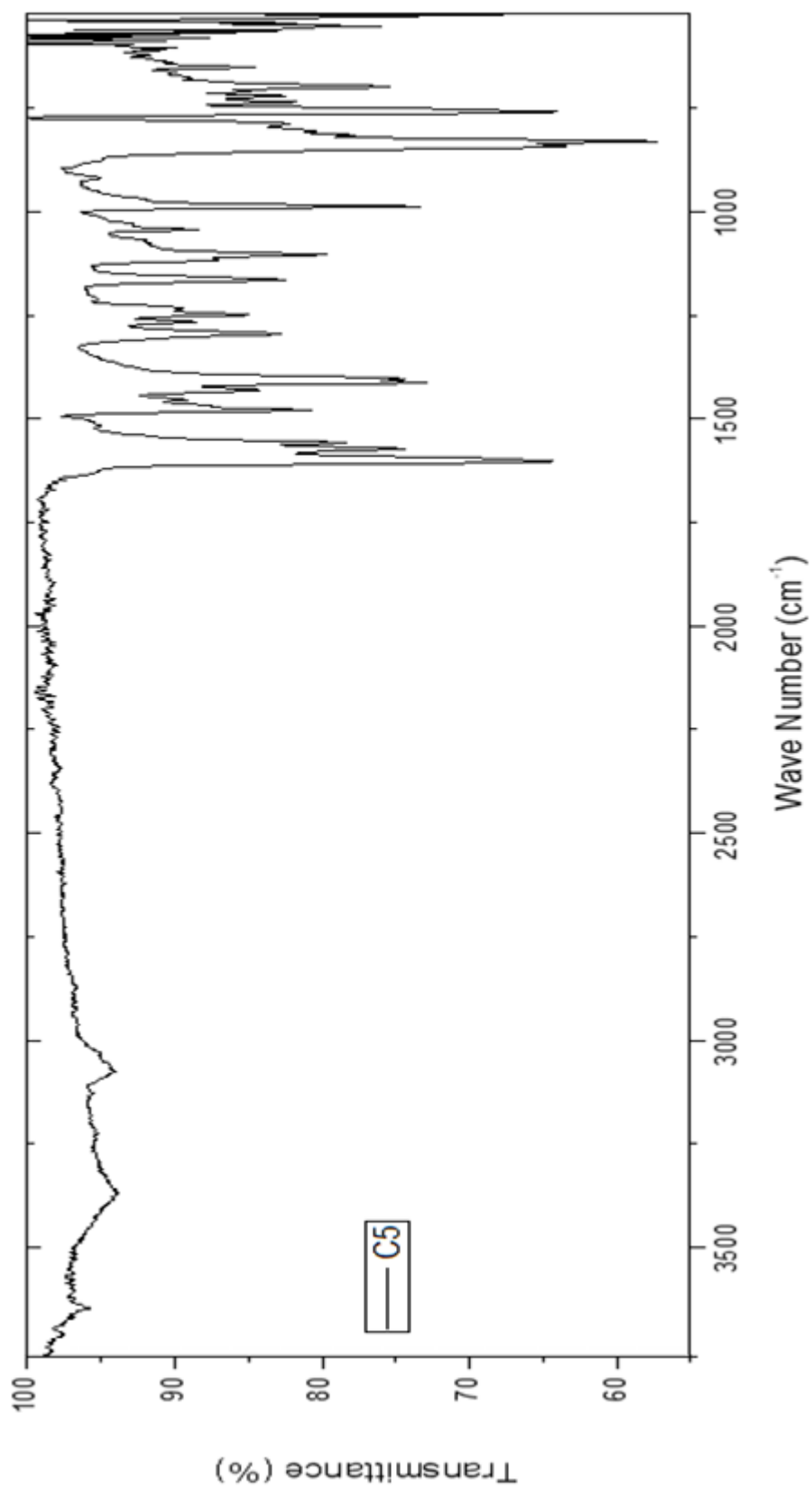
Figure A.28: FTIR spectrum of C4.

Figure A.29: FTIR spectrum of C5.
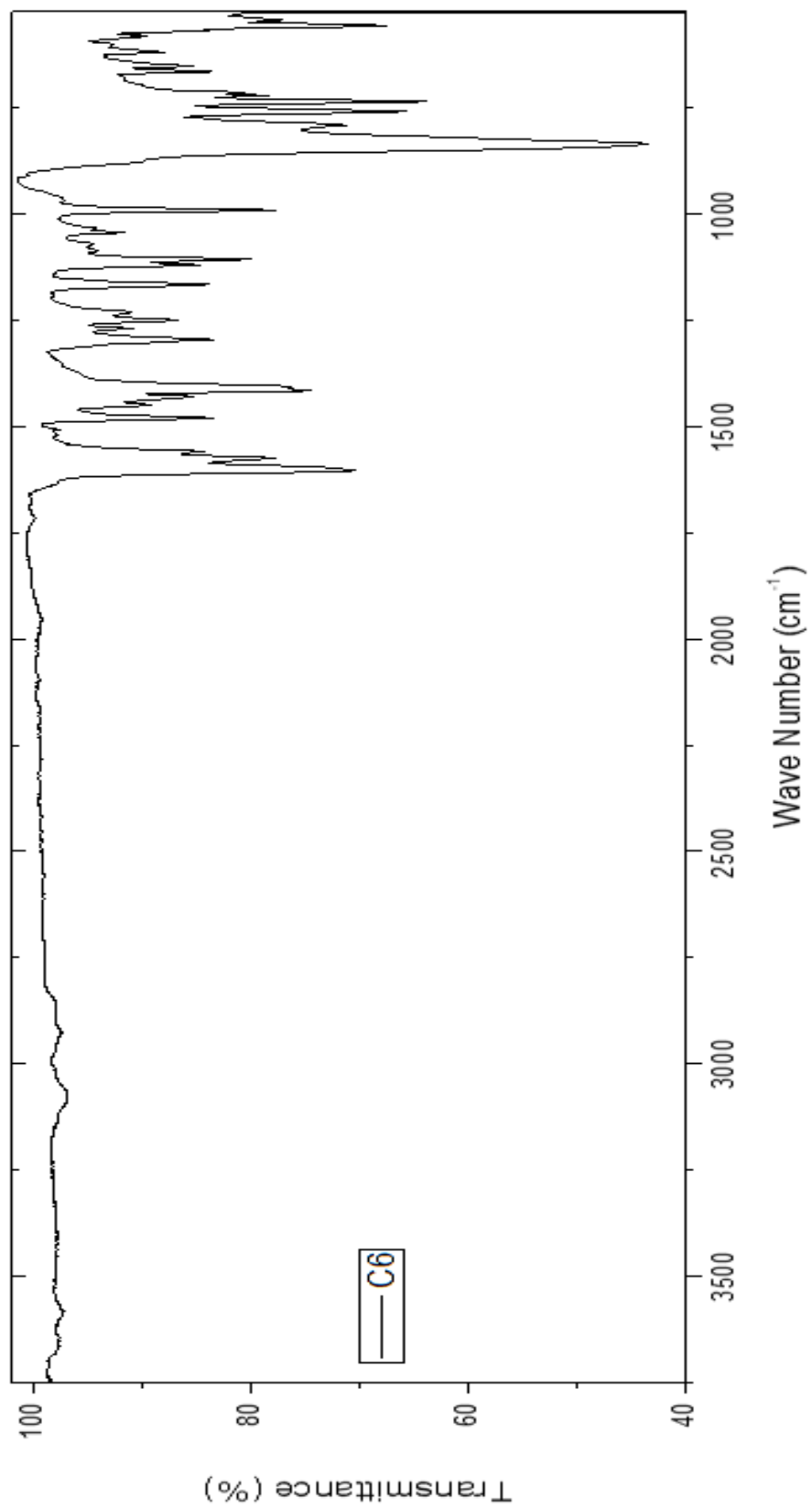
Figure A.30: FTIR spectrum of C6.
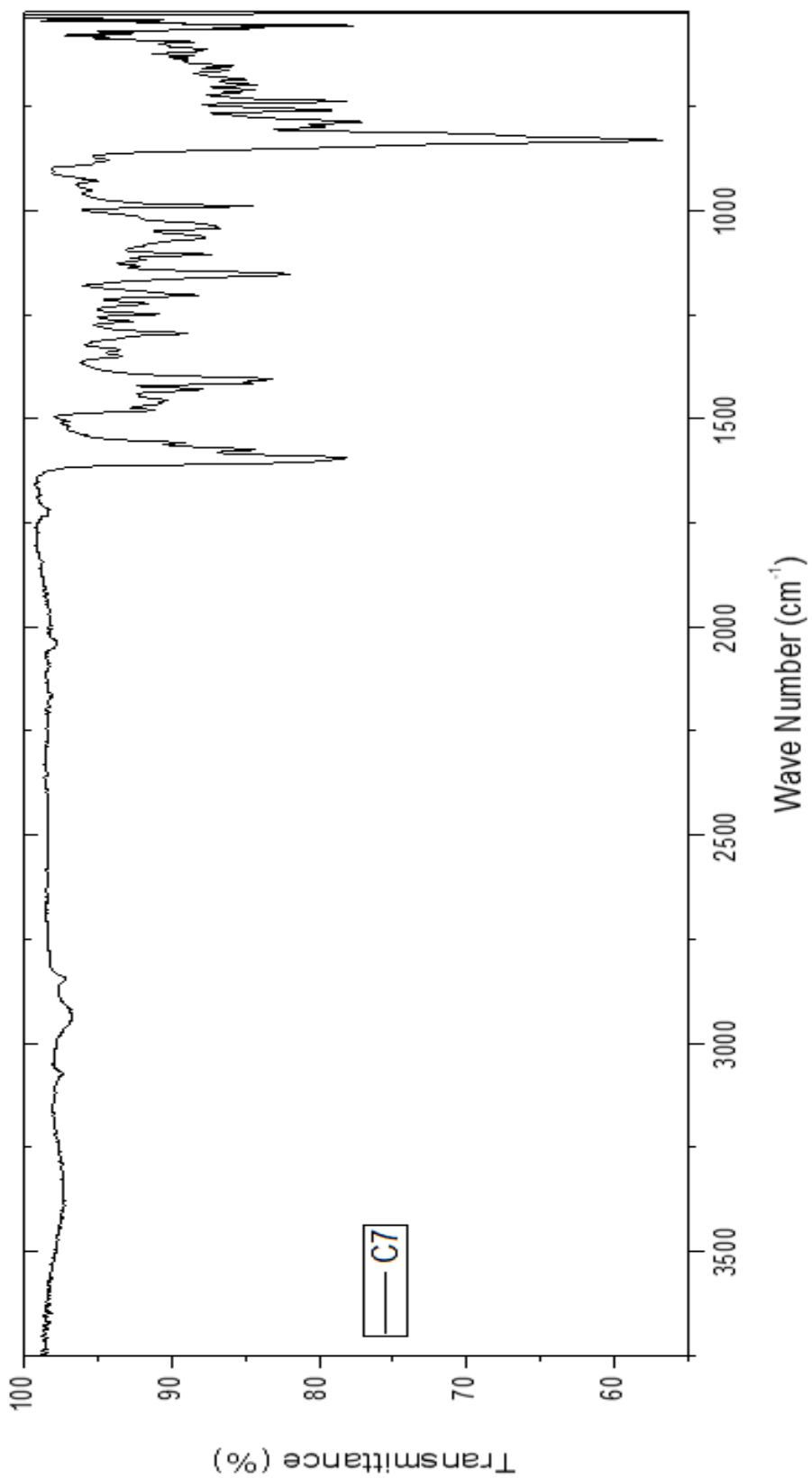
Figure A.31: FTIR spectrum of C7.
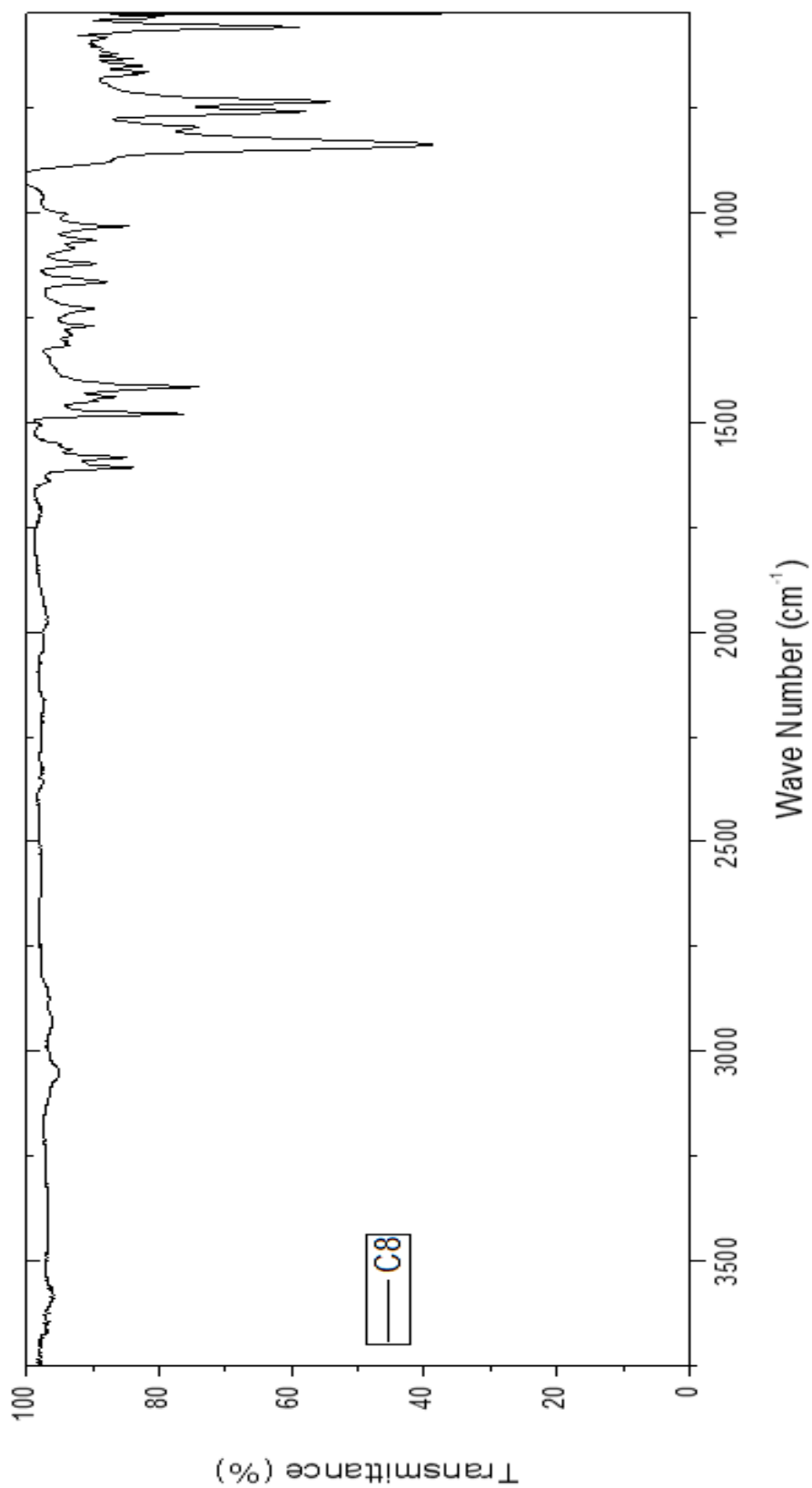
Figure A.32: FTIR spectrum of C8.

CURRICULUM VITAE

Name Surname	: **Caner KARAKAYA**
Place and Date of Birth	: **Tekirdağ / Malkara 15.07.1984**
E-Mail	: **cnrkarakaya@gmail.com**

EDUCATION :

- **B.Sc.** : 2009, Ondokuz Mayıs University, Faculty of Science, Chemistry Department
- **M.Sc.** : 2012, Süleyman Demirel University, Faculty of Science, Chemistry Department

PUBLICATIONS, PRESENTATIONS AND PATENTS :

1. Aydin, Hasan; Bacaksız, Cihan; Yagmurcukardes, Nesli; Karakaya, Caner; Mermer, Omer; Can, Mustafa; Senger, Tugrul; Sahin, Hasan; Selamet, Yusuf Experimental and Computational Investigation of GrapheneSAMsn-Si Schottky Diodes" Applied Surface Science,2018

2. Eyyup Yalcin, Duygu Akin Kara, Caner Karakaya, Mesude Zeliha Yigit, Ali Kemal Havare, Mustafa Can, Cem Tozlu, Serafettin Demic, Mahmut Kus, Abdelkhalk Aboulouard ''Functionalized different small molecules as interface to enhance charge carrier injection in Electroluminescent Cell'', Optic Materials, 2017

3. Aysenur Erdogan, Caner Karakaya, Mehmet Kerem Gonce, Sumeyra Buyukcelebi, Ahmet Nuri Ozcivan, Mustafa Can, Mahmut Kus and Serafettin Demic "Surface modification CdSeS nanocrystals for Polymer Hybrid Solar Cells", RSC Advance 2016

4. Karakaya, C., B. Dede, and E. Cicek, Novel Metal (II) Complexes with Bidentate Schiff Base Ligand: Synthesis, Spectroscopic Properties and Dye Decolorization Functions. Acta Physica Polonica A, 2016. 129(2): p. 208-212.

5. Eyüp Yalçın, Duygu Akın Kara, Caner Karakaya, Mustafa Can, Nusret Kaya, Şerafettin Demiç, ''Using SelfAssembled Monolayer to Improve Device

Performance of Organic Light Emitting Diodes'',Porto, Portugal, Jully 17-20 2017

6. Şerafettin Demiç, Ayşenur Erdoğan, Caner Karakaya, Mehmet Kerem Gönce, Sümeyra Büyükçelebi, E. Yenel, Koray Kara, Ahmet Nuri Özcivan, Mustafa Can, Mahmut Kuş, Surface Modification of CdSeS Nanocrystals for Hybrid Solar Cell Applications 28. Kimya kongresi 2016, No:0685-B3

7. Karakaya, C., Dede, B., Çiçek, E., "Novel Co(II), Ni(II), Cu(II) and Zn(II) Complexes with Bidentate Schiff Base Ligand: Synthesis, Spectroscopic Properties and Dye Decolorization Functions", 50. Zakopane School of Physics, 18-23 May 2015, Zakopane, Poland.